BURNUP IN A MOLTEN SALT FAST REACTOR

L.L.W. Frima

Master Thesis
NERA-131-2013-010

Committee:
Dr. ir. J.L. Kloosterman
Dr. ir. D. Lathouwers
Dr. E. van der Kolk

Delft University of Technology
Faculty of Applied Sciences
Department of Radiation Science and Technology
Section of Nuclear Energy and Radiation Applications

September 27$^{\text{th}}$, 2013

Abstract

The Molten Salt Fast Reactor (MSFR) is a proposed generation-IV nuclear reactor with increased safety and sustainability aspects. To assess MSFR's performance a new burnup tool was developed to model nuclide transformation in the fuel region taking into account online refueling and reprocessing. The adopted volume lumped parameter model assumes the fuel is homogeneously mixed for all times and models online reprocessing due to helium bubbling and offline reprocessing of lanthanides by introducing an effective decay rate for nuclides concerned. The results show good agreement with those obtained by Politecnico di Milano (POLIMI), but also show substantial differences with those obtained by Laboratoire de Physique Subatomique et de Cosmologie (LPSC), especially in the ^{234}U concentration, due to adoption of another cross section library. After 200 years of operation, the reactor reaches an equilibrium condition which requires $1.1 \cdot 10^3$ kg per year of ^{232}Th and 61 kg per year of ^{233}U. Different offline lanthanide reprocessing rates influence the required fissile material feed and switching between one refueling rate and another can be accomplished with a step function by changing the offline lanthanide reprocessing rate, which was varied between 20 and 60 liters per day. Nuclear waste from the MSFR exists of reprocessed fission products that are slightly more radiotoxic than those of a PWR and are not influenced by the offline lanthanide reprocessing rate in the investigated domain. After approximately 300 years, MSFR's waste is as radiotoxic as the equivalent amount of uranium ore needed to generate the same amount of energy in a PWR. Concerning safety, the temperature coefficient of reactivity is strongly negative throughout operation, starting at -6.95 pcm/K for fresh fuel and rising a little to -5.27 pcm/K at equilibrium. The effective delayed neutron fraction is lowered in comparison with the delayed neutron fraction due to precursor decay in the external circuit (290 pcm versus 310 pcm). If cooling of the fuel fails, the predicted rapid temperature increase solely due to decay heat requires a passive safety system, based on a freeze plug, to drain the core within 11 minutes. Unless the melting time of 15 minutes can be greatly reduced, a mechanical valve should be considered to close and open the drainage system.

Acknowledgements

First of all I would like to thank my daily supervisors Jan Leen Kloosterman and Danny Lathouwers who made this project possible. I enjoyed working with you. But I would also like to thank Frank Wols and Zoltán Perkó with whom I had many discussions that influenced my thesis. To the rest of the group I would like to say I had a good time here and I hope to see you in the future.

Contents

Chapter 1

Introduction

People's objections to nuclear energy are mainly induced by the longevity of nuclear waste and the possibility of accidents similar to Fuskushima (Japan, 2011) or Chernobyl (USSR, 1986). To accommodate the world's rising demand for an affordable and a sustainable supply of electricity, as well as to effectively address these concerns, thirteen countries and institutions collaborate in the Generation-IV International Forum (GIF-IV) to lay the groundwork for the next generation of nuclear energy systems, which will outperform current designs in terms of sustainability, non-proliferation, use of resources, safety and waste management. The Molten Salt Fast Reactor (MSFR), one of six selected candidates[17], is a radical new design compared to traditional Light Water Reactors (LWRs) and promises extensive (passive) safety features as well as waste reduction due to adoption of the thorium fuel cycle combined with fuel in a liquid form.

1.1 Thorium Fuel Cycle

A reactor utilizing the thorium fuel cycle, like the MSFR, converts thorium to uranium and is called a 'converter reactor' or a 'breeder reactor' if producing even more than what it consumes. Thorium is approximately three to four times more abundant than uranium and is found in many countries as an easily exploitable resource[6]. In this fuel cycle, the fertile ^{232}Th is converted into fissile ^{233}U in three steps: first ^{232}Th absorbs a neutron to become ^{233}Th, which decays by two subsequent beta emissions via protactinium to ^{233}U. ^{233}Th has a very short half life of $t_{1/2} = 22.3$ min, but ^{233}Pa has a half life of 27 days, allowing for considerable parasitic neutron capture reactions (^{233}Pa captures a neutron to become ^{234}Pa, which decays by beta emission to ^{234}U, a non-fissile nuclide contaminating the fuel). Another important type of reaction is the (n,2n) reaction on ^{233}Pa and ^{233}U, which both result in ^{232}U. This uranium isotope yields strong gamma emitters in its decay chain (mainly ^{208}Tl), making the fuel harder to handle and reprocess, but also more proliferation resistant. Figure 1.1 gives a summary of the ^{233}U production routes and some associated reactions. Achieving net production of ^{233}U

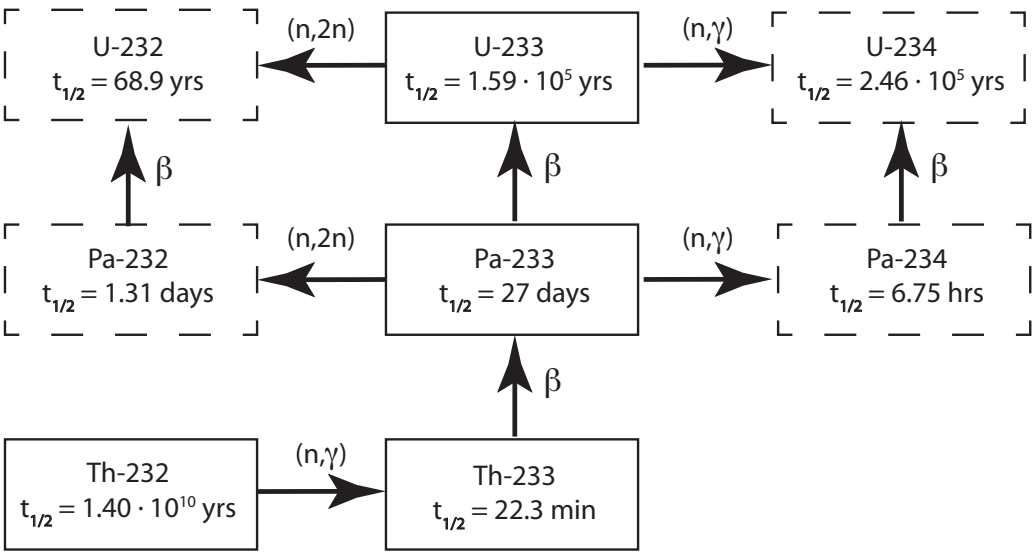

Figure 1.1: **Production paths of fissile ^{233}U, fuel contaminating ^{234}U and two possible paths of the strong gamma emitter ^{232}U,.**

is difficult, because on average only 2.5 neutrons per fission are produced of which 1 is needed to convert ^{232}Th into ^{233}U and 1 more to actually fission ^{233}U. This leaves on average only 0.5 neutrons for leakage and radiative capture reactions, mainly in ^{233}Pa, fission products and also in ^{233}U.

1.2 From the 1940s to current days

To use a liquid fuel containing thorium as fertile material in a nuclear reactor was pioneered at Oak Ridge National Laboratory (ORNL, Tennessee, United States) from the late 1940s to end of the 1960s; at first as part of America's 'Aircraft Nuclear Propulsion program' and in a later stadium for civilian purposes as well. The first experiments to establish the feasibility of molten salts as fuel for nuclear reactors, indicated salts based on fluorides are most suitable[29]:

> The fluorides appeared particularly appropriate because they have high solubility for uranium, are among the most stable of chemical compounds, have very low vapor pressure even at red heat, have reasonably good heat transfer properties, are not damaged by radiation, do not react violently with air or water, and are inert to some common structural metals.

These salts subsequently became the focal point of research into liquid fuels. The first step was to study nuclear stability of the circulating fuel system by constructing the 'Aircraft Reactor Experiment' (ARE), a small nuclear reactor of 2.5 MW_{th} to power (military) aircraft. In 1954, ARE became critical and operated in a stable and self-regulating manner for nine days without

Figure 1.2: **The ARE building at Oak Ridge National Laboratory was first used for the Aircraft Reactor Experiment and later for the Molten Salt Reactor Experiment.**

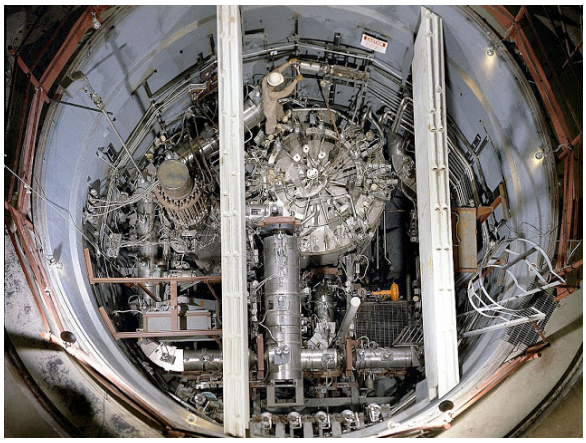

Figure 1.3: **Construction of ORNL's Molten Salt Reactor Experiment.**

mechanical or chemical problems. In 1956 research into civilian power applications began. At the time, graphite moderated thermal reactors seemed most promising, mainly because breeding ratios of resonance spectrum reactors were expected to be lower. The efforts culminated in the design and construction of the 'Molten Salt Reactor Experiment' (MSRE), a 8 MW_{th} graphite moderated reactor at ORNL, reaching criticality in 1965. Although the MSRE resembled in its engineering features a converter reactor, it did not use thorium (the fuel mixture was comprised of uranium, lithium, beryllium and zirconium fluorides). The MSRE-program ended in 1969 and proved viability of reactors based on molten salt [29].

The end of the MSRE-program marked the end of ORNL's research program concerning Molten Salt Reactors and not much has been done since. At the time, a rapid expansion of nuclear energy, combined with thought-to-be limited uranium reserves, made a high breeding ratio top priority. The MSR lost competition to the Liquid Metal Fast Breeder Reactor (LMFBR) which, operating on a ^{238}U - ^{239}Pu mixture has a higher breeding ratio, due to more neutron production per fission and less loss of neutrons due to parasitic capture [25].

However, uranium reserves are more plentiful than was anticipated and electricity demand did not increase as much. These days, breeding is still a desirable characteristic, but is not as indispensable as in the 1960s and as such, Molten Salt Reactors have regained interest and are now topic of investigation world wide. The Chinese have initiated a 350 million dollar program at the Shanghai Institute of Nuclear and Applied Physics to build a 2 MW_{th} demonstration plant, based on the MSRE, by 2020 and then scale it up to commercial size [11]. EU's 1.86 million Euro 'Evaluation and Viability of Liquid Fuel Fast Reactor Systems' (EVOL) - project, of which this work is a part, aims to demonstrate the Molten Salt Fast Reactor, a modern variant of the MSRE without graphite moderator and using an epithermal neutron spectrum, meets the generation-IV requirements of sustainability, non-proliferation, use of resources, safety and waste management [27].

1.3 Advantages and disadvantages of the Molten Salt Fast Reactor

As discussed, requirements for generation-IV nuclear energy systems range from sustainability to non-proliferation and from economics to safety. Advantages unique to the Molten Salt (Fast) Reactor (MSFR) indicate the concept is a good candidate indeed. For instance, its epithermal neutron spectrum let the reactor accept any mixture of higher actinides as fuel, enabling the MSFR to 'burn' existing waste stocks and due to adoption of the thorium fuel cycle, the reactor also generates very little of them. From the safety point of view, its

1. large negative temperature feedback of around -7 pcm/K at startup and -5 pcm/K at equilibrium (see chapter 4 on 'Results') ensures stability and quick dampening of power excursions;

2. online fuel reprocessing capabilities decrease the amount of decay heat present after shut down;

3. online refueling requires the reactor to run on little excess reactivity, decreasing the possibility of a recriticality accident after shut down;

4. molten salt lets the reactor operate at atmospheric pressure, compared to 155 bar for modern Pressurized Water Reactors;

5. freeze plug in the bottom of the reactor core, composed of solidified fuel salt, will liquefy when its cooling fails (for instance due to a power outage), and the fuel salt is then passively drained by gravity in specially designed drainage tanks, which are very unfavorable to nuclear chain reactions and are easy to cool;

Unfortunately, there are also some disadvantages unique to Molten Salt Reactors. These include:

1. fission of ^{233}U creates less delayed neutrons, imperative to reactor control, than fission of ^{235}U (but more than ^{239}Pu);

2. the number of available delayed neutrons is further diminished by fuel flow, which causes precursors to decay outside the core where they are of no use to reactor control;

3. online reprocessing forms an extra route for creating a nuclear explosive device as protactinium can be separated from the fuel to decay outside the core to ^{233}U. However, in order to successfully built and operate the MSFR, the uranium fuel cycle needs to be understood and implemented first, as the MSFR can only be started by using fissile material from that cycle. If a country has intentions of developing a nuclear weapon, the logical course of action would be to utilize the uranium fuel cycle and not this new route.

1.4 EVOL's MSFR Reference Configuration

All EVOL-partners[a] use the same Reference Configuration of the MSFR, from hereon referred to as the 'Reference Configuration', describing an initial fuel composition (with associated characteristics), a reprocessing scheme and a simplified, axially symmetric geometry making an adequate comparison of all partners' results possible. It can be found in Appendix A. This section is a description of the reactor itself as outlined in that Reference Configuration.

1.4.1 Reactor design

Figures 1.4 and 1.5 display the 3D and 2D reactor geometries. The 3D geometry incorporates 16 pipes of about 30 cm in diameter through which the salt flows in and out of the core. The research object of this thesis is the 2D simplified (axially symmetric) version that differs mainly from the 3D geometry in modeling of the pipes, which are not individually accounted for and in the absence of drainage tanks (visible in purple). The 2D version consists of four different materials, fuel (yellow), fertile blanket (red), neutron absorber (blue) and structural material (green and white). The fuel salt volume is 18 m^3 and is distributed equally between the core and the external circuit (or out-of-core-region), i.e. pipes, heat exchangers, pumps and other systems.

Fission takes place mainly in the core-region surrounded by a reflector of structural material and by the fertile blanket, which increases the MSFR's global breeding performance. The neutron absorber protects heat exchangers and pumps against neutrons emanating from the core and the fertile blanket. Due to precursor decay in the out-of-core region, a non-zero neutron flux remains, however.

1.4.2 Material compositions

The Reference Configuration discerns two initial compositions. Both are made up of a LiF-ThF_4-$(HN)F_4$ mixture, but the Heavy Nuclides (HN) composition differs and consists either of transuranic elements (TRU) coming from 60 GWd/ton waste from a PWR with plutonium as the main element or of ^{233}U. In this work only the latter composition of LiF-ThF_4-UF_4 in a 77.5-19.985-2.515 mol% mixture is used. In the model the uranium concentration is adjusted slightly such that the reactor is exactly critical at startup. The salt in the fertile blanket is a LiF-ThF_4 mixture in a 77.5-22.5 mol% ratio and lithium is enriched to 99.999 mol% ^7Li in both salts. The process of enriching lithium from 92.5% (natural) to 99.999% ^7Li is based on hazardous mercury and is at this moment only done by China and Russia, as the United States have shut down their enrichment program at Oak Ridge National Laboratory. In a nuclear reactor, ^6Li captures a neutron and forms tritium, to be avoided in the MSFR, but

[a]Centre National de la Recherche Scientifique, France; Karlsruher Institut für Technologie, Germany; Helmholtz-Zentrum Dresden-Rossendorf, Germany; Politecnico di Torino, Italy; INOPRO, France; BME Institute of Nuclear Techniques, Hungary; Delft University of Technology, Netherlands

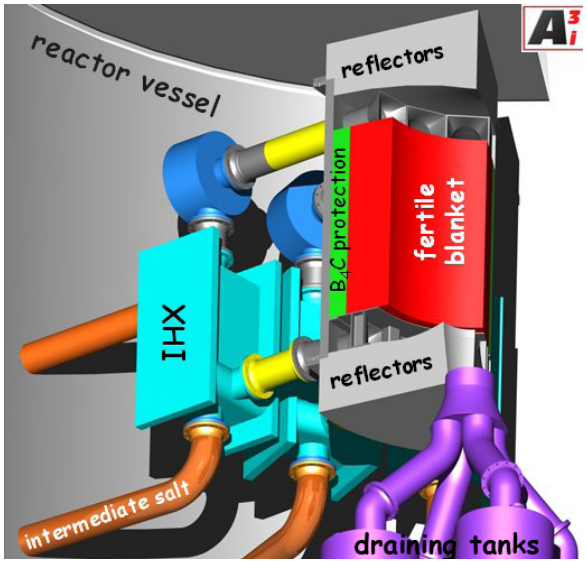

Figure 1.4: **The 3D geometry, not to scale, with the core, fertile blanket, neutron absorber, reflectors, drainage tanks and external circuit formed by pipes, heat exchangers (IHX) and pumps.**

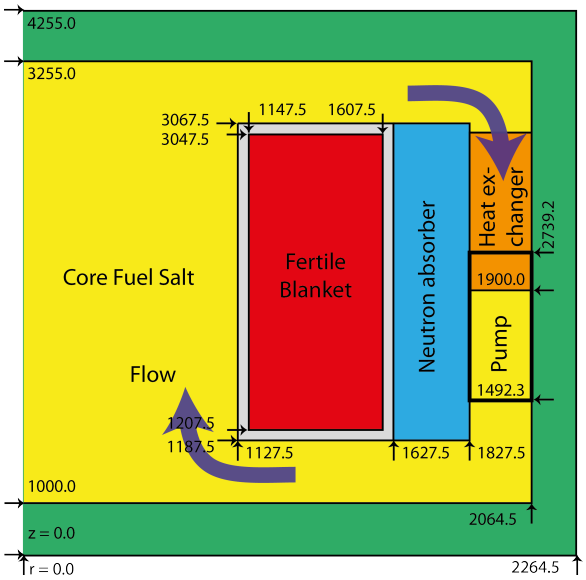

Figure 1.5: **The 2D model geometry of the MSFR depicts the core- and out-of-core-region, the fertile blanket, structural materials, the pump and the heat exchanger. The picture is not to scale.**

Table 1.1: **Atomic composition (mol%) of structural material.**

Ni	W	Cr	Mo	Fe	Ti	C
79.432	9.976	8.014	0.736	0.632	0.295	0.294

Mn	Si	Al	B	P	S
0.257	0.252	0.052	0.033	0.023	0.004

also one of the components of thermonuclear warheads. Enriching lithium will thus be strictly regulated [14].

The structural material is a nickel-based alloy designed to be able to withstand high temperatures as well as high neutron fluxes and its composition is displayed in table 1.1. During the project the structural material density is 10 g cm^{-3} and all of its properties are assumed to be temperature independent.

The neutron absorber is boron carbide B_4C, made of natural boron (19.8 mol% ^{10}B and 80.2 mol% ^{11}B) and has a density of 2.52016 g cm^{-3} (independent of temperature).

Table 1.2: **Physicochemical properties of the fuel and fertile salt.**

Property	Formula	Value at 700 °C	Validity Range °C
ρ [g cm^{-3}]	$4.094 - 8.82 \cdot 10^{-4}(T_{(\mathrm{K})} - 1008)$	4.1249	[620 - 850]
μ [Pa · s]	$\rho_{(\mathrm{g\ cm^{-3}})} \cdot 5.54 \cdot 10^{-5} \exp(3689/T_{(\mathrm{K})})$	$1.01 \cdot 10^{-2}$	[625 - 846]
λ [W m^{-1} K^{-1}]	$0.928 + 8.397 \cdot 10^{-5} \cdot T_{(\mathrm{K})}$	1.0097	[618 - 747]
C_p [J kg^{-1} K^{-1}]	$(-1.111 + 0.00278 \cdot T_{(\mathrm{K})}) \cdot 10^3$	1594	[594 - 634]

1.4.3 Physicochemical properties

During reactor operation, the salt is contaminated only a little with fission products (up to some mol%) and according to the Reference Configuration, this does not impact the salt's physicochemical properties needed for our studies. Therefore, for both the fuel and the fertile salt, the same characteristics apply, as measured at 78 mol% LiF - 22 mol% ThF_4. These properties are summarized in table 1.2.

Chapter 2

Modeling the Molten Salt Fast Reactor

2.1 Neutronics

DALTON-MSR, simply called DALTON from this point onwards, is the in-house developed code designed to calculate the neutron flux in the MSFR by solving the time-(in)dependent multigroup diffusion equation. Derivation of this equation is thoroughly discussed in other works, such as in Duderstadt & Hamilton[9]. The final result without external sources for G neutron groups for the time dependent case is given in equation 2.1.

$$\frac{1}{v_g}\frac{\partial \phi_g}{\partial t} - \nabla \cdot D_g \nabla \phi_g + \Sigma_g^r \phi_g - \sum_{g' \neq g}^{G} \Sigma_{g' \to g}^s \phi_{g'} = \chi_g \sum_{g'=1}^{G} (1-\beta)\nu_{g'} \Sigma_{g'}^f \phi_{g'} + \sum_{i=1}^{I} \lambda_i \chi_{d,g,i} C_i \quad (2.1)$$

The first term describes the neutron flux rate of change in group g and every other term describes a contribution to this rate of change: neutron streaming, neutrons leaving group g by absorption and scattering, neutrons scattering from other groups to group g, prompt neutron production from fission and delayed neutron production from precursor decay, respectively. Contrary to conventional nuclear reactors, MSFR's fuel is liquid and precursors thus flow. According to Wilcox[38], convection diffusion equations form an adequate tool for modeling turbulent flow of scalar quantities, such as precursors. Equation 2.2 is the convection diffusion equation characterizing precursor time evolution and table 2.1 includes a summary of all used quantities.

$$\frac{\partial C_i}{\partial t} + \nabla \cdot (C_i \mathbf{u}) - \nabla \cdot D_{eff} \nabla C_i = \beta_i \sum_{g=1}^{G} \nu \Sigma_g^f \phi_g - \lambda_i C_i \quad (2.2)$$

However, for depletion analysis, it is not practical, nor necessary to actually calculate time dependent behavior in such a detailed fashion. An alternative is to consider the steady-state

Table 2.1: **Overview of quantities used in the time-dependent and steady state multigroup diffusion equation as well as in the time-dependent and steady-state equations describing precursor transport.**

Quantity	Explanation
v_g	neutron speed in group g [cm s^{-1}]
ϕ_g	neutron flux in group g [cm^{-2} s^{-1}]
D_g	effective neutron diffusion constant of group g ($= 1/3\Sigma_g^{tr}$) [cm]
Σ_g^r	macroscopic removal constant of group g [cm^{-1}]
$\Sigma_{g'\to g}^s$	macroscopic scattering cross section from group g' to group g [cm^{-1}]
χ_g	fraction of prompt neutrons produced in group g due to fission
β	total fraction of delayed neutrons
ν_g	average number of neutrons produced due to fission induced by a neutron from group g
Σ_g^f	macroscopic fission cross section of group g [cm^{-1}]
λ_i	decay constant of precursors in precursor group i [s^{-1}]
$\chi_{d,g,i}$	fraction of delayed neutrons produced in group g due to precursor decay in precursor group i
C_i	number of precursors in precursor group i [cm^{-3}]
$\mathbf{u}$	velocity vector [cm s^{-1}]
D_{eff}	effective (turbulent) diffusion constant [cm^2 s^{-1}]
β_i	fraction of delayed neutrons in group i

diffusion equation, as given in equation 2.3.

$$-\nabla \cdot D_g \nabla \phi_g + \Sigma_g^r \phi_g - \sum_{g' \neq g}^{G} \Sigma_{g' \to g}^s \phi_{g'} = \frac{1}{k} \chi_g \sum_{g'=1}^{G} (1-\beta) \nu_{g'} \Sigma_{g'}^f \phi_{g'} + \sum_{i=1}^{I} \lambda_i \chi_{d,g,i} C_i \tag{2.3}$$

where k is the multiplication factor. The eigenvalue k adjusts the magnitude of the fission source, such that this equation always has a solution. $k = 1$ corresponds to a situation in which loss and production of neutrons in all groups g are balanced such that the flux corresponds to the true solution for longer times, while $k < 1$ or $k > 1$ indicate neutron production is either lower or higher than neutron loss.

The steady-state precursor convection diffusion equation is part of the same problem and is an eigenvalue problem with the same $1/k$ scaling of the fission source term (see equation 2.4).

$$\nabla \cdot (C_i \mathbf{u}) - \nabla \cdot D_{eff} \nabla C_i = \frac{1}{k} \beta_i \sum_{g=1}^{G} \nu \Sigma_g^f \phi_g - \lambda_i C_i \tag{2.4}$$

Again, terms describe convection of precursors, (turbulent) diffusion of precursors, a source of precursors due to fission and a sink due to decay, respectively. Each quantity in equations 2.1 through 2.4 is explained in table 2.1.

Duderstadt and Hamilton[9] also discuss three important assumptions forming the basis for (multigroup) diffusion theory: the angular neutron flux depends only weakly on angle, i.e. the

angular flux is only linearly anisotropic, neutron sources are isotropic and the rate of time variation of the neutron current density is much slower than the collision frequency. Therefore, the diffusion approximation breaks down near boundaries, where material properties change dramatically, near localized sources and in strongly absorbing media.

In the Reference Configuration there are no sources and the only strongly absorbing medium is located behind the fertile blanket to protect heat exchangers against neutrons emanating from the core. Because of the presence of this blanket only a very small fraction of neutrons reaches the absorber, which has therefore very little influence on the flux in the core. Material properties do differ in the fertile blanket and in the core, where the presence of fissile uranium causes a relatively high absorption cross section. However, Erik van der Linden [36] shows the difference between transport and diffusion theory is very small in the current design. The multigroup diffusion equation is thus a good description of MSFR neutronics.

2.2 Flow and Turbulence

Correctly modeling fuel flow will increase validity of the temperature distribution in the core, which influences cross sections and also allows for correctly solving precursor densities across the core. Erik van der Linden [36] describes modeling of MSFR's turbulent flow (in the core, Reynolds number is about $Re = \rho v D/\mu \approx 2.5 \cdot 10^6$) in detail and because this part of the MSFR model has almost not changed since then, only a short summary is given here.

The most accurate, but computationally infeasible method would be to solve the Navier-Stokes equations in full, using Direct Numerical Simulation (DNS). Erik van der Linden chose to use Reynolds Averaged Navier-Stokes (RANS) equations with Boussinesq's closure hypothesis and the standard $k-\epsilon$ model instead, due to expected implementation time and computational power needs.

The RANS methodology describes the flow in a macroscopic or statistical manner by splitting every quantity in a mean and a fluctuating part and then averaging over a time ensemble. For instance, $\mathbf{u} = \bar{\mathbf{u}} + \mathbf{u}'$ where $\mathbf{u}$, $\bar{\mathbf{u}}$ and $\mathbf{u}'$ are the actual, mean and fluctuating velocity, respectively. Boussinesq's closure hypothesis assumes Reynolds stresses $-\rho_F \overline{\mathbf{u_i}' \cdot \mathbf{u_j}'}$ are proportional to the mean rate of deformation. For an incompressible flow, the RANS equations with Boussinesq's closure hypothesis are stated in equation 2.5, as discussed in Versteeg and Malalasekera [37], and table 2.2 gives an explanation of each quantity and term.

$$\rho_F \frac{\partial \bar{\mathbf{u}}}{\partial t} + \rho_F (\bar{\mathbf{u}} \cdot \nabla)\bar{\mathbf{u}} = -\nabla \cdot \left(\bar{p}\mathbf{I} + \frac{2}{3}\rho_F k \mathbf{I} \right) + \nabla \cdot \left[(\mu + \mu_t) \left(\nabla \bar{\mathbf{u}} + (\nabla \bar{\mathbf{u}})^T \right) \right] + \mathbf{f}_b \tag{2.5}$$

Temperature induced density differences cause a variable gravitational pull on the fluid throughout the reactor (buoyancy effects), resulting in a spatially dependent body force term in equation 2.5, modeled using a first order Taylor expansion of the density.

Table 2.2: **Overview of quantities used in the RANS equations and the k-ϵ model.**

Quantity	Explanation	Unit
ρ_F	fluid density	[kg m^{-3}]
$\bar{\mathbf{u}}$	Reynolds average velocity	[m s^{-1}]
$\bar{p}$	Reynolds averaged pressure	[Pa]
k	turbulent kinetic energy per unit mass	[J kg^{-1}]
μ	dynamic viscosity of the fluid	[Pa $\cdot$ s]
μ_t	eddy viscosity or turbulent viscosity	[Pa $\cdot$ s]
$\mathbf{f}_b$	body force, i.e. gravity	[N m^{-3}]
$\rho_F \frac{\partial \bar{\mathbf{u}}}{\partial t}$	momentum rate of change	[kg m^{-2} s^{-2}]
$\rho_F(\bar{\mathbf{u}} \cdot \nabla)\bar{\mathbf{u}}$	convection of momentum	[kg m^{-2} s^{-2}]
$-\nabla \cdot \left(\bar{p}\mathbf{I} + \frac{2}{3}\rho_F k \mathbf{I}\right)$	pressure (isotropic stresses)	[kg m^{-2} s^{-2}]
$\nabla \cdot \left[(\mu + \mu_t)\left(\nabla\bar{\mathbf{u}} + (\nabla\bar{\mathbf{u}})^T\right)\right]$	diffusion and turbulent mixing	[kg m^{-2} s^{-2}]
ϵ	dissipation of turbulent kinetic energy	[J kg^{-1} s^{-1}]
σ_k	turbulent Prandtl number	-
σ_ϵ	turbulent Prandtl number	-
C_i	model constants	-
P_k, P_b	rate of production	[J m^{-3} s^{-1}]

Two yet undefined quantities, eddy viscosity and turbulent kinetic energy per unit mass, have entered equation 2.5 as a result of Boussinesq's closure hypothesis and require an extra model. The standard $k-\epsilon$ model is most widely used and validated, according to Versteeg and Malalasekera[37]. In this model, eddy viscosity is expressed in the large-eddy velocity scale $\mathcal{V}$ and large-eddy length scale $\mathcal{L}$, which are in there turn expressed in k, turbulent kinetic energy per unit mass, and ϵ, dissipation of turbulent kinetic energy, as shown in equation 2.6.

$$\mathcal{V} \equiv k^{1/2} \qquad \mathcal{L} \equiv \frac{k^{3/2}}{\epsilon} \qquad \mu_t = C_\mu \rho_F \mathcal{V}\mathcal{L} = C_\mu \rho_F \frac{k^2}{\epsilon} \tag{2.6}$$

The $k-\epsilon$ model also describes transport of k and ϵ as shown in equation 2.7. Used quantities are tabulated in table 2.2.

$$\rho_F \frac{\partial k}{\partial t} + \rho_F \nabla \cdot (k\bar{\mathbf{u}}) = \nabla \cdot \left[\left(\mu + \frac{\mu}{\sigma_k}\right)\nabla k\right] + P_k + P_b - \rho_F \epsilon \tag{2.7}$$

$$\rho_F \frac{\partial \epsilon}{\partial t} + \rho_F \nabla \cdot (\epsilon\bar{\mathbf{u}}) = \nabla \cdot \left[\left(\mu + \frac{\mu_t}{\sigma_\epsilon}\right)\nabla \epsilon\right] + C_{\epsilon 1}\frac{\epsilon}{k}[P_k + C_{\epsilon 3}\max(P_b, 0)] - C_{\epsilon 2}\rho_F \frac{\epsilon^2}{k} \tag{2.8}$$

The scalar quantity 'thermal energy', very closely linked to the temperature, is calculated using the convection diffusion equation 2.9 with the flow field resulting from equation 2.5. The terms describe rate of change, convection, turbulent diffusion and a source term, respectively.

Table 2.3: **Overview of quantities used in the convection diffusion equation for temperature**

Quantity	Explanation	Unit
ρ_F	fluid density	[kg m^{-3}]
c_P	specific heat capacity	[J kg^{-1} K^{-1}]
T	temperature	[K]
$\bar{\mathbf{u}}$	Reynolds average velocity	[m s^{-1}]
λ_T	thermal conductivity	[J K^{-1} m^{-1} s^{-1}]
μ_t	eddy viscosity or turbulent viscosity	[Pa · s]
Pr_t	turbulent Prandtl number (= 0.85)	[-]
$\rho_F c_P \frac{\partial T}{\partial t}$	thermal energy rate of change	[J m^{-3} s^{-1}]
$\rho_F c_P \nabla \cdot (T\bar{\mathbf{u}})$	convection of thermal energy	[J m^{-3} s^{-1}]
$\nabla \cdot \left[\left(\lambda_T + c_P \frac{\mu_t}{Pr_t}\right) \nabla T\right]$	thermal energy transport by turbulent diffusion	[J m^{-3} s^{-1}]
P	production of thermal energy	[J m^{-3} s^{-1}]

Table 2.3 presents an overview of relevant quantities.

$$\rho_F c_P \frac{\partial T}{\partial t} + \rho_F c_P \nabla \cdot (T\bar{\mathbf{u}}) = \nabla \cdot \left[\left(\lambda_T + c_P \frac{\mu_t}{Pr_t}\right) \nabla T\right] + P \tag{2.9}$$

The k-ϵ model is reported[37] to perform poorly in, among other cases, flows with strongly curved boundary layers or swirling flows, such as exist in the MSFR core, and in fully developed flows in non-circular ducts, like the entrance of the core. However, this probably does not influence results much due to the fact that the precise temperature distribution is less important to burnup.

2.3 Burnup

In a traditional LWR, the fuel is stationary and burnup is a space dependent problem. In the MSFR however, by considering the flowing fuel homogeneously mixed for all times, the problem simplifies to burnup in a single point, at the cost of finding representative cross sections and a flux for the entire fuel region. Homogeneously mixed means the density of a nuclide (mol cm^{-3}) relative to the density of another nuclide does not depend on space. This important assumption is more closely looked at in subsection 3.6.3 on page 44, but is warranted due to the highly turbulent flow (Reynolds number is approximately 10^6), short fuel cycle time of 4 seconds and relative slow change of the nuclide density in time). This section discusses the adopted 'volume-lumped parameter model' and its derivation, starting with modifying the Bateman equations, which describe burnup in stationary fuel, by considering time dependence of nuclide densities

Table 2.4: **Description of each physical quantity in the burnup model.**

$N_i(\mathbf{r},t)$	Concentration of nuclide i at position $\mathbf{r}$	[mol cm^{-3}]
$N_i^0(t)$	Average concentration of nuclide i in the core	[mol cm^{-3}]
$\sigma_{j\to i}(\mathbf{r},E,t)$	Microscopic transmutation cross section of nuclide j to nuclide i	[barn^{-1}]
$\phi(\mathbf{r},E,t)$	Scalar neutron flux at position $\mathbf{r}$, energy E and time t	[barn^{-1} s^{-1} eV^{-1}]
λ_i	Decay constant of nuclide i	[s^{-1}]
$b_{j\to i}$	Branching ratio of nuclide j to nuclide i	
$\mathbf{u}_i(\mathbf{r},t)$	Nuclide velocity vector at position $\mathbf{r}$ and time t	[cm s^{-1}]
$\rho(\mathbf{r})$	Fuel salt density at position $\mathbf{r}$	[g cm^{-3}]

and then volume averaging over the entire fuel region. During the last step, final definitions for cross sections and fluxes are developed. Equation 2.10 describes nuclide i's local concentration rate of change. Different physical quantities and their meaning are given in table 2.4.

$$\begin{aligned}\frac{\partial N_i(\mathbf{r},t)}{\partial t} + \nabla\cdot(\mathbf{u}_i(\mathbf{r},t)N_i(\mathbf{r},t)) &= \sum_{j\neq i}\int_E dE\sigma_{j\to i}(\mathbf{r},E,t)\phi(\mathbf{r},E,t)N_j(\mathbf{r},t)\\ &- \sum_{i\neq j}\int_E dE\sigma_{i\to j}(\mathbf{r},E,t)\phi(\mathbf{r},E,t)N_i(\mathbf{r},t)\\ &+ \sum_{j\neq i} b_{j\to i}\lambda_j\cdot N_j(\mathbf{r},t) - \lambda_i N_i(\mathbf{r},t)\end{aligned} \tag{2.10}$$

If the fuel is perfectly mixed, solving for the full space dependent nuclide concentrations is not necessary. Instead, a volume averaged concentration of nuclide i is introduced, $N_i^0(t) = \frac{1}{V}\int_V dV N_i(\mathbf{r},t)$, which can still not be solved, due to the fact that $N_i(\mathbf{r},t)$ is unknown. However, one can multiply and divide $N_i(\mathbf{r},t)$ by $N_i^0(t)$, assume that the ratio $\frac{N_i(\mathbf{r},t)}{N_i^0(t)}$ only depends on the local fuel salt density, i.e. homogeneously mixed and related to a known temperature distribution. Equation 2.11 summarizes these statements.

$$\begin{aligned}N_i^0(t) &= \frac{1}{V}\int_V dV N_i(\mathbf{r},t)\\ \rho_0 &= \frac{1}{V}\int_V dV\rho(\mathbf{r})\\ N_i(\mathbf{r},t) &= \frac{N_i(\mathbf{r},t)}{\int_V dV N_i(\mathbf{r},t)}\int_V dV N_i(\mathbf{r},t) = \frac{N_i(\mathbf{r},t)}{N_i^0(t)}N_i^0(t) \approx \frac{\rho(\mathbf{r})}{\rho_0}N_i^0(t)\end{aligned} \tag{2.11}$$

Using these definitions and volume averaging equation 2.10 yields equation 2.12.

$$\begin{aligned}\frac{\int_V dV \frac{\rho(\mathbf{r})}{\rho_0}}{V}\frac{\partial N_i^0(t)}{\partial t} + \frac{1}{V}\int_V dV \nabla \cdot \left(\mathbf{u}_i(\mathbf{r},t)\frac{\rho(\mathbf{r})}{\rho_0}N_i^0(t)\right) = \\ \sum_{j\neq i}\frac{1}{V}\int_V dV \int_E dE \frac{\rho(\mathbf{r})}{\rho_0}\sigma_{j\to i}(\mathbf{r},E,t)\phi(\mathbf{r},E,t)N_i^0(t) - \\ \sum_{i\neq j}\frac{1}{V}\int_V dV \int_E dE \frac{\rho(\mathbf{r})}{\rho_0}\sigma_{i\to j}(\mathbf{r},E,t)\phi(\mathbf{r},E,t)N_i^0(t) + \\ \sum_{j\neq i}\frac{1}{V}\int_V dV \frac{\rho(\mathbf{r})}{\rho_0}b_{j\to i}\lambda_j N_j^0(t) - \frac{1}{V}\int_V dV \frac{\rho(\mathbf{r})}{\rho_0}\lambda_i N_i^0(t)\end{aligned} \tag{2.12}$$

The last step consists of rearranging terms, as well as multiplying and dividing by $\int_V \int_E \phi(\mathbf{r},E,t)dEdV$ which leads to the final form of the volume lumped parameter model of burnup adopted for this project (see equation 2.13).

$$\begin{aligned}\frac{\partial N_i^0(t)}{\partial t} = &\sum_{j\neq i}\overline{\sigma_{j\to i}(t)}\cdot\overline{\phi(t)}\cdot N_j^0(t) - \sum_{i\neq j}\overline{\sigma_{i\to j}(t)}\cdot\overline{\phi(t)}\cdot N_i^0(t) \\ &+ \sum_{j\neq i} b_{j\to i}\lambda_j \cdot N_j(\mathbf{r},t) - \lambda_i \cdot N_i^0(t) + F_i(t)N_i^0(t) - R_i(t)N_i^0(t)\end{aligned} \tag{2.13}$$

where,

$$\begin{aligned}\overline{\phi(t)} &= \frac{\int_V dV \int_E dE \phi(\mathbf{r},E,t)}{V} \\ \overline{\sigma_{j\to i}(t)} &= \frac{V\cdot\int_V dV\int_E dE\rho(\mathbf{r})\phi(\mathbf{r},E,t)\sigma_{j\to i}(\mathbf{r},E,t)}{\int_V dV\rho(\mathbf{r})\int_V dV\int_E dE\phi(\mathbf{r},E,t)} \\ \lambda_i^{eff} &= \lambda_i \\ F_i(t) - R_i(t) &= -\frac{\int_S d\mathbf{S}\rho(\mathbf{r})\mathbf{u}_i(\mathbf{r},t)}{\int_V dV\rho(\mathbf{r})}\end{aligned} \tag{2.14}$$

$F_i(t)$ and $R_i(t)$ represent feeding and reprocessing and comes in the equation by means of the second term of equation 2.12, because this term represents net flow across the reactor boundary (see equation 2.15). Only at the boundary, the nuclide velocity $\mathbf{u}_i(\mathbf{r},t)$ is not equal to the fuel salt's velocity, due to the fact that the boundary is permeable for reprocessed nuclides as well as for fed nuclides, but not for other nuclides (then $\mathbf{u}_i(\mathbf{r},t) = 0$ at the boundary). The

'velocity' with which nuclides flow through the boundary is a free parameter and the feeding and reprocessing rates can thus be chosen at will.

$$\begin{aligned}\frac{V\rho_0}{\int_V dV\rho(\mathbf{r})}\frac{1}{V}\int_V dV\nabla\cdot\left(\mathbf{u}_o(\mathbf{r},t)\frac{\rho(\mathbf{r})}{\rho_0}N_i^0(t)\right) &= \frac{1}{\int_V dV\rho(\mathbf{r})}\int_S d\mathbf{S}\rho(\mathbf{r})\mathbf{u}_i(\mathbf{r},t)N_i^0(t) \\ &= (R_i(t)-F_i(t))N_i^0(t)\end{aligned} \tag{2.15}$$

2.4 Radiotoxicity

Waste from nuclear reactors emits ionizing radiation that is detrimental to human health because it can break molecular bonds of biological molecules and damage DNA, possibly leading to cancer. A brief overview of radiotoxicity and relevant vocabulary is given here and a full description can be found in other works, such as[3]. In this project, only stochastic effects due to relatively low doses are considered and not immediate deterministic effects such as radiation sickness resulting from a large dose. Several pathways exist through which radiation can enter the body. The source can be external, only leading to exposure as long as it is nearby. Two other ways are via inhalation and ingestion, and only the latter is considered here. Then, contrary to external exposure, the source is inside the body and radiation will continue to damage tissue until the source has completely decayed or is secreted.

The 'radiation dose' is the total amount of energy per kg absorbed from ionizing radiation by biological tissue. Radiation is traditionally subdivided into α, β and γ radiation which are formed by respectively helium nuclei, electrons or positrons and photons. There are, however, more particles posing a health risk, for instance neutrons, protons and fission fragments. Depending on the mass, energy and charge, a dimensionless weighting factor is given to each type, ranging from 1 for photons and electrons up to 20 for α particles, as different types of radiation inflict different amounts of damage to biological tissue. Correcting absorbed amount of energy (dose, measured in Grays or J/kg) for the type of radiation results in the 'equivalent dose' (measured in Sieverts).

Another correction takes into account differences in biological tissue as not all types of tissues are equally vulnerable to radiation. Each organ is assigned a dimensionless weighting factor depending on the method of intake (ingestion or inhalation), residence time and location of the nuclide in the body, and chemical characteristics. Correcting the equivalent dose for biological factors results in the 'committed effective dose' and a 'dose coefficient' can be calculated, which is the total effective dose per Becquerel received by the body over 50 years time due to ingestion of a substance.

Actinides usually form the majority of the radiotoxicity of spent nuclear fuel, due to their high specific radiotoxicity (usually alpha emitters) and long decay chains. For actinides, these daughter elements are included in their specific radiotoxicity. For fission products however, only the isotope itself is considered and in order to properly evaluate the radiotoxicity of fission products, their decay chains have to be solved for. All data, i.e. dose coefficients, are according to ICRP 61[22].

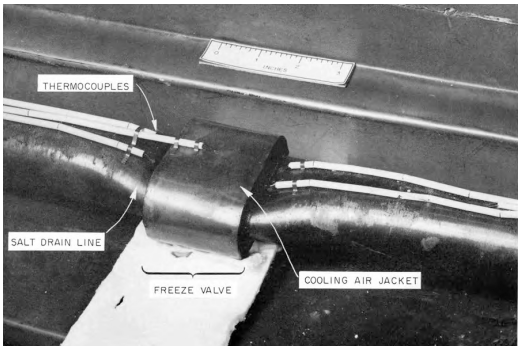

(a) **A freeze valve as used in the MSRE.**

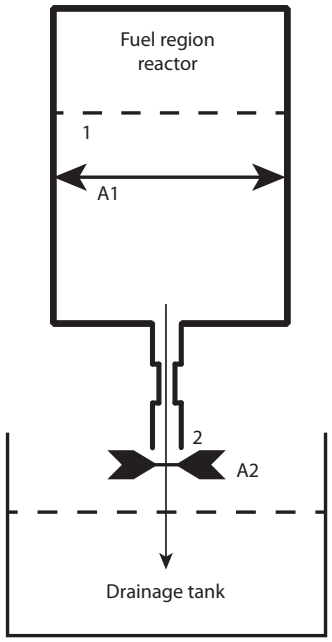

(b) **An overview of the reactor and drainage tank. Point 1 is the fuel level in the reactor and point 2 is the exit of the reactor, i.e. the end of a pipe.**

Figure 2.1:

2.5 Draining the core

Freeze valves were used in the MSRE to drain the fuel salt in case of an emergency into specially designed drainage tanks[28] and consisted of flattened parts of piping in which the fuel salt was cooled by a fan to below its melting point. It is a passive safety system, i.e. it does not require active systems to function, because in case of a power outage, the liquid fuel on top will melt the now uncooled solid fuel in the valve, which will eventually open. Depending on the amount of applied cooling, the time it took to thaw the freeze valves varied from just under 15 minutes to several hours. Figure 2.1(a) displays a freeze valve as was used in the MSRE[2].

In order to evaluate possible use of freeze valves in the MSFR, the time it takes to completely drain the core is an important parameter. With a stationary mechanical energy balance[35] the flow out of the reactor, driven by gravity, can be calculated, see equation 2.16,

$$0 = \phi_m \left[\frac{1}{2} v_1^2 - \frac{1}{2} v_2^2 + g(z_1 - z_2) + \int_2^1 \frac{1}{\rho(p)} dp \right] - \phi_m e_{fr} \tag{2.16}$$

in which v_i, z_i, $\rho(p)$ are the velocity, altitude and density at point i, ϕ_m is the mass flow (in kg/s) and e_{fr} is the amount of mechanical energy per kg which is lost due to friction. In this case, point '1' is the fuel salt level and point '2' is the exit, as can be seen in figure 2.1(b). The pressure is considered to be equal to the atmospheric pressure both above the fuel level in the reactor and at the exit, and since the pipe is small, $v_1 = 0$. The loss due to friction in a pipe is described by equation 2.17 [35].

$$e_{fr} = \left(4f\frac{L}{D} + K_{w,tot}\right)\frac{1}{2}v^2 \tag{2.17}$$

in which '4f' is the Fanning friction factor which can be determined with the aid of a Moody chart, L and D are the length and diameter of the pipe and $K_{w,tot}$ is the total friction coefficient due to objects such as entrances, exits, contractions and enlargements and is the sum of all individual friction coefficients. For the entrance, $K_w = 0.5$, for the sudden contraction (start freeze valve), $K_w = 0.45(1 - \frac{D2}{D1})$, for the sudden enlargement $K_w = (\frac{D2}{D1} - 1)^2$ (D2 and D1 are the diameters downstream and upstream of the tube part respectively) and the free jet exit has $K_w = 0$ for Reynolds number $> 10^5$ downstream of the tube part [23]. Combining equations 2.16 and 2.17 results in equation 2.18 linking the fuel level $h(t)$ and the geometry together to describe the exit velocity v_2:

$$v_2 = \sqrt{\frac{2gh}{1 + 4f\frac{L}{D} + K_{w,tot}}} \tag{2.18}$$

This then results in a differential equation describing the fuel level h as a function of time, see equation 2.19.

$$\begin{aligned} h(t) &= \frac{m(t)}{A_1\rho(t)} \\ v(t) &= \sqrt{\frac{2gh}{1 + 4f\frac{L}{D} + K_{w,tot}}} \\ \frac{\partial m}{\partial t} &= -A_2\rho(t)v(t) \end{aligned} \tag{2.19}$$

where $m(t)$ is the residual mass still in the reactor, A_1 and A_2 are the cross sections of the reactor and the pipe exit and ρ is the fuel density which depends on temperature and thus on time, in case of a transient. Results are shown in section 4.4 on page 62.

Chapter 3

Computational programs

The purpose of the developed computer model is to calculate the isotopic fuel composition as a function of time, measured in months or years, as well as various physical quantities relevant for nuclear reactor calculations, like k_{eff}, the neutron spectrum, β, cross sections etc. Since all quantities depend on time and influence each other, the system is highly coupled and therefore each module, responsible for calculating some quantities, is run for a certain period of simulated time, assuming results from other modules remain constant. LOWFAT is an in-house developed code for burnup calculations and uses results from the neutronics code DALTON, CFD code HEAT, and diverse cross section preparation modules. One run of LOWFAT, with a varying time step, is called a 'burnup' step. This chapter provides a detailed overview of computational implementation of the three sub models of chapter 2 (neutronics, CFD and burnup), and starts with cross section development. Erik van der Linden[36] describes in detail how to obtain a steady state flow and temperature distribution and these distributions are assumed to be known and available. It will not be repeated here.

3.1 Cross section preparation

Input to the models consists for a large part of cross section data. In the simulations DALTON needs macroscopic, temperature, and thus space dependent cross sections while LOWFAT needs microscopic cross sections. Preparation of these cross sections is divided in three parts:

1. Data preparation common for both DALTON and LOWFAT entails creating libraries for approximated geometries at homogeneous temperatures at 100K intervals;

2. Creation of a DALTON input library by the program 'Mixer.pl', which interpolates macroscopic cross sections between adjacent temperatures;

3. Creation of a LOWFAT input library by updating an existing burnup library with microscopic cross sections developed by the program 'Burnup_mixer.pl;

3.1.1 Common cross section preparation for DALTON and LOWFAT

Depending on the importance to neutronics and availability of data, nuclear data of 1486 isotopes is taken into account with varying accuracy. The ENDF/B-VII.0 library contains 417 nuclides frequently used for general purpose criticality calculations in a 238 energy group structure[10] and forms the basis for cross sections for DALTON and LOWFAT. Among these isotopes are also specific moderators and cladding materials not used in this project. Depending on the isotope, nuclear cross sections are on file at different temperatures (600 K, 900 K, 1200 K and 2400 K for most nuclides). In a few steps, this library is processed to obtain spatially dependent macroscopic and microscopic cross section libraries at temperature intervals of 100 K called 'lib_coll_T_K for the macroscopic libraries and 'lib_T_K' for the microscopic ones, where T is in the relevant domain (900 K up to 1300 K).

CSASI For all actinides in the ENDF/B library and for the main fission products, as determined by their macroscopic absorption cross section (46 isotopes turn out to be sufficient to keep their combined macroscopic absorption cross section well above 99% of the total macroscopic absorption cross section), the first step is to produce five libraries (in 238 groups) called CSAS_lib_900_K, CSAS_lib_1000_K, ..., CSAS_lib_1300_K, in which the number represents temperature, by calling SCALE 6's CSASI routine to perform resonance shielding. The nuclides are treated as if they were in an infinite homogeneous medium, which is the most suitable method for 'large masses of materials where the size of each material is large compared to the average mean-fee path', according to the manual[18]. This procedure is repeated every burnup step and creates output like the example in figure 3.1.

The identity of the mentioned 46 nuclides is stored in the file 'in_AMPX' and as they have been selected by LOWFAT on the basis of neutron absorption, plenty of nuclides are not accounted for. In order to take into account all other nuclides that are described in the ENDF/B library, a lumped artificial nuclide is produced in such a way to efficiently calculate their contribution to scattering, absorption and fission. This procedure is also described by Tabuchi and Aoyama[34] and is demonstrated in equation 3.1.

$$\sigma_i^{eff} = \frac{\sum_k N^k \sigma_i^k}{\sum_k N^k} \tag{3.1}$$

where the sums run over all nuclides to be lumped k. The created nuclide is assigned identification number 99999 and is added to the CSAS_lib_T_K libraries. Microscopic cross section data of these nuclides is obtained by one CSASI run with approximate concentrations for all nuclides after 20 years of operation. To save computation time, changes in resonance shielding over time are neglected for this class of nuclides. From figure 3.1 it can be seen this is only a small approximation.

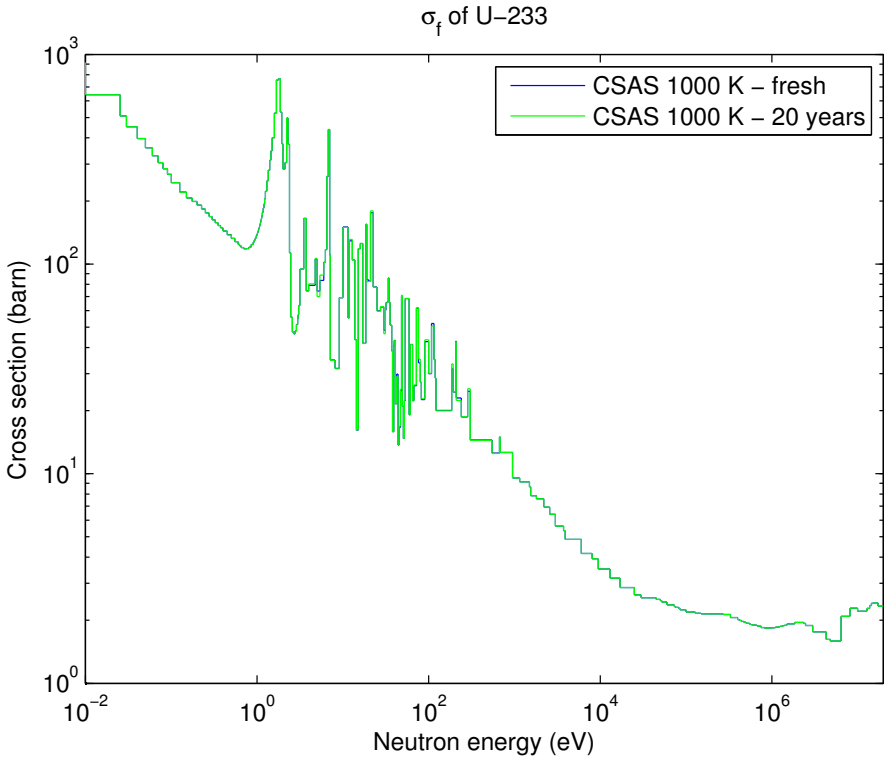

Figure 3.1: **238 group fission cross section of ^{233}U in fresh fuel and after 20 years of operation, as determined by the CSASI routine.**

Table 3.1: **Boundaries of the 11 energy groups.**

Boundary	Neutron energy (eV)	Boundary	Neutron energy (eV)
1	$2.000 \cdot 10^7$	7	$1.860 \cdot 10^2$
2	$1.400 \cdot 10^6$	8	$5.200 \cdot 10^1$
3	$1.010 \cdot 10^6$	9	$3.325 \cdot 10^1$
4	$5.730 \cdot 10^5$	10	$1.290 \cdot 10^1$
5	$7.300 \cdot 10^4$	11	$6.250 \cdot 10^{-1}$
6	$2.290 \cdot 10^3$	12	$1.000 \cdot 10^{-5}$

Exactly the same procedure, including resonance shielding by CSASI, is carried out for the same nuclides, but without lumping a part of them. The result is the library CSAS_lib_ENDF, which is only relevant for LOWFAT's input.

XSDRNPM To calculate the scalar neutron flux and k_{eff} with DALTON in 238 groups requires solving for 66 x 78 x 238 = $1.2 \cdot 10^6$ unknowns, which is computationally impractical (there are 66x78 spatial elements). Therefore, using an approximation to the geometry, the 238 group cross sections are collapsed into an 11 group structure displayed in table 3.1 using XSDRNPM, which is also part of the SCALE 6 system.

XSDRNPM is a 1D transport code and computes the neutron flux for a 1D slab or cylindrical geometry using a criticality calculation and then collapses fine cross sections into broader groups, conserving reaction rates in a designated spatial region[19]:

$$\bar{\sigma}_G \int_{space} d\mathbf{r} N_D(\mathbf{r}) \int_G dE \phi(E, \mathbf{r}) = \int_{space} d\mathbf{r} N_D(\mathbf{r}) \int_G dE \sigma(E, \mathbf{r}) \phi(E, \mathbf{r}) \tag{3.2}$$

in which $\bar{\sigma}_G$ is the collapsed cross section of broad group G, $N_D(\mathbf{r})$ is the atomic number density and $\phi(E, \mathbf{r})$ is the weighting spectrum. XSDRNPM allows for different types of spatial weighting and uses 'zone' weighting in this project to obtain a set of unique cross sections for every designated spatial zone. Converting to a discrete multi group notation and introducing σ_g^j as the fine group cross section with energy g and at position j and W_g^j as the weighting function (i.e. the neutron flux [cm^{-2} s^{-1}]), this yields the following expression:

$$\bar{\sigma}_G = \frac{\sum_j^{zone} \sum_{g \in G} \sigma_g^j W_g^j}{\sum_j^{zone} \sum_{g \in G} W_g^j} \tag{3.3}$$

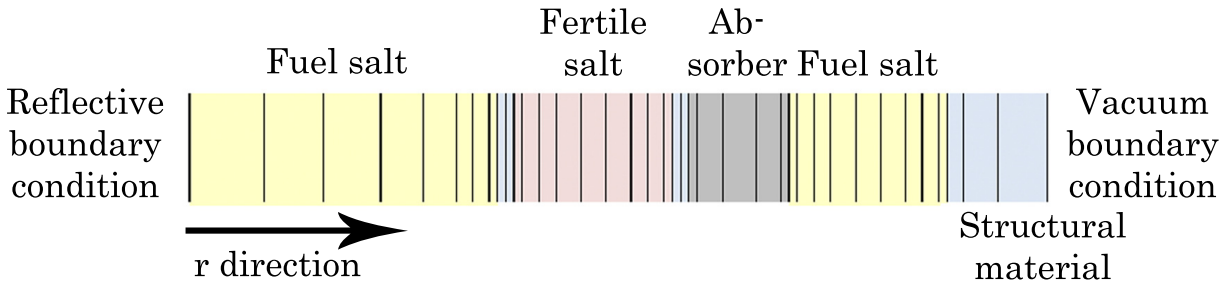

Figure 3.2: **A sketch of R1's geometry (courtesy to Erik van der Linden).**

Since XSDRNPM is a 1D transport code, the geometry is approximate. To represent the actual 2D system, the reactor is subdivided into 28 zones and both 1D radial and axial influences are taken into account. Cross sections are first collapsed to 54 groups using radial geometries, of which an example is depicted in figure 3.2 and in a second stage cross sections are collapsed with the axial geometries from 54 groups to the final 11 group structure. In this stage of cross section preparation, this is the main difference compared to the method adopted by Erik van der Linden[36]. In figure 3.3, the two radial calculations (R1 and R3), 'R' for 'radial' and index numbers 1 and 3, are indicated, as well as the five axial ones (A1, A2, A3, A5, A6). R2 is skipped to save computation time, just as A4 and because of the small amount of material involved, this approximation is justified. Note it is not possible to perform R4 and A7 due to absence of fissile material in those parts. Therefore, A1 is performed twice, the second time from 238 groups to 54 groups in order to create structural material cross section in 54 groups. These cross section are used in subsequent calculations whenever 54 group cross sections for structural materials are unavailable. A zone's id-number is the radial calculation number followed by the axial calculation number. For instance, zone 11 in the core is the combination of radial calculation 1 and axial calculation 1. Zone 21 does in principle not exist, but cross sections from zone 11 suffice. Cross sections for the right reflector are also unavailable and for that region, cross sections from zone 12 are taken. Obviously, these are a bit off, but due to the very low total neutron flux ($1.18 \cdot 10^{12}$ cm^{-2} s^{-1} in the right reflector, but $3.82 \cdot 10^{15}$ cm^{-2} s^{-1} in the core), this does not matter.

Another module within the SCALE 6 system, ICE[20], converts microscopic cross section libraries into macroscopic cross section ones:

$$\Sigma_G = \sum_{i}^{all\ nuclides} \sigma_G^i N_D^i \tag{3.4}$$

where Σ_G is the macroscopic cross section, and N_D^i the atomic number density [barn^{-1} cm^{-1}].

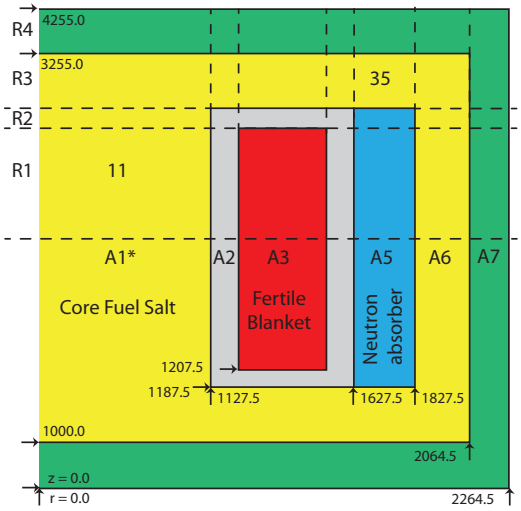

Figure 3.3: **The MSFR geometry is subdivided into 28 different zones. Each XSDRNPM calculation is designated with a letter standing for either 'Radial' or 'Axial' and an index number. Each zone id-number consists of first the radial index number followed by the axial index number. Some zones are not explicitly taken into account, for instance if the amount of material is very small. Then, other comparable cross sections are assigned to that region.**

3.1.2 Creation of a DALTON input library

A module called 'Mixer.pl' transforms five zone dependent macroscopic cross section libraries at 900 K, 1000 K, 1100 K, 1200 K and 1300 K into one library with spatially dependent cross sections at the appropriate temperature for each element. For every element in the DALTON mesh, Mixer.pl

1. reads the temperature of the element, which is saved in 'T.bin', a result of HEAT;

2. selects the two libraries closest to the actual temperature, i.e. for an element with a temperature of 1022 K, the libraries 'lib_coll_1000_K' and 'lib_coll_1100_K' are selected and uses macroscopic cross sections of the appropriate zone;

3. interpolates the cross sections using square root interpolation, because cross sections in the resonance region follow approximately a square root law[24]:

$$\Sigma(T) = \omega_1 \Sigma(T_1) + \omega_2 \Sigma(T_2) \qquad \omega_2 = \frac{\sqrt{T} - \sqrt{T_1}}{\sqrt{T_2} - \sqrt{T_1}} \qquad \omega_1 \equiv 1 - \omega_2 \tag{3.5}$$

3.1.3 Creation of a LOWFAT input library

LOWFAT will eventually read an ORIGEN working library, based on the fast reactor master library 'ABTR', containing among other things cross sections, decay constants, fission yields and recoverable energy per disintegration released by radioactive decay for 1487 nuclides, in a one group energy structure. Primary data source for the ORIGEN-S master library ABTR is the ENDF/B-VI, while nuclides not present in this library have been obtained from the JEFF-3/A library. Cross sections are collapsed using the neutron spectrum from the inner core of the Advanced Burner Test Reactor at equilibrium [16].

To better represent cross sections from important nuclides, this master library is updated with the COUPLE procedure [15] using a library in SCALE6's AMPX format. Three different approximations to the burnup model described in section 2.3 on page 17, differing in accuracy and computational cost, eventually lead to a set of cross sections used by LOWFAT.

Exact method The exact method is the computational implementation of equation 2.14 and computes average microscopic cross sections representative for the entire fuel region for all nuclides in the file 'in_AMPX'. The first part of a specially designed program, called 'Burnup_mixer.pl' takes computed zone dependent microscopic cross sections and applies the same square root temperature interpolation as discussed in subsection 3.1.2. This results in space and temperature dependent cross sections in a 11 group energy structure. DALTON has already computed the flux distribution and the second part of the program creates the final one group cross section by carrying out equation 3.6.

$$\begin{aligned}\overline{\sigma_{j\to i}(t)} &= \frac{V\cdot\int_V dV\int_E dE\rho(\mathbf{r})\phi(\mathbf{r},E,t)\sigma_{j\to i}(\mathbf{r},E,t)}{\int_V dV\rho(\mathbf{r})\int_V dV\int_E dE\phi(\mathbf{r},E,t)}\\ &= \frac{\sum_{g}^{groups} V\sum_{k}^{volume}\rho_k\phi_{k,g}(t)\sigma_{k,g,j\to i}(t)\Delta V_k}{\sum_{g}^{groups}\left[\sum_{l}^{volume}\rho_l\Delta V_l\sum_{m}^{volume}\phi_{m,g}(t)\Delta V_m\right]}\end{aligned} \tag{3.6}$$

For every documented reaction, every nuclide in the file 'in_AMPX' now has effective cross sections stored in the AMPX library 'library_burn.xs'.

Approximated method The previous described method requires lots of computational power and is therefore not feasible to perform for every nuclide. An approximation to equation 3.6 is to neglect spatial fuel salt density differences ($\rho(\mathbf{r}) \approx \rho_0$) and to consider broad group cross sections independent from space ($\sigma_{j\to i}(\mathbf{r}, E, t) \approx \sigma_{j\to i}(E, t)$). This results in equation 3.7:

$$\begin{aligned}\overline{\sigma_{j\to i}}(t) &= \frac{V \int_V dV \int_E dE \rho(\mathbf{r}) \phi(\mathbf{r}, E, t) \sigma_{j\to i}(\mathbf{r}, E, t)}{\int_V dV \rho(\mathbf{r}) \int_V dV \int_E dE \phi(\mathbf{r}, E, t)} \\ &\approx \frac{\int_E dE\, \sigma_{j\to i}(E, t) \int_V dV \phi(\mathbf{r}, E, t)}{\int_E dE \int_V dV \phi(\mathbf{r}, E, t)} \\ &= \frac{\sum_{g}^{groups} \sum_{k}^{volume} \phi_{k,g}(t) \sigma_{g,j\to i}(t) \Delta V_k}{\sum_{g}^{groups} \sum_{m}^{volume} \phi_{m,g}(t) \Delta V_m}\end{aligned} \tag{3.7}$$

where the number of groups is 11. This method is used for all nuclides included in the ENDF/B-VII library but not in the 'in_AMPX'-file and the 11 group cross sections are determined with the neutron flux in the reactor center (using XSDRNPM), while DALTON calculates the space and energy dependent neutron flux in 11 groups. The program 'Burnup_mixer.pl' creates libraries called 'lib_ENDF_burn_1,2 and 3' with cross sections of the nuclides updated with the Approximate method. Each library contains a maximum of 150 nuclides, due to restrictions imposed by COUPLE to update the ABTR-library. This method neglects more thermal influences of the 238-group spectrum present near the reflectors and the fertile blanket and only takes thermal contributions into consideration when using the volume averaged DALTON flux in 11 groups to collapse to 1 group. As cross sections usually rise with decreasing neutron energy, cross sections calculated by this method are expected to be a bit too low. In practice, it turns out this method is a good approximation to the exact method, as determined by studying the cross sections development methods in section 3.6.2 on page 41.

Coarse method For all other nuclides present in the ABTR library (approximately 1000 nuclides), detailed cross section information is unavailable and cross sections from the inner core of the conceptual design of the Advanced Test Burner Reactor (ABTR) at equilibrium are taken instead. The spectrum is fast, causing cross sections to be too low in general. The method's accuracy is also addressed in section 3.6.2 on page 41 and it turns out this method is rather inaccurate.

COUPLE, part of SCALE 6, updates the ORIGEN library ABTR, with the discussed AMPX libraries and uses a total flux normalization (as opposed to a thermal flux normalization, frequently used for depletion analysis in Light Water Reactors).

3.2 Neutronics

Provided with a flow field by HEAT and an input library containing nuclear data for every cell, DALTON solves the steady-state multigroup diffusion equation with precursors (equation 2.3 together with 2.4) with the 'power method' as discussed by Y. Saad [31]. Only the main idea behind this method is explained here, starting with solving an eigenvalue problem in standard form:

$$Ax = \lambda x \tag{3.8}$$

The solution has eigenvalues λ_i and associated eigenvectors $\mathbf{v}_i$ which can be ordered:

$$|\lambda_1| \geq |\lambda_3| \geq |\lambda_3| \geq |\lambda_4| \geq \ldots \geq |\lambda_n|$$

By successive multiplication of matrix A to an arbitrary initial vector $\mathbf{x}_0$, such that

$$\mathbf{x}_{l+1} = A\mathbf{x}_l = A^{l+1}\mathbf{x}_0 \tag{3.9}$$

the ratio of subsequent vectors $\mathbf{x}_{l+1}$ and $\mathbf{x}_l$ will tend to the dominant eigenvalue and $\mathbf{x}_{l+1}$ to its associated eigenvector:

$$\begin{aligned} \lim_{l\to\infty} \mathbf{x}_l &= \mathbf{v}_1 \\ \lim_{l\to\infty} \frac{\mathbf{x}_{l+1}}{\mathbf{x}_l} &= \lambda_1 \end{aligned} \tag{3.10}$$

The power method also efficiently solves the multi-group diffusion equation without precursors, which is a generalized eigenvalue problem:

$$\begin{aligned} M\phi = \frac{1}{k}F\phi \;\leftrightarrow\; kM\phi = F\phi \\ M = -\nabla\cdot D\nabla + \Sigma^r - \sum_{g'\neq g}^{G} \Sigma^s_{g'\to g} \\ F = \chi\nu\Sigma^f \end{aligned} \tag{3.11}$$

In this situation, at every iteration, we want to solve the matrix equation for ϕ_{l+1}:

$$M^{-1}F\phi_l = \phi_{l+1} \;\leftrightarrow\; F\phi_l = \phi* = M\phi_{l+1} \tag{3.12}$$

Precursors can be included by again scaling the total fission source with 1/k and adjusting the neutron emission spectrum χ to include precursor effects, because in the steady state, the 'delay' in neutron emission caused by precursors is not noticably, but precursors do change the emission spectrum. Equation 3.13 gives the rescaling of χ for the case only one material is present.

$$\chi = (1-\beta)\chi_p + \sum_{i}^{I} \beta_i \chi_{d,i} \tag{3.13}$$

Table 3.2: **The six precursor groups with their characteristic decay time and delayed neutron production.**

i	decay constant $[s^{-1}]$	$\nu_{d,i}$ x 100
1	0.0129 ± 0.0002	0.053 ± 0.003
2	0.0311 ± 0.0005	0.197 ± 0.012
3	0.134 ± 0.003	0.175 ± 0.025
4	0.331 ± 0.012	0.212 ± 0.013
5	1.26 ± 0.12	0.047 ± 0.014
6	3.21 ± 0.26	0.016 ± 0.006

DALTON solves the large matrix equation using the Generalized Minimal Residual Method (GMRES) in 11 energy groups, six precursor groups and a spatial mesh of 66x78 elements. See table 3.1 for the energy boundaries of the flux and table 3.2 for decay constants and delayed neutron production of the precursor groups.

3.3 Computational Fluid Dynamics

HEAT is the Computational Fluid Dynamics program that solves Reynolds Averaged Navier Stokes equations (equation 2.5), the $k - \epsilon$ model (equation 2.7) and scalar transport of temperature (equation 2.9) with the finite volume method (thoroughly discussed in for instance Versteeg and Malalasekera[37]). HEAT uses a 264 x 312 staggered grid with rectangular cells, which becomes finer near the walls. Figure 3.4 displays part of the mesh for both HEAT and DALTON.

Energy transport is modeled only in the fuel region and energy leaves the system solely via the heat exchanger, modeled as a sink and occupies 36% of the out-of-core region. The Nusselt number is determined according to the Dittus-Boelter correlation[23] and thus depends both on the velocity profile and temperature difference. Structural materials and the fertile blanket remain at the average core temperature. The pump is modeled as a body force and the pressure difference amounts to approximately 27 kPa.

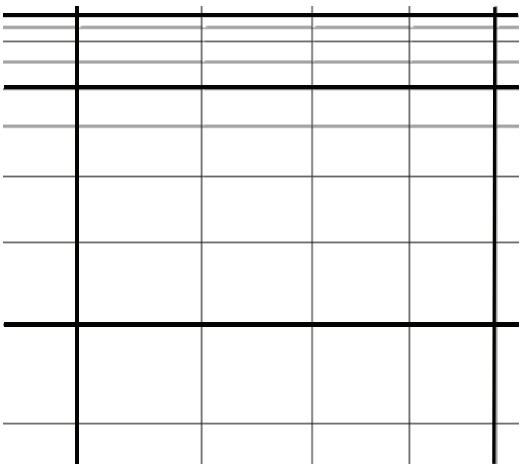

Figure 3.4: **The finer (staggered) HEAT mesh (264 x 312 cells), here displayed in gray, has element boundaries exactly on top the coarser DALTON mesh (68 x 78 cells, displayed in black) everywhere. Only a part of the mesh is displayed.**

In the fertile blanket, the flow is also neglected. Heat transfer in this blanket is not modeled and neither is heat production due to occasional fission of thorium (expected to be around $0.90MW = 0.03\%$ of nominal power) and is assumed to be extracted by the same system that removes fission products. 0.9 MW is little compared to the amount of decay heat present in the reprocessing facility, which is a few per cent of nominal power.

3.4 LOWFAT and the burnup model

Assuming proper values for all constants are available, LOWFAT will calculate concentrations for all nuclides for each burnup step by solving the coupled system of partial differential equations (equation 3.14), as discussed in section 2.3 on page 17.

$$\begin{aligned}\frac{\partial N_i^0(t)}{\partial t} &= \sum_{j\neq i} \overline{\sigma_{j\to i}}(t)\overline{\phi}(t)N_j^0(t) - \sum_{i\neq j} \overline{\sigma_{i\to j}}(t)\overline{\phi}(t)N_i^0(t) \\ &+ \sum_{j\neq i} b_{j\to i}\lambda_j N_j(\mathbf{r},t) - \lambda_i N_i^0(t) + F_i(t)N_i^0(t) - R_i(t)N_i^0(t)\end{aligned} \tag{3.14}$$

3.4.1 Read data and calculate relevant quantities

Each nuclide's concentration, cross sections, reprocessing and feeding rates need to be known to set up system 3.14. Part of the data, including information about time, cross sections, concentrations and k_{eff}, is stored in files and after reading it, LOWFAT prepares and adjusts the data in the following manner:

An overflow tank is modeled as a zero flux area to accommodate variations in the fuel salt quantity over time due to reprocessing and feeding. Although not incorporated in the Reference Configuration, an overflow tank will be required in a MSFR design to allow for thermal expansion while operating or overfilling. The Molten Salt Reactor Experiment at Oak Ridge National Laboratory (discussed in the Introduction) also featured a similar tank[28]. Another possibility is to add a void region in the reactor core's upper part to accommodate fuel expansion. Advantages and disadvantages of both methods will have to be investigated further. In this model, the overflow tank's only function is to conserve mass in the system, i.e. reactor and overflow tank, when the reactor alone is not large enough to accommodate the total fuel volume that will slightly vary due to reprocessing and feeding. To understand the effect of an overflow tank, consider the total amount of fuel at time t when it exactly equals the total mass required by equation of state in table 1.2 on page 11. At that time, equation 3.15 is valid.

$$\sum_{i=1}^{n} m_i N_i^t V_{core} = \rho(\bar{T}) V_{core} \tag{3.15}$$

where, m_i is nuclide's i molar mass, ρ is the density, $\bar{T}$ is the average temperature in the fuel region and V is volume. After LOWFAT calculates new concentrations this condition is in general no longer met, because of feeding and reprocessing. The new situation at time $t+1$ is as follows:

$$\sum_{i=1}^{n} m_i N_i^{t+1} V_{core} = \rho(\bar{T})(V_{core} + \Delta V) = \rho(\bar{T}) V_{tot} \tag{3.16}$$

where a small extra volume ΔV in the overflow tank is required for the extra fuel (the density, thus temperature, is the same in the overflow tank as in the reactor). By enforcing condition 3.15, the concentration in the reactor is such that the fuel density is the same as is required by thermodynamic properties:

$$\sum_{i=1}^{n} m_i N_i^{t+1} \frac{V_{core}}{V_{tot}} = \sum_{i=1}^{n} m_i \tilde{N}_i^{t+1} V_{core} = \rho(\bar{T}) V_{core} \tag{3.17}$$

When LOWFAT is called, it reads the concentration as it is in the core (i.e. $\tilde{N}_i$ for all i) and calculates the total amount of atoms present in the core and overflow tank using the actual volume V_{tot} and uses these numbers in its calculations.

Total flux and decay heat is calculated by LOWFAT instead of by DALTON, since DALTON does not have enough data to precisely calculate the magnitude of the flux. The flux needs to be such that the total amount of power equals 3 GW throughout operation. To this end, LOWFAT first calculates the decay heat and then uses the prompt energy release per fission and per neutron capture to determine the flux, see equation 3.18.

$$\overline{\phi} = \frac{P_{nom} - \sum_{i}^{n} \gamma_{\lambda,i} \lambda_i N_i}{\sum_{k \in actinides} \gamma_{p,k} \sigma_{f,k} N_k + \sum_{i}^{n} \gamma_{c,i} \sigma_{c,i} N_i} \tag{3.18}$$

where $\overline{\phi}$ is the total flux, P_{nom} is nominal power, i.e. 3 GW_{th}, γ is the amount of energy released per specified reaction, λ_i is nuclide i's decay rate and σ_f and σ_c are the fission and capture cross sections of a nuclide, respectively. Energy release data is derived from the ENDF-B/VII library: the prompt fission energy is all recoverable fission energy minus delayed beta and gamma energy releases. Energy releases for certain radiative capture reactions are listed in the ORIGEN-S Data Libraries manual, while for all other radiative capture reactions a value of 5 MeV is taken, consistent with the ORIGEN-S methodology[16].

Reprocessed nuclides are given in the Reference Configuration and separated in two groups. A gaseous extraction system, utilizing helium bubbling, extracts all non-soluble fission products, i.e. some noble metals and gaseous fission products and is modeled by introducing a removal period of $T_{1/2} = 30\ s$ for nuclides concerned (nuclides shown in blue in figure 3.5). Also, a fraction of the salt, 40 liters per day in the nominal scenario, is withdrawn daily, reprocessed offline to extract mainly lanthanides (shown in red), and fed back into the core. Introduction of an effective decay rate for the relevant nuclides models this offline extraction (with 100% efficiency, i.e. 40 liters is cleaned completely and without removing any other nuclides than the desired ones).

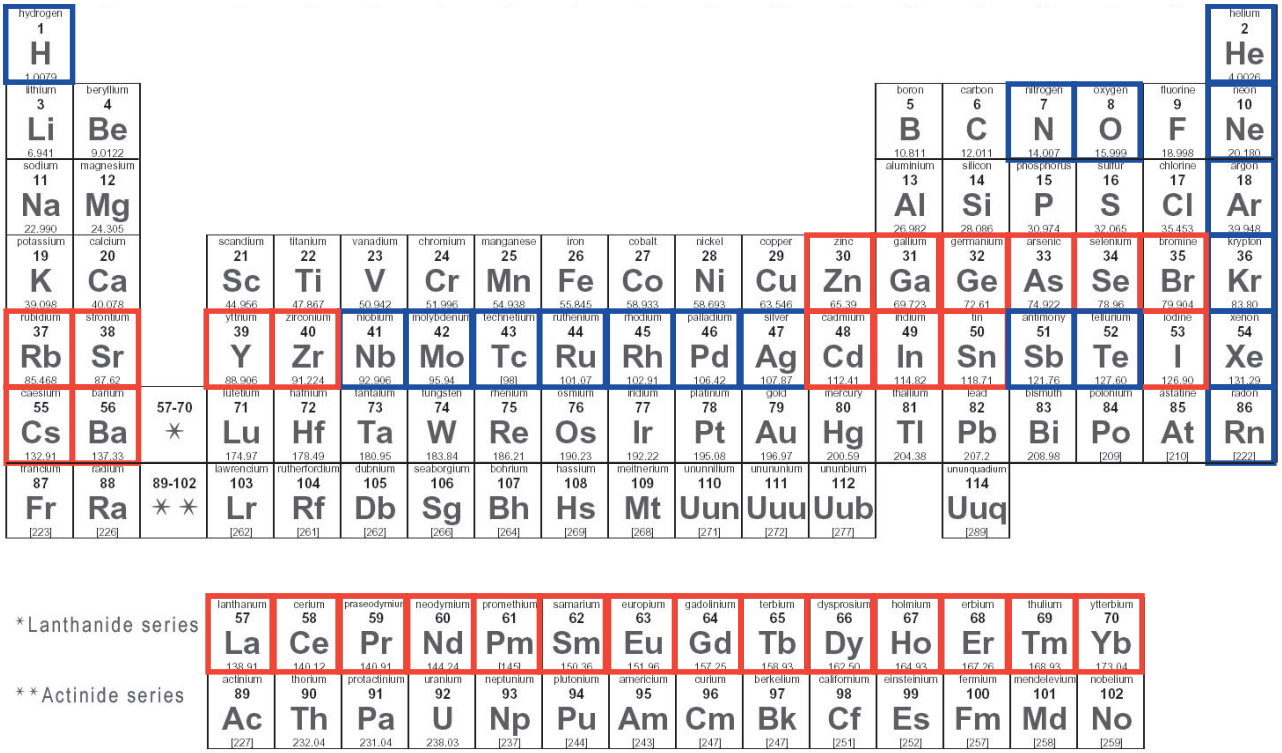

Figure 3.5: **All nuclides reprocessed offline are shown in red, while all nuclides subject to helium bubbling are shown in blue.**

Feeding of ^{232}Th and ^{233}U into the reactor core can also be done in a continuous manner. ^{232}Th is fed to ensure the amount of actinides ($90 \leq Z \leq 99$) relative to the amount of lithium and fission products is kept at the eutectic point, i.e. the composition having a melting point at a lower temperature than any other mixture with the same compounds [33], throughout reactor operation. Therefore, condition 3.19 must hold for all times. Z is the atomic number of nuclide N_i and fluor (Z=9) is left out, because in an ideal situation, all fluor is bounded to actinides or fission products, i.e. there is no free fluor in the system.

$$\frac{\sum_{90 \leq Z \leq 99} N_i^t}{\sum_{Z \neq 9} N_i^t} = 0.225 \tag{3.19}$$

Therefore, the amount of ^{232}Th at the end of each burnup step can be estimated by taking into account the current ratio, decay, and loss due to absorption. Equation 3.20 gives the amount of ^{232}Th needed at the end of each burnup step to satisfy condition 3.19. In the following equations, the actinide id is formed by the combination ij where $i = Z - 90$ and $j = A \, mod \, 10$ (Z is the atom number and A the mass number). The amount of ^{232}Th,

^{233}Pa and ^{233}U is thus indicated by N^{02}, N^{13} and N^{23} respectively.

$$\mathrm{N}^{02}_{t+1} = \frac{0.225 \cdot \sum_{(Z \neq 9 \ \& \ N^i \neq \mathrm{N}^{02})} N^i - \sum_{(90 \leq Z \leq 99 \ \& \ N^i \neq \mathrm{N}^{02})} N^i}{1 - 0.225} \tag{3.20}$$

Observing equation 3.21 describing the rate of change of ^{02}N, one can derive the feed of ^{232}Th necessary to achieve condition 3.19.

$$\begin{aligned} \frac{\partial \, \mathrm{N}^{02}}{\partial t} &= -\sigma_a^{02} \phi \, \mathrm{N}^{02} - \lambda^{02} \, \mathrm{N}^{02} + F^{02} \, \mathrm{N}^{02} \\ \frac{\mathrm{N}^{02}_{t+1} - \mathrm{N}^{02}_t}{\Delta t} &= -\sigma_a^{02} \phi \, \mathrm{N}^{02}_t - \lambda^{02} \, \mathrm{N}^{02}_t + F^{02} \, \mathrm{N}^{02}_t \\ F^{02} \, \mathrm{N}^{02}_t &= \frac{\mathrm{N}^{02}_{t+1} - \mathrm{N}^{02}_t}{\Delta t} + \sigma_a^{02} \phi \, \mathrm{N}^{02}_t + \lambda^{02} \, \mathrm{N}^{02}_t \end{aligned} \tag{3.21}$$

Note the time discretization is done explicitly and as long as time steps are sufficiently small, this yields correct results.

The ^{233}U feed can be estimated in a similar manner and is used to ensure criticality ($k_{eff} = 1$) at a thermal power output of 3 GW throughout operation. The method uses a prediction of the amount of ^{233}U needed to have $k_{eff} = 1$, and loss due to absorption and production of ^{233}U due to decay of ^{233}Pa. Equation 3.22 gives the predicted amount of ^{233}U necessary to achieve $k_{eff} = 1$, everything but the ^{233}U concentration remaining constant.

$$\frac{\partial k^{eff}}{\partial \, \mathrm{N}^{23}} = \frac{k^{eff}_{t+1} - k^{eff}_t}{\mathrm{N}^{23}_{t+1} - \mathrm{N}^{23}_t} \ \rightarrow \ \mathrm{N}^{23}_{t+1} = \frac{1 - k^{eff}_t}{\partial k^{eff} / \partial \, \mathrm{N}^{23}} + \mathrm{N}^{23}_t \tag{3.22}$$

It turns out it is sufficient to evaluate $\partial \, k^{eff} / \partial \, N^{23}$ only once at reactor startup. This method will be more accurate when time steps are smaller, especially directly after startup as some fission products will build up quickly. Analogue to equation 3.21, equation 3.23 describes the feed to get $k^{eff} = 1$.

$$\begin{aligned} \frac{\partial \, \mathrm{N}^{23}}{\partial t} &= -\sigma_a^{23} \phi \, \mathrm{N}^{23} + \lambda^{13} \, \mathrm{N}^{13} + F^{23} \mathrm{N}^{23} \\ F^{23} \, \mathrm{N}^{23}_t &= \frac{1 - k^{eff}_t}{\partial \, k^{eff} / \partial \, \mathrm{N}^{23} \Delta t} \, \mathrm{N}^{23}_t + \sigma_a^{23} \phi \, \mathrm{U}^{23}_t - \lambda^{13} \mathrm{N}^{13}_t \end{aligned} \tag{3.23}$$

In order to force the reactor to criticality more quickly, an extra adaptive term is added compensating for errors and approximations introduced in the derivation. To this end the quantity k_{forced} is decreased slightly if the reactor is super critical after a burnup step and increased if sub critical, see equation 3.24:

$$F^{23} \mathrm{N}^{23}_t = \frac{k_{forced} - k^{eff}_t}{\partial \, k^{eff} / \partial \, \mathrm{N}^{23} \Delta t} \, \mathrm{N}^{23}_t + \sigma_a^{23} \phi \mathrm{N}^{23}_t - \lambda^{13} \mathrm{N}^{13}_t \tag{3.24}$$

3.4.2 Set up coupled differential equations

Since every term in equation 3.14 contains a factor of N_i^t, the system can be rewritten in the following format, in which A is the 'transition matrix':

$$\mathbf{N}^{t+1} = A\,\mathbf{N}^t \tag{3.25}$$

The nuclide vector **N** is concatenated with a 'waste stock' vector of length N and the matrix A is expanded appropriately to, for every nuclide, keep track of the amount extracted from the core and taking into account decay of this stock. For this part, exactly the same set of equations is used as for calculating burnup in the fuel, but with the flux equal to zero and including a source term for every waste stock opposite to the sink terms in the volume lumped parameter model, due to reprocessing. The two parts are thus only coupled through reprocessing, i.e. the waste stocks depend on nuclide densities in the core, but not vice versa.

3.4.3 Solve the system

The program VODE, developed by Lawrence Livermore National Laboratory, is eventually called to actually solve the system for which it uses the fixed leading coefficient Backward Differentiation Formula (BDF) method[5]. Only a very brief summary of the solver is given here, but a full description of VODE and associated mathematical methods are given by Brown et al.[5] and Skeel[32]. The general problem is:

$$\dot{y} = f(t, y), \quad y(t_0) = y_0, \quad y \in \Re^N \tag{3.26}$$

For our stiff problem, the Backward Differentiation Formula with order q and variable time step size h_n (a burnup step includes many time steps) is as follows:

$$\sum_{i=0}^{q} \alpha_{n,i} y_{n-i} + h_n \dot{y}_{n,0} = 0 \tag{3.27}$$

Coefficients $\alpha_{n,i}$ depend on the size of previous time steps and a modified Newton iteration is used to solve the non-linear system originating from this formula. After each time step an error test is performed and the error of each component is tested to absolute and relative tolerances provided in an input file. Depending on the result of this test, the result is passed, repeated with a smaller time step or the order q is changed. After the system has been solved, all relevant data is written to files to be used by other modules.

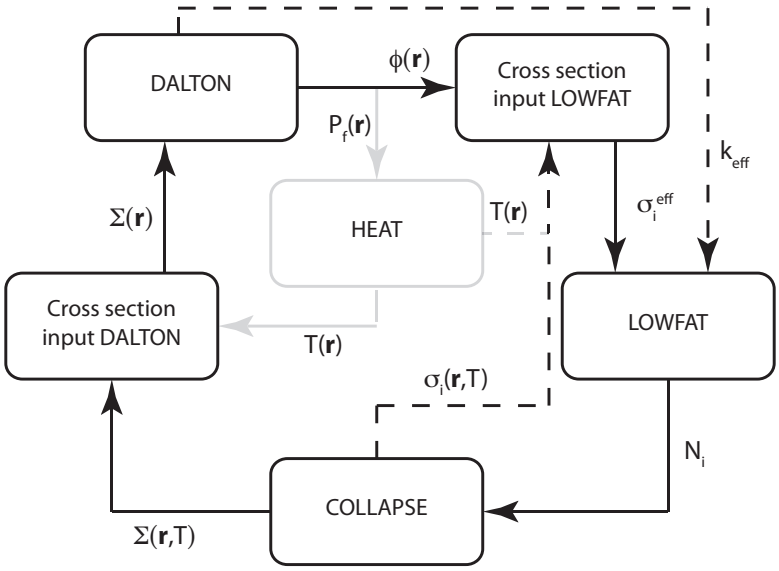

Figure 3.6: **Coupling of different modules. The arrows indicate the execution sequence, while dashed arrows only indicate transfer of information. HEAT and related arrows are more transparent, since HEAT is part of the model, but it's not updated during execution.**

3.5 Coupling different modules

Previous paragraphs describe the computational implementation of six different modules (general cross section processing, cross section input for DALTON, HEAT, cross section input for LOWFAT and LOWFAT) individually. The perl script IMP_burn.pl couples these modules such that time dependent behavior over many months and years is modeled properly. The model assumes a temperature profile is available for all times (it turns out the temperature profile is independent of fuel composition since it is mostly determined by the steady state flow and total power, while variations in the power distribution are minimal). Note that since IMP_burn.pl only uses eigenvalue calculations to calculate the flux distribution, running DALTON in time-dependent mode is not necessary.

Once a steady state solution has been obtained, IMP_burn.pl calculates transmutation of the fuel by coupling different modules (see also figure 3.6 for the calling sequence and data transfer between different modules). Using an initial fuel composition, 'Collapse.exe' (section 3.1.1) creates cross section libraries forming the basis Mixer.pl, which prepares nuclear data input for DALTON, which is called after Collapse.exe finishes (section 3.1.2). DALTON calculates the flux distribution (section 3.2), used to further collapse the 11 group structure to 1 group and to weight all cross sections spatially (section 3.1.3. k_{eff}, also calculated by DALTON , is used by LOWFAT (section 3.4) to calculate the ^{233}U feed. The new material composition is fed into Collapse, and the procedure is repeated as many times as desired.

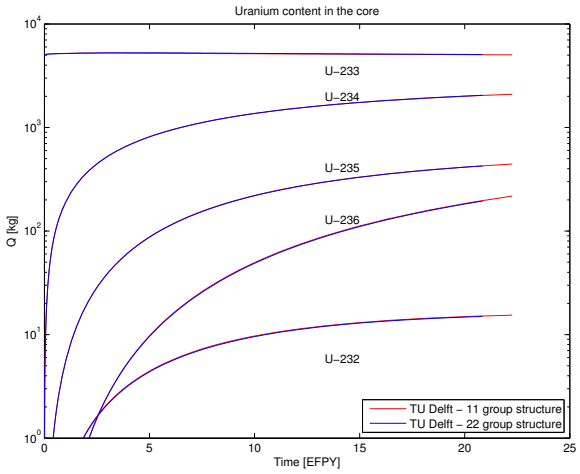

Figure 3.7: **Uranium content in simulations of 11 and 22 energy groups.**

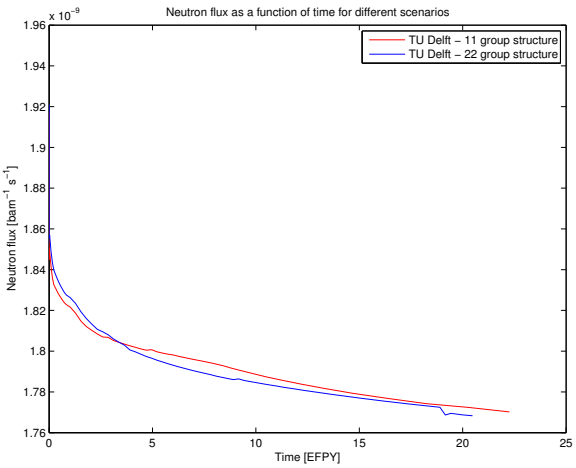

Figure 3.8: **A comparison of the flux in simulations of 11 and 22 energy groups.**

3.6 Parameter studies

In this section, various aspects and assumptions of the model are investigated to test their validity and impact on the model. Different burnup steps have been tested and further decreasing the burnup step does not yield different results.

3.6.1 Energy structure and temperature profile

The influence of the chosen energy structure is analyzed by splitting every group in half, e.g. the fine groups making up one broad group are distributed equally over two new broad groups, thus doubling the number of broad groups to 22. Figure 3.7 displays the uranium isotope content in the core for both energy structures. The agreement between both simulations is very good, although a small difference in the ^{233}U is observed, which is due to a slight change in k_{eff}. The ^{232}U content also differs slightly, probably due to a more precise description of the fast flux responsible for the important (n,2n) threshold reaction. Other nuclides show similar agreement and the difference in the flux is 0.2%.

In this work, the temperature distribution is taken into account via temperature induced density differences relevant for spatial weighting and cross section collapsing at different temperatures. The isotopic composition was found not to differ significantly if a homogeneous temperature of 973.15 K was chosen instead (midway between the inlet and outlet temperature, opposed to a non homogeneous temperature distribution with a mean of 1022 K that was used in this work). The ^{233}U differs approximately 0.6% after 20 years. The uranium feed, however, differs approximately 5% due to a slight change in the breeding ratio.

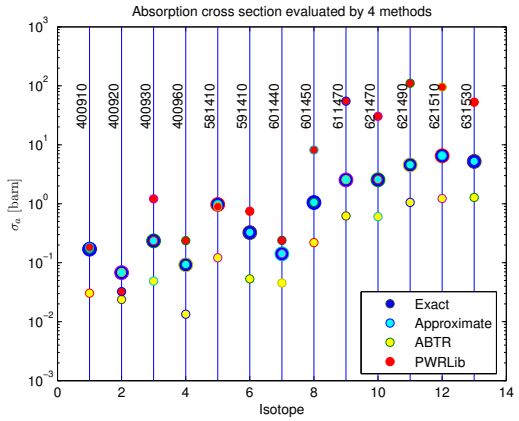

Figure 3.9: **Absorption cross sections of randomly selected fission products calculated with all four methods. The Approximate method is very close to the Exact method.**

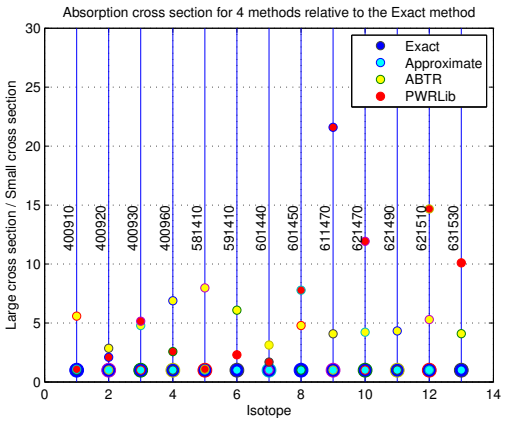

Figure 3.10: **Absorption cross sections relative to results of the Exact method. The larger cross section is always divided by the smaller one. The Exact method thus yields 1.**

3.6.2 Comparison of cross section development methods

The program uses three distinct approaches to calculate cross sections for LOWFAT, which have been discussed in subsection 3.1.3 on page 29. The 'Exact method' fully takes into account spatial cross section variations of homogeneously mixed fuel and is the first and preferred method, but due to computational restrictions, this method is only utilized for the majority of the actinides and the main fission products. The 'Approximate method' approximates cross sections of nuclides present in the ENDF/B library which have not been processed with the Exact method, by collapsing the 238 energy groups to 11 with the weighting function derived from the inner MSFR core and then further to 1 group using the volume averaged DALTON neutron flux. SCALE 6's ABTR library, where cross sections have been collapsed with the weighting function derived from the fast spectrum of the inner core of the Advanced Burner Test Reactor, provides cross sections for all other nuclides. A fourth possibility would be not to use the ABTR library, but SCALE 6's PWRLib library instead which is specially made for thermal reactors, since a typical LWR weighting function is used to collapse cross sections to 3 groups, allowing for some problem specific updating. Figure 3.9 displays the absorption cross section of the fission products with the largest macroscopic cross section after approximately 20 years of operation for all methods and figure 3.10 compares the methods by displaying the multiplication factor between results of two methods as calculated by dividing the larger cross section by the smaller one.

In general, the Approximate methods is accurate (differing less than 1% with the Exact method), while both the ABTR and PWRLib libraries tend to give results that are too low or too high respectively. These findings are confirmed by results from other nuclides, not

Table 3.3: **Calculating ^{135}Xe absorption cross section with different methods.**

Method	Cross section [barn]
The Approximate method	0.30
PWRLib method	127.4
PWRLib method - typical LWR weighting function to 3 groups	99.13

presented in this work. The error is induced by the weighting function which is used to collapse fine energy groups into broad groups and is demonstrated with ^{135}Xe, a very strong thermal absorber. Here the Approximate method yields an absorption cross section of 0.30 barn, while the PWRLib method yields 127.4 barn, over 400 times as much. Table 3.3 illustrates the effect of using different weighting functions to collapse cross sections. The first line shows the results of the Approximate method and the second line the result of the PWRLib method. To show the weighting function is the cause of the discrepancy, the third line is the result of mimicking the PWRLib method by using a 'typical' LWR weighting function (not the same as the one used to generate PWRLib, which is unknown) to collapse 238 groups to PWRLib's 3 group structure and then using the DALTON volume averaged flux (in 3 groups) to collapse them to 1 group. Figure 3.12 displays the two weighting functions (not neutron spectra, which are not relevant here). As can be seen, MSFR's weighting function is very small in the thermal domain and peaks in the resonance region, indicated with 'Res'. Therefore, an accurate description of the 'res-cross section' is important, but a clear difference can be seen between the two functions for the lower part of the resonance region (between 1 and 100 eV). There, the LWR weighting function is significantly higher and since cross sections increase at lower energies (the absorption cross section of ^{135}Xe is depicted in figure 3.11), the PWRLib method will tend to produce cross sections that are too high, especially in the important resonance region. Although the result from the 'mimicked PWRLib method' is not the same as the real PWRLib, it definitely shows the discrepancy is caused by the 238 group weighting function. The relatively high cross section in the lower energy epithermal groups weighs heavily on the result and introduces an error. However, the Exact method updates 99.88% of all particles in the reactor at equilibrium, and the Approximate method further updates 0.12% of the particles, summing up to a total of 99.99983%. The Coarse method is thus almost not used in practice and errors from this source can be regarded as negligible.

To summarize, the Approximate method is a good approximation to the Exact method. Considerable differences are observed however for ABTR cross sections, which are still better than those generated with the PWRLib. The weighting function used to determine these cross sections is the cause of this discrepancy.

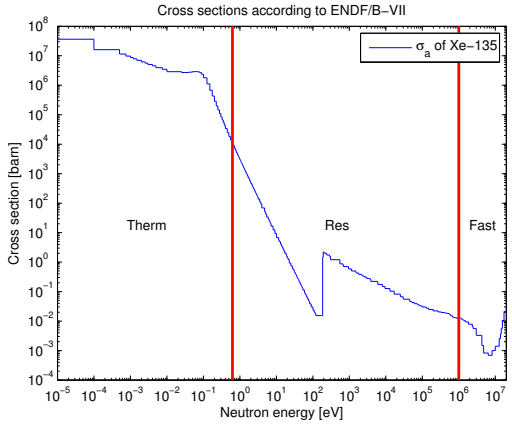

Figure 3.11: ^{135}**Xe is a very strong thermal absorber, having a thermal absorption cross section of millions of barns. The cross section is still very large in epithermal groups close to the thermal region (around 1 eV).**

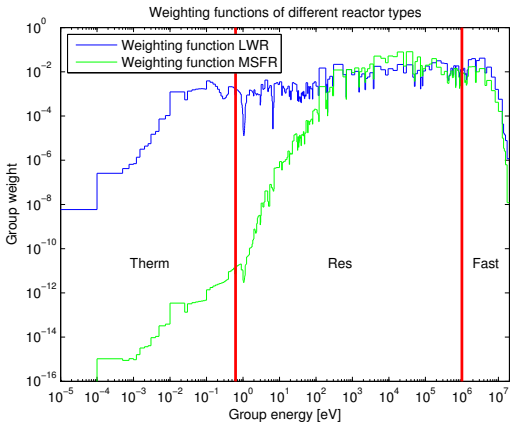

Figure 3.12: **Two different weighting functions yield different broad group cross sections. Here, one weighting function with a large thermal flux is typical for a LWR, while the other belongs to the MSFR.**

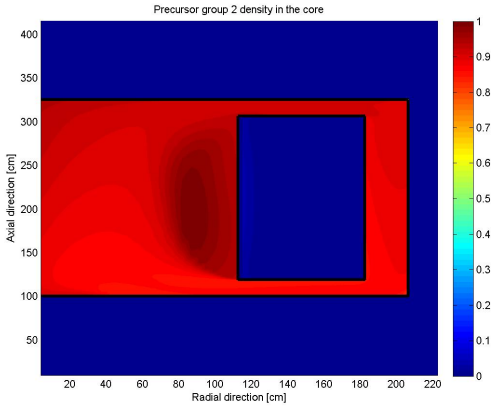

Figure 3.13: **Precursor density of group 2 (λ = 0.0334 s^{-1}) across the core normalized to the maximum. Some inhomogeneities occur.**

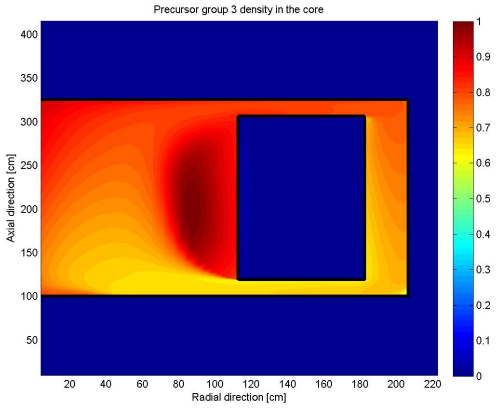

Figure 3.14: **Precursor density of group 3 (λ = 0.121 s^{-1}) across the core normalized to the maximum. Substantial density differences occur.**

3.6.3 Effects of incomplete mixing

In section 2.3 definitions for the flux, cross sections and decay constants (equation 2.14) relied on the assumption that the fuel is homogeneously mixed, i.e. the only space dependence in the nuclide density is a result of temperature induced fuel density fluctuations. A fluid will be homogeneously mixed when its components change slowly compared to the mixing time, which is in this case, due to highly turbulent flow, similar to the fuel circulation time (4 seconds). Precursors are a straightforward example of MSFR fuel components which are not completely, i.e. homogeneously, mixed, see for instance figure 3.13 and 3.14 which depict precursor concentrations across the fuel region for precursor groups 2 and 3 (normalized such that the maximum in both figures equals 1). In order to investigate possible inaccuracies due to the neglect of these spatial density variations, the definition for the effective cross section, as given in equation 2.14 on page 19 was modified (equation 3.28) to include non-homogeneous distributions and precursor densities form a model for an inhomogeneous distributed mixture. Here, the nuclide capturing a neutron (nuclide j) is considered inhomogeneously mixed with the distribution of precursor groups 2 and 3 respectively, while nuclide i is homogeneously distributed.

$$\frac{\partial N_i^0(t)}{\partial t} = f(\overline{\sigma_{j\to i}}(t)) \to \overline{\sigma_{j\to i}}(t) = \frac{V \cdot \int_V dV \int_E dE \frac{\rho_j}{\rho_j^0}(\mathbf{r})\phi(\mathbf{r},E,t)\sigma_{j\to i}(\mathbf{r},E,t)}{\int_V dV \frac{\rho_i}{\rho_i^0}(\mathbf{r}) \int_V dV \int_E dE \phi(\mathbf{r},E,t)} \tag{3.28}$$

where $\rho_j^0 = \frac{1}{V}\int dV N_j(\mathbf{r},t)$, which has a known integrand. Figure 3.15 visualizes the discrepancy between three cases: a homogeneous case (with only temperature induced density variations, as used in this project) and case two and three in which the precursor densities form the

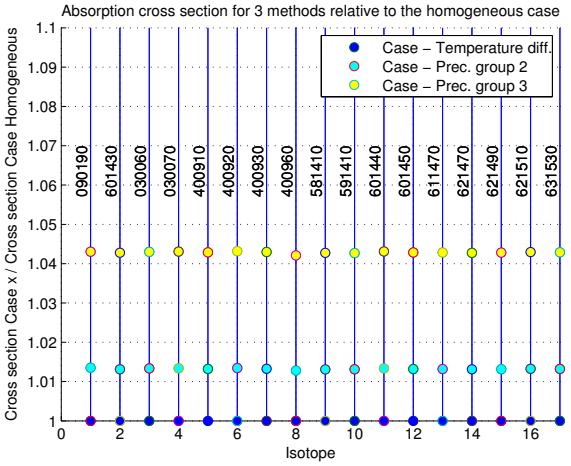

Figure 3.15: **Absorption cross sections for the most important fission products for three cases (homogeneous distribution, and densities of precursor group 1 and 2) normalized to the homogeneous case. In reality, nuclides in this graph are homogeneously distributed and the picture serves to illustrate a possible source of error only.**

density weighting function ρ_j. All cross sections are normalized to cross sections generated for the assumed homogeneous distribution. The picture is for illustrative purposes only, as these fission products are actually homogeneously distributed. Inhomogeneities occur if fuel components change quickly with respect to the circulation time (this is definitely true for these precursor groups), for instance due to a large decay rate and if large enough to produce a notable error, its concentration is therefore also very low and absorption is not important. In the simulations, approximately 500 nuclides have a decay rate larger than 0.01 s^{-1} (similar to precursor group 3) and none of them has a non negligible absorption cross section (in fact, on file their absorption cross section is 0) or a total abundance larger than a milli mol in the entire reactor. Helium bubbling is modeled by incorporating an effective removal 'decay' constant of $2.31 \cdot 10^{-2}$ s^{-1}, which is slightly less than the decay rate of precursor group 2. Cross sections belonging to this group of quickly reprocessed fission products, can be expected to be a bit off (about 1% when inspecting figure 3.15) and some nuclides have an absorption cross section of a few barns), but their abundance is also very low due to the reprocessing, never exceeding a milli mol in the reactor per nuclide. None of the nuclides has an absorption rate large enough to result in an inhomogeneous distribution (^{148m}Pm has the largest absorption cross section of 12.55 barn, resulting in a reaction rate of $2.21 \cdot 10^{-8}$ s^{-1}). For other sources of inhomogeneities, similar arguments hold. The homogeneous mixing assumption is thus an accurate way of describing the fuel.

Chapter 4

Results

In this chapter all results, divided into four parts, will be discussed: the section 'Neutronic benchmark results' discusses nuclear reactor physics quantities at BOL, e.g. the neutron flux, precursor, temperature and velocity distributions and the delayed neutron fraction as well as evolution of the fuel salt composition, in the section 'Reprocessing scenarios' the offline lanthanide reprocessing rate is varied to evaluate the possibility of changing the feeding rate of fissile material, nuclear waste of the MSFR and its associated radiotoxicity is discussed in the section 'Nuclear waste and radiotoxicity', and lastly, feasibility of the freeze plug is examined in the section 'Decay heat and core draining'.

4.1 Neutronic benchmark results

This section describes results determined for a Neutronic Benchmark, carried out under WP2 of the EVOL project[12]. Complete TU Delft Neutronic Benchmark results can be found in Appendix B.

4.1.1 Initial composition and startup parameters

In order to achieve criticality of the reactor at startup, the uranium concentration is slightly increased to 2.61 mol%, compared to 2.515 mol% given in the Reference Configuration[13] and the ^{232}Th concentration is adjusted accordingly, such that the total heavy nuclide concentration remains at the eutectic point, i.e. 22.5 mol%. The startup procedure (filling the core, warming up the fuel salt, reaching criticality etc.) is neglected, i.e. it is assumed the reactor reaches its steady state temperature and velocity field without fissioning uranium.

4.1.2 Temperature and velocity field

At beginning-of-life, figures 4.1 and 4.2 give the temperature distribution and the velocity profile across the core as calculated by HEAT according to a RANS-model (discussed in section

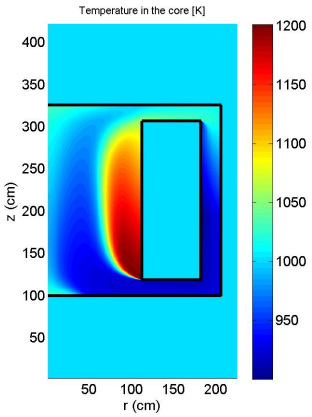

Figure 4.1: **Temperature distribution in the core as calculated with a mesh of 264x312 elements.**

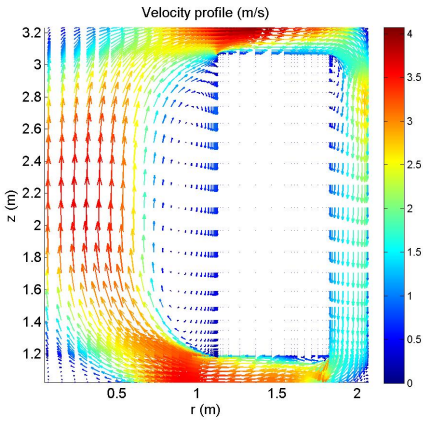

Figure 4.2: **Velocity profile across the core in m/s. Near corners, recirculation zones are visible.**

2.2 on page 15). Note that the velocity profile is the average velocity profile as fluctuations due to turbulence are split off from the average velocity in RANS models. When the fuel enters the core, it has a temperature of 920.6 K (647.5 °C), heating up to 1021.1 K (748.0 °C) when leaving the core. The temperature difference across the core therefore amounts to 100.5 K, close to the Reference Configuration specification of an inlet and outlet temperature of 650 and 750 °C, respectively. The pump is simulated with a pressure drop of 26.267 kPa, resulting in a volumetric flow of 4.50 m^3 s^{-1} equivalent to a fuel circulation time of 4.0 seconds as specified in the Reference Configuration. A large recirculation zone is present next to the fertile blanket, yielding a very high maximum temperature of 1201 K on structural materials enclosing the fertile blanket. Structural material will weaken more quickly if subject to the higher temperatures associated with these zones making a new geometry without them desirable. The temperature distribution is mainly determined by the velocity field and energy conservation (total power extracted from the core equals total prompt fission power plus decay heat). Since neither the salt's physicochemical properties, nor the primary system change by the slight variation in composition over time, these distributions were found to be time independent under normal operation.

4.1.3 Neutron flux and precursors

The total flux $\phi(\mathbf{r}, t)$ at beginning-of-life, i.e. the sum of all group fluxes, is plotted in figure 4.3 and reaches its maximum of $9.77 \cdot 10^{15}$ cm^{-2} s^{-1} in the core center. The core's mean flux according to DALTON is $3.81 \cdot 10^{15}$ cm^{-2} s^{-1} while the mean flux in the fertile blanket is $2.65 \cdot 10^{14}$ cm^{-2} s^{-1}, or about 7% of the average flux in the core. The flux in the fertile blanket, as indicated by figure 4.4 is more thermal due to absence of fast fission neutrons.

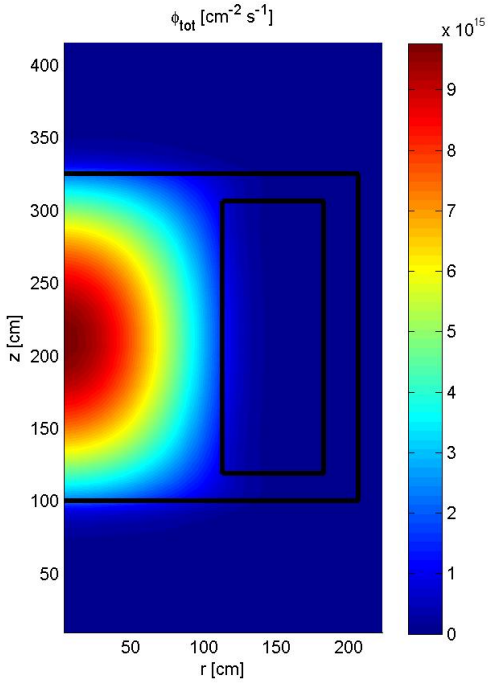

Figure 4.3: **Sum of group fluxes as a function of space.**

For other compositions than the starting composition, DALTON's ability to predict the total flux is limited by its energy per fission data (187.5 MeV per fission is assumed independent of composition and not taking into account changes in decay heat due to reprocessing).

The neutron spectrum in the core is epithermal, i.e. the highest flux is reached in the epithermal energy groups. Figure 4.5 depicts MSFR's relative neutron spectrum in the core at startup calculated by a radial XSDRN run at 1000 K and by scaling the flux such that its maximum is 1. Towards the reflectors and the fertile blanket, some thermal contribution to the spectrum exists as well.

Flowing fuel causes precursors to flow in and out of the core and reactor control benefits less from precursor decay outside the core. Figure 4.6 displays precursor densities across the fuel region at startup and the associated composition yields a delayed neutron fraction β of 310 pcm and an effective beta, i.e. β corrected for precursor decay outside the core, of 290 pcm.

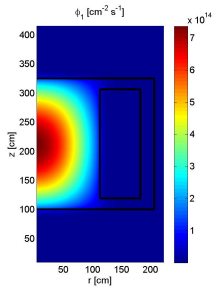

(a) 20 MeV - 1.4 MeV

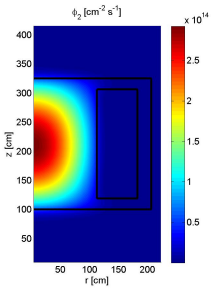

(b) 1.4 MeV - 1.01 MeV

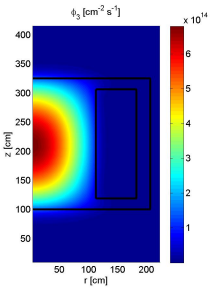

(c) 1.01 MeV - 573 keV

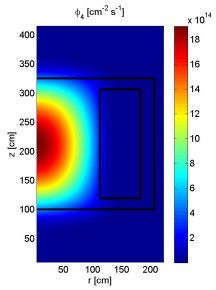

(d) 573 keV - 73 keV

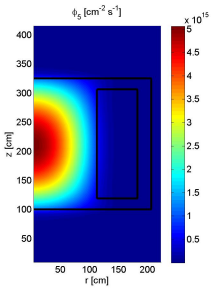

(e) 73 keV - 2.29 keV

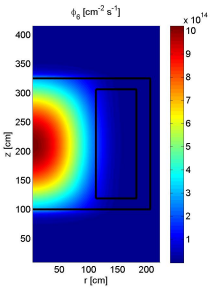

(f) 2.29 keV - 186 eV

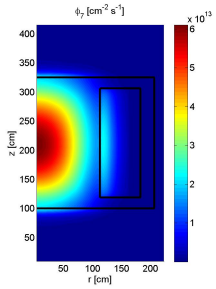

(g) 186 eV - 52 eV

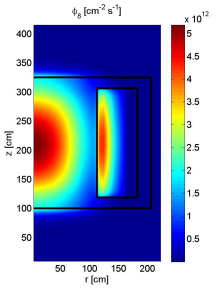

(h) 52 eV - 33.25 eV

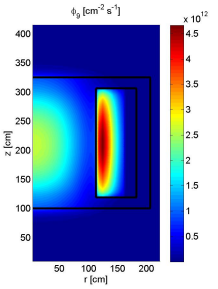

(i) 33.25 eV - 12.9 eV

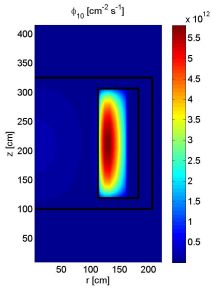

(j) 12.9 eV - 0.625 eV

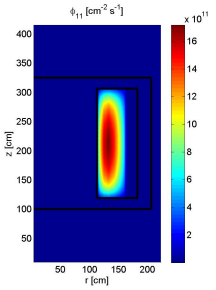

(k) 0.625 eV - 10 μeV

Figure 4.4: **Neutron flux as a function of space for every energy group.**

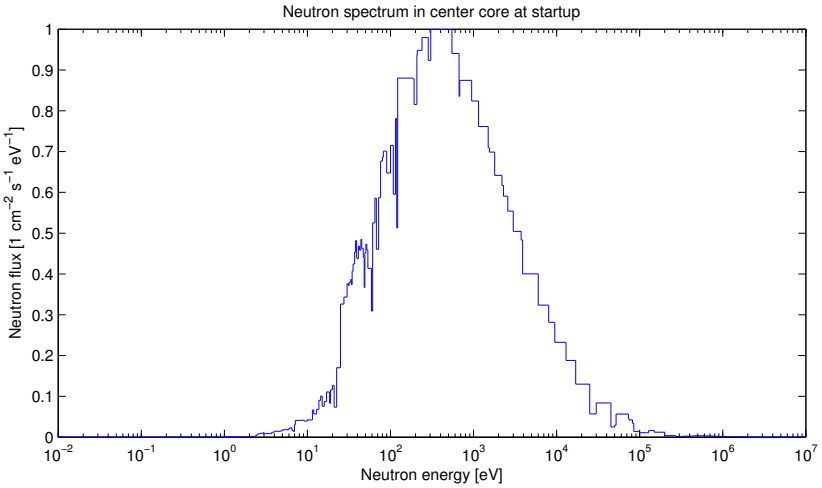

Figure 4.5: **MSFR's relative epithermal neutron spectrum at center core.**

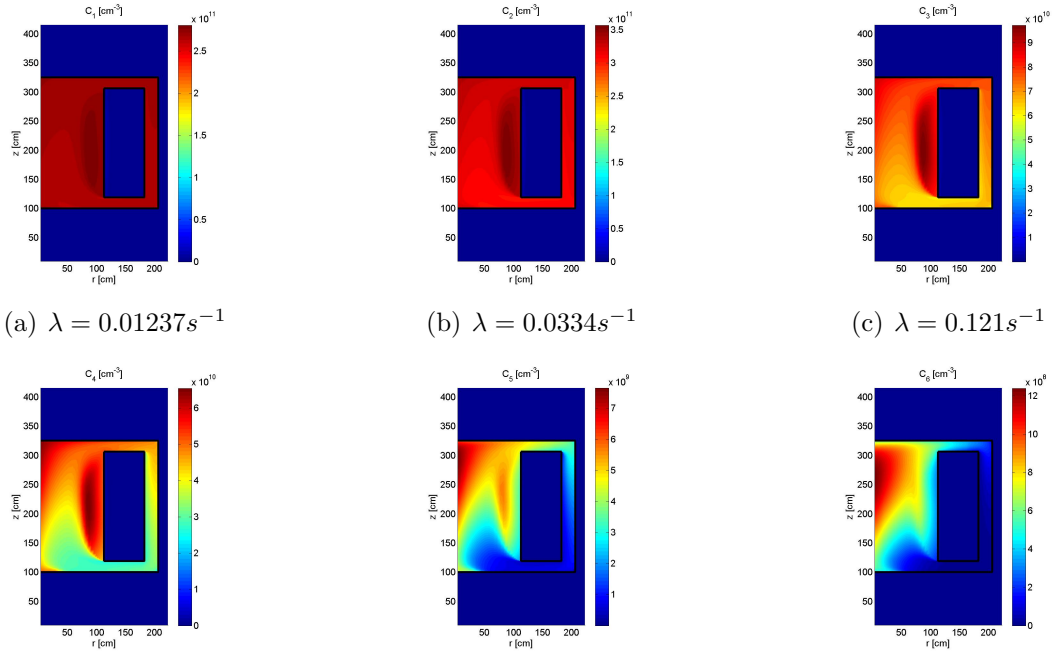

(a) $\lambda = 0.01237s^{-1}$ (b) $\lambda = 0.0334s^{-1}$ (c) $\lambda = 0.121s^{-1}$

(d) $\lambda = 0.321s^{-1}$ (e) $\lambda = 1.21s^{-1}$ (f) $\lambda = 3.29s^{-1}$

Figure 4.6: **Precursor distribution for six groups as function of space.**

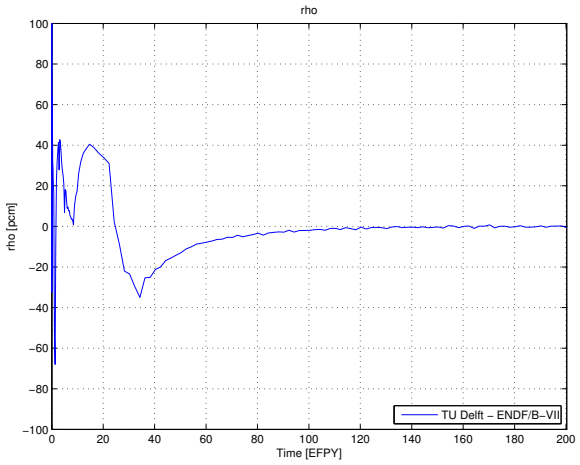

Figure 4.7: **Reactivity as a function of time.**

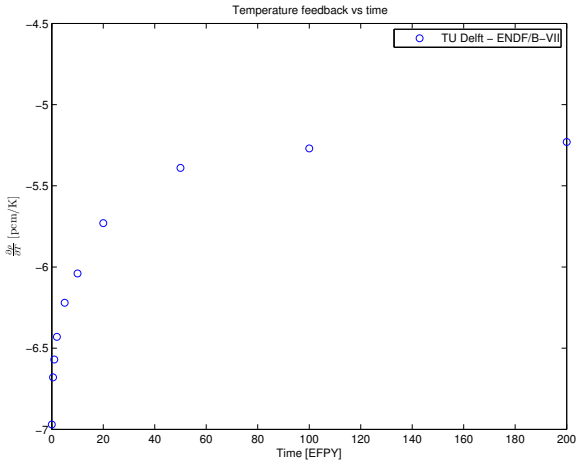

Figure 4.8: **Temperature feedback as a function of time.**

4.1.4 Composition evolution

As discussed in section 2.3 on page 17 a volume lumped parameter model is used to calculate the fuel salt composition as a function of time. In this model the fuel is considered homogeneously mixed, i.e. the density of nuclide A relative to the density of nuclide B does not depend on space, but temperature differences can induce slight spatial density variations. Depending on the nuclide, its cross sections are calculated either with the 'Exact', 'Approximate' or 'Coarse' method, which have been discussed in section 3.1.3 on page 29. In the Reference Configuration, two possible starting composition are considered. Only the ^{233}U started MSFR is considered in this project. To realistically calculate formation of fission products and actinides, the reactivity, displayed in figure 4.7, must be close to zero and during the simulation, it almost never exceeds 40 pcm in either direction. Figure 4.8 displays temperature feedback and suggests a reactivity of 40 pcm will induce a temperature difference of less than 10 K, shown in section 3.6 on parameter studies to be negligible for composition evolution calculations.

The total flux, as calculated by LOWFAT (discussed in section 3.4.1 on page 33) is another important parameter for burnup calculations and is visualized in figure 4.9.

Some of the actinides formed are fissile themselves and contribute to the fission power, of which ^{235}U and ^{239}Pu are the most important. Figure 4.10 displays the evolution of uranium, plutonium and americium concentration as well as evolution of ^{232}Th and ^{233}Pa. The results are in good agreement with results obtained by researchers from Politecnico di Milano (POLIMI)[a] who use a modified version of the Monte-Carlo based burnup tool 'SERPENT' for their calculations as well as the same cross section library (ENDF-B/VII). Only some difference between the ^{232}U and ^{242m}Am concentrations is observed. The ^{242m}Am concentration differs the most: POLIMI predicts 0.21 kg and TU Delft's prediction is 0.37 kg after 200 years of operation. This

[a]The results were provided by Manuele Aufiero of POLIMI's Energy Department.

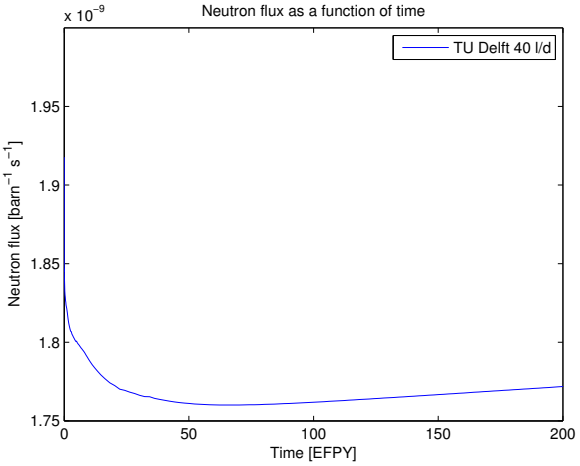

Figure 4.9: **Total flux in the fuel region.**

is probably due to uncertainty in the yield when ^{241}Am captures a neutron. As can be seen from figures 4.11 and 4.12, displaying dominant production routes for actinides, TU Delft's model has a yield of 8.6% for the transition from ^{241}Am to ^{242m}Am. However, if SCALE 6's PWRLib (a burnup library developed for thermal reactors) would have been used, the yield is 16.2%. Although the yield in POLIMI's model appears to be lower than in TU Delft's model and not higher, the large variation hints that another burnup library might use yet another value. The difference in the ^{232}U concentration probably has to do with the energy group structure. The (n,2n) reaction on ^{232}Th imperative for production of ^{232}U is a reaction with a threshold and if no energy boundary exists on this threshold, this introduces an error. Some substantial differences can be observed however with results obtained by LPSC[b] with cross section library ENDF/B-VI, especially with regard to uranium isotopes (mainly ^{234}U) and plutonium isotopes (mainly ^{238}Pu). Another difference is the expected conversion of thorium to uranium: LPSC's uranium feed is only 17 kg/y after 100 years of EFPY, opposed to 61.5 and 60.4 kg/y predicted by TU Delft and POLIMI respectively.

[b]The results were provided by Mariya Brovchen of LPSC.

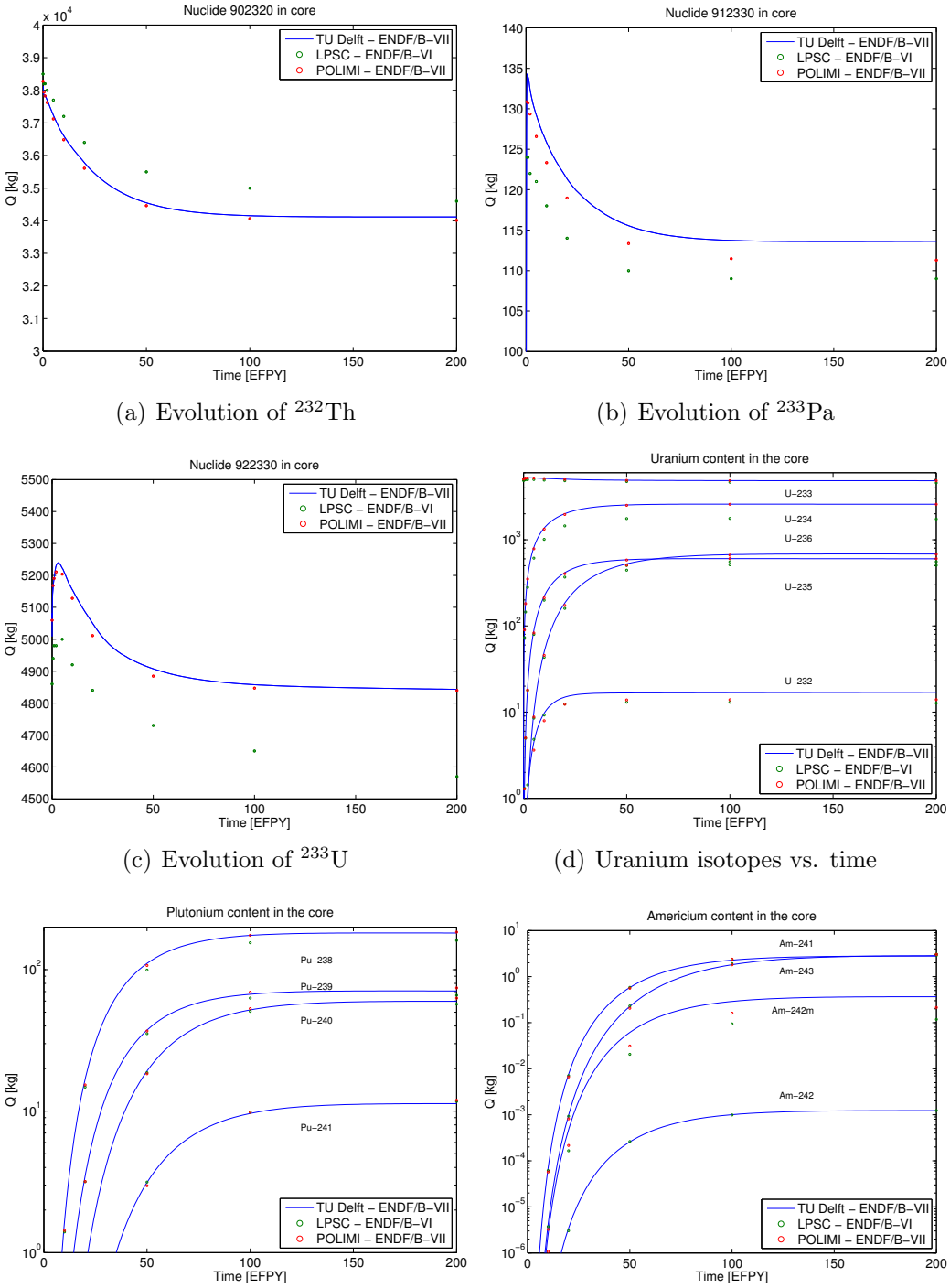

(a) Evolution of ^{232}Th

(b) Evolution of ^{233}Pa

(c) Evolution of ^{233}U

(d) Uranium isotopes vs. time

(e) Plutonium isotopes vs. time

(f) Americium isotopes vs. time

Figure 4.10: **Core composition as a function of time for nominal reprocessing of 40 l/d for TU Delft (ENDF/B-VII), POLIMI (ENDF/B-VII) and LPSC (ENDF/B-VI). ^{242}Am is not shown for POLIMI.**

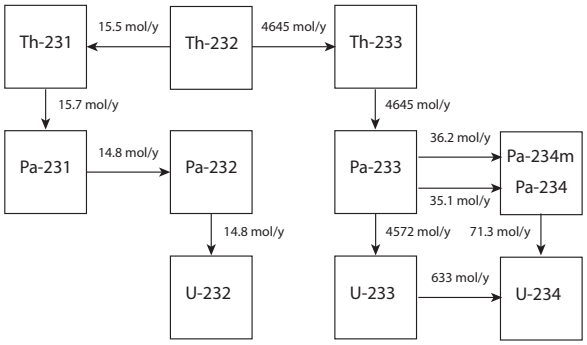

Figure 4.11: **Dominant production routes of isotopes from thorium up to ^{234}U as included in the TU Delft model.**

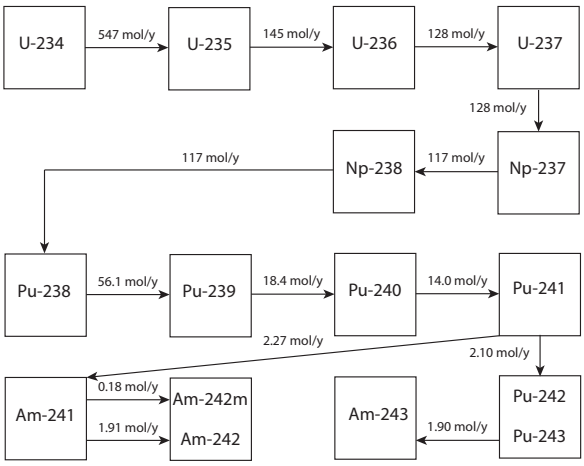

Figure 4.12: **Dominant production routes of isotopes from ^{234}U up to americium at equilibrium.**

4.2 Reprocessing scenarios

Previous section described results obtained with the nominal offline lanthanide reprocessing rate of 40 liters per day (l/d) of which the model is discussed in section 3.4.1 on page 33. The influence of this reprocessing rate on required feeding rates of thorium and uranium is investigated by changing this rate to 20 l/d and 60 l/d linearly in 10 weeks time after running for approximately 100 Equivalent Full Power Years. Figure 4.13 depicts the uranium quantity in the fuel region, i.e. core, external circuit and overflow tank, as well as the salt volume in the overflow tank and expected uranium and thorium feeds necessary to keep the fuel at its eutectic composition and the reactor critical.

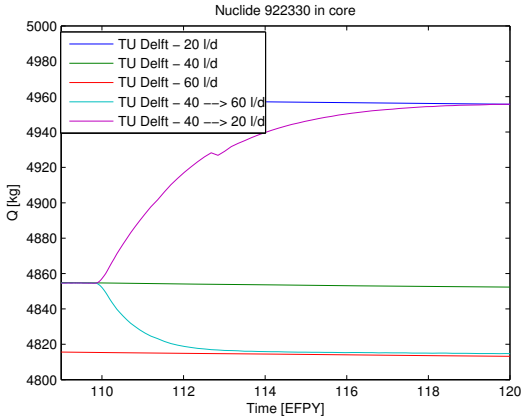

(a) ^{233}U concentration in the core

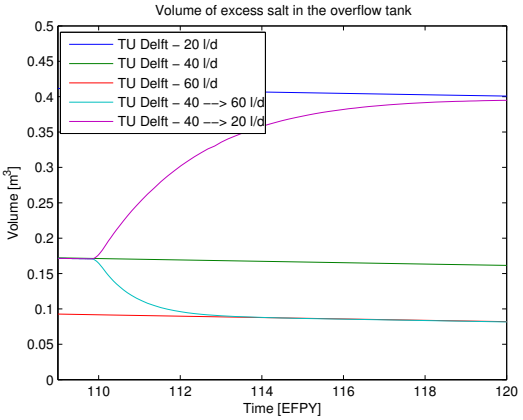

(b) Salt volume in the expansion tank

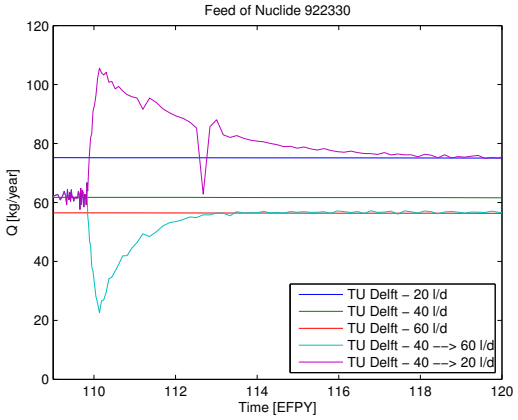

(c) ^{233}U feed to keep the reactor critical

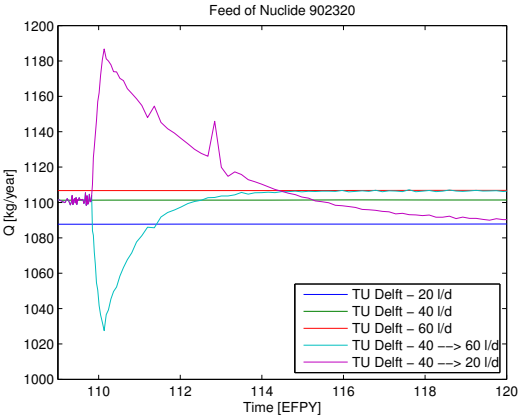

(d) ^{232}Th feed to keep the salt at its eutectic point

Figure 4.13: **Development of ^{233}U concentration and other quantities over time after a transient involving a change in the lanthanide reprocessing rate from 40 l/d to 20 and 60 l/d.**

Decreasing the reprocessing rate has an immediate and temporary as well as a belated and lasting effect. At first, the amount of fuel in the overflow tank increases rapidly due to decreased fission product removal requiring a large feed to not dilute thorium and uranium in the core. The extra fission products also absorb neutrons and the relative uranium concentration needs to be higher to compensate for this increased neutron loss, decreasing the thorium concentration in the process (the heavy metal concentration is maintained at the eutectic point, 22.5 mol%). As a consequence the internal production of uranium drops requiring a lasting increased feed. The thorium feed also increases at first, but stabilizes at a lower level than before the transient due to decreased thorium demand. An increase in reprocessing rate has exactly the opposite effect: less material is needed at first and the uranium feed stabilizes at a lower level than before the transient while the thorium feed does so at a higher level. In this domain, the offline lanthanide reprocessing rate does not influence the decay heat after shutdown and thus does not form a potential safety risk.

For a reprocessing rate of 20 l/d, the uranium feed equals 75 kg/y, while for reprocessing rates of 40 and 60 l/d, the feed is 61.5 kg/y and 56.3 kg/y respectively. Therefore decreasing the reprocessing rates from 60 l/d to 20 l/d, increases the necessary uranium feed by 33% on top of a one time supply of 142 kg ^{233}U. The feed of fissile material can thus be increased or decreased very rapidly by changing the reprocessing rate.

The wobbly behavior of the feed just prior to the transient is a result of the very short burnup step used there (1 week). A peak in the uranium and thorium feed can also be observed, which is the result of either a small deviation in the calculated feed or a small deviation (35 pcm) in the k_{eff} calculated by DALTON. Its influence on the results is negligible.

Note the rather large uncertainty in the absolute value of the uranium feed with respect to the cross section library used as it is the amount of fissile material not produced in the core, as shown in the following rough calculation. Using a burnup value at equilibrium of 1000 GWd/tHM, the MSFR fissions approximately 1 ton of fissile material per year, but produces approximately 940 kg/year requiring a feed of 60 kg/y. An uncertainty in the production of uranium of 1% then results in an uncertainty in the feed of approximately 15%. This uncertainty grows as the MSFR's conversion ratio comes closer to unity. As discussed in the previous section, POLIMI, using the same cross section library, predicts a uranium feed of 60.43 kg/y opposed to LPSC's prediction, using ENDF/B-VI instead of ENDF/B-VII, of 17 kg/y (both after 100 EFPY).

4.3 Nuclear waste and radiotoxicity

Nuclear waste and its associated (radio)toxicity is one of people's main concerns regarding nuclear energy. The thorium fuel cycle greatly reduces the amount of waste compared to 'traditional' Boiling Water Reactors (BWRs) or Pressurized Water Reactors (PWRs). The MSFR has great potential in further reducing the amount of nuclear waste, due to its capability to 'burn' higher actinides as found in waste from mentioned reactors. As discussed in section

2.4 on page 20 radiotoxicity of waste from a nuclear power plant, due to ingestion, is evaluated in Sieverts (per GWy) and compared with the radiotoxicity of the uranium or thorium ore needed to produce the fuel. The radiotoxicity of natural uranium and thorium ore (i.e. 99.27% ^{238}U, 0.7% ^{235}U and 0.0054% ^{234}U for natural uranium and 100% ^{232}Th for natural thorium [26]) is displayed in figures 4.14 and 4.15, as well as the main contributors to its long term toxic behavior.

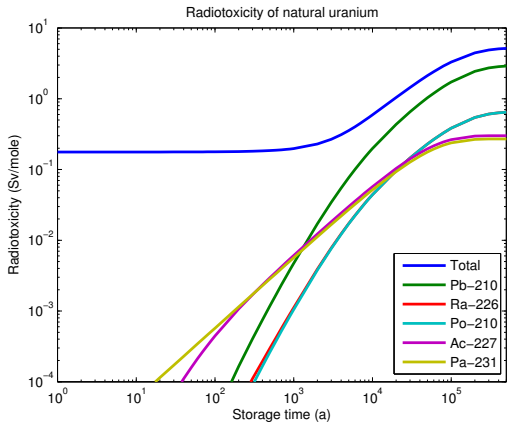

Figure 4.14: **Radiotoxicity of natural uranium due to decay of its components and daughter elements.**

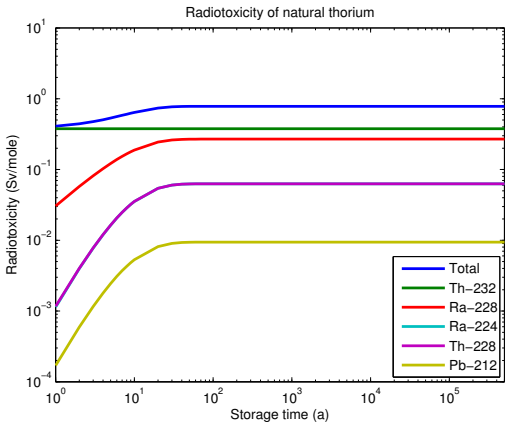

Figure 4.15: **Radiotoxicity of natural thorium due to decay of its components and daughter elements.**

It can be clearly seen both thorium and uranium become more radiotoxic as time progresses due to decay of daughter products and radioactive waste is compared with the long term radiotoxicity of the ore. The thorium feed in the MSFR is approximately 1100 kg/year, and equals to a demand of 4.33 mol/GWd, combined with a radiotoxicity of 0.78 Sv/mole yields 3.38 Sv/GWd ($= 1.23 \cdot 10^3$ Sv/GWy). The waste is also compared with nuclear waste from a PWR, using a typical burnup value of 50 GWd/tU, one 18 month cycle without multi-recycling and an enrichment of 4% (the depleted uranium still has 2% ^{235}U), as well as with the radiotoxicity of uranium ore needed to generate 1 GWy of thermal energy in that PWR. Following the same procedure as for thorium and a radiotoxicity of 5.15 Sv/mol yields $1.28 \cdot 10^6$ Sv/GWy for uranium ore.

An important distinction between traditional nuclear power plants and the MSFR is near closure of the fuel cycle. In principle, the fuel salt can be used indefinitely and as a consequence, long lived radiotoxic waste from actinides does not need to exist, but it can, however, be created in two ways. Inefficiencies in the offline lanthanide reprocessing due to chemical similarities between reprocessed lanthanides and actinides, will result in some actinide waste and are neglected in this project. The other course of action resulting in this type of waste would be to not use the salt anymore and 'declare' it as such, unlike fission products which are separated from the salt continuously. In case of the MSFR at equilibrium, the amount of

reprocessed fission products must equal the amount of actinides (in this project thorium and uranium) fed into the core, i.e. approximately 1170 kg/y. Figure 4.16 displays waste due to reprocessing of fission products (including major short term contributors) for 20, 40 and 60 l/d as well as long term contributors for 40 l/d. The radiotoxicity of MSFR's nuclear waste does not vary for the considered reprocessing rates. This is due to the fact that reprocessing of the main contributors to radiotoxicity like ^{99}Tc is their dominant removal route, and, since production stays equal, the concentration in the core will rise if reprocessing is decreased, such that the total removal rate is only a little less. After approximately 300 years, the radiotoxicity is decreased to the level of uranium ore. Figures 4.17 and 4.18 display the radiotoxicity of actinides and fission products resulting from the described PWR (50 GWd/tU burnup). Per GWy, the radiotoxicity of MSFR's reprocessed fission products is actually higher than that of a PWR, due to the fact that fission products with a high specific radiotoxicity as well as a substantial absorption cross section, like ^{99}Tc, do not 'burn', but are removed from the system instead.

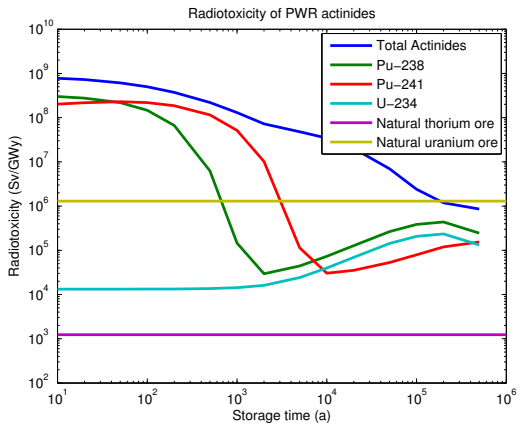

Figure 4.17: **Actinide waste of PWR with a burnup of 50 GWd/tHM after five years of cooling, without recycling.**

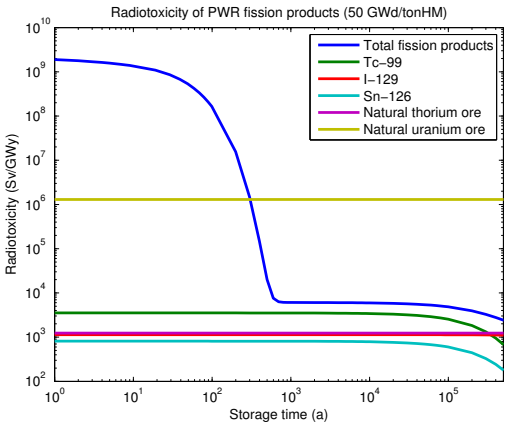

Figure 4.18: **Radiotoxicity of fission products from PWR fuel with a burnup of 50 GWd/tHM.**

Suppose, for some reason, the fuel salt is not reused, then the total inventory is waste. There will still be fission products in the core, as well as a large amount of actinides which will have to be stored. Figure 4.19 displays fission product waste as well as actinide waste per installed gigawatt of thermal power for the 40 l/d scenario. If the reactor starts with fresh fuel, then after 200 years of operation the inventory is slightly more radiotoxic than after 60 years due to formation of some higher actinides, which tend to be more radiotoxic. Fission products in the inventory do not significantly contribute to the total radiotoxicity as they are relatively less radiotoxic and the quantity is little compared to fission products extracted by reprocessing (the inventory equals 210 kg/GW, while reprocessing of fission products yields 390 kg/GWy).

In the MSFR, radiotoxicity of actinide waste does not diminish as much as the PWR's (due

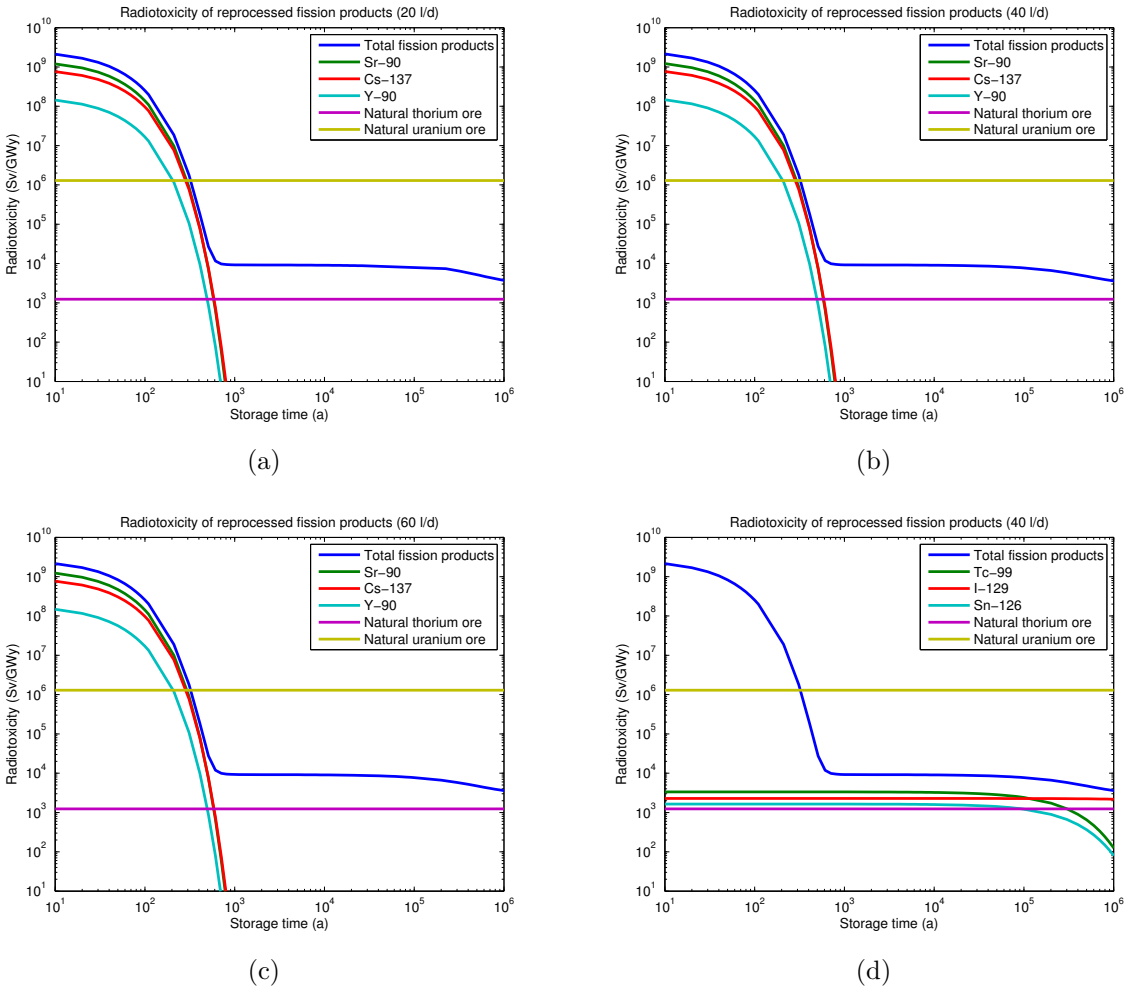

Figure 4.16: **^{90}Sr, ^{137}Cs and ^{90}Y are responsible for the relatively high radiotoxicity for the first hundreds of years, while ^{99}Tc, ^{129}I and ^{126}Sn determine radiotoxicity in the long term.**

to ^{233}U and ^{234}U) but is formed only in comparatively little quantities, when the fuel salt is not reused. Considering spent nuclear fuel after 10 years of cooling, one could only operate the PWR used in this case study for 13.6 years to obtain the same amount of radiotoxicity as the total actinide inventory of the MSFR, consisting of 9.1 tons of uranium and transuranic elements and 34.4 tons of thorium at equilibrium. Due to relative fast decay of ^{238}Pu (the main plutonium isotope in the MSFR), this ratio further improves to only 1.4 years after 1000 years, to then deteriorate to 63 and 174 years after $50 \cdot 10^3$ and $5 \cdot 10^5$ years respectively.

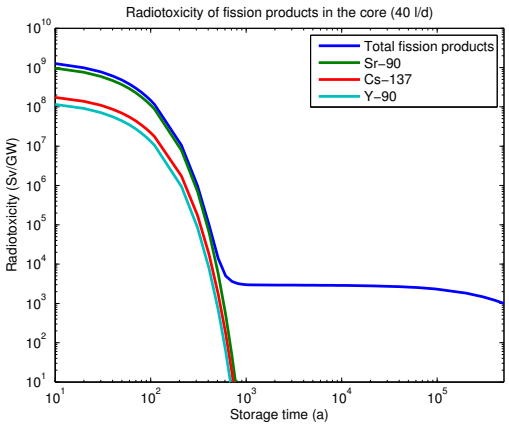

(a) Reprocessing rate is at 20 l/d.

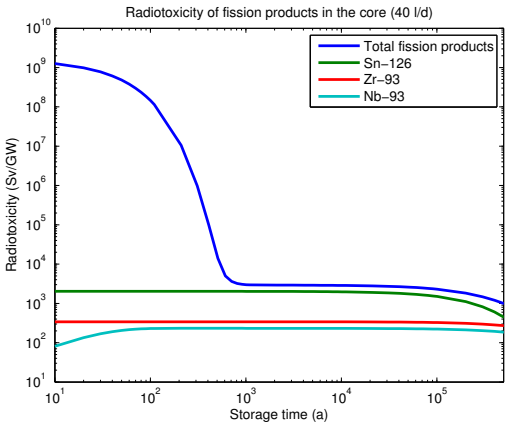

(b) Reprocessing rate is at 40 l/d.

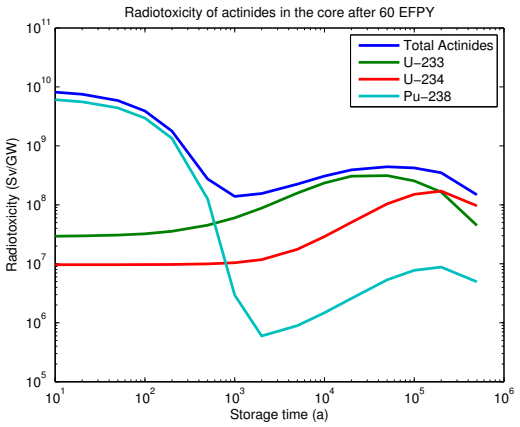

(c) Actinide radiotoxicity after 60 years of operation.

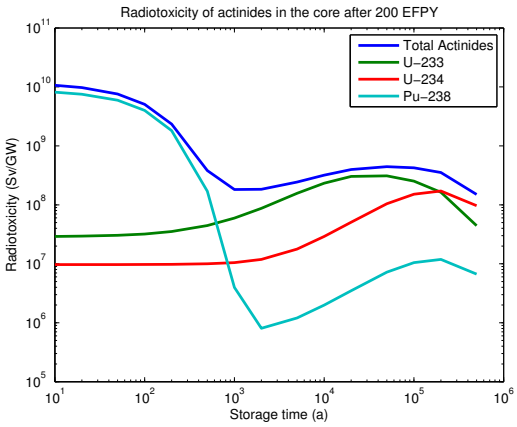

(d) Actinide radiotoxicity after 200 years of operation.

Figure 4.19: **Radiotoxicity of the inventory per installed GW of thermal power capacity. Only the 40 l/d scenario is shown.**

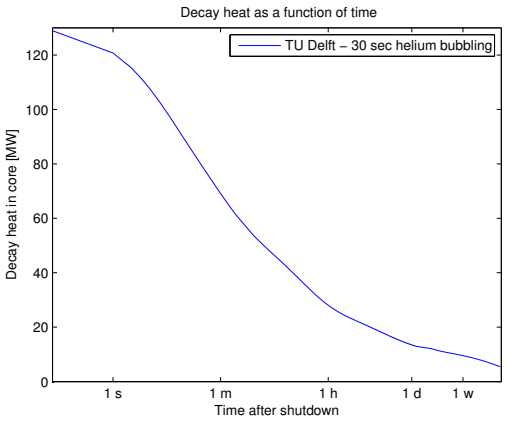

Figure 4.20: **Decay heat as a function of time after shutdown is homogeneously distributed over the salt's volume. Helium bubbling lowers the initial rate.**

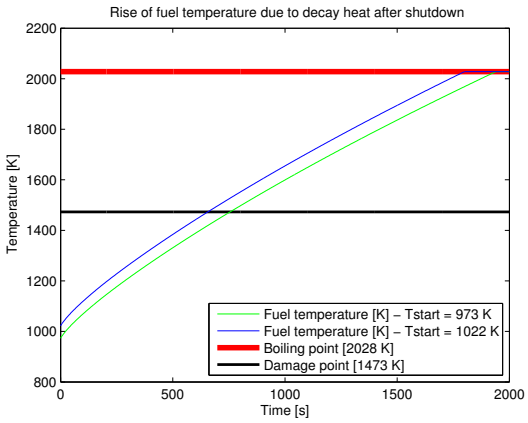

Figure 4.21: **Due to decay heat, the fuel temperature rises from either 973 K (in between the inlet and outlet temperature) or 1022 K, the outlet temperature.**

4.4 Decay heat and core draining

Heat produced by decay of fission products and actinides is a major safety concern in a nuclear power plant due to necessary prolonged cooling after shutdown. In a typical PWR using UO_2 as fuel, decay heat at shutdown is approximately 6% of nominal power, i.e. 180 MW_{th} for a 3 GW_{th} reactor (as is the MSFR). The decay heat as a function of time after shutdown is thus an important parameter in a safety assessment of a nuclear reactor. The situation in a MSFR differs from a PWR, as fission products and actinides are dissolved in the salt and non soluble fission products are continuously reprocessed by means of helium bubbling. Therefore, some of the decay takes place outside the core in the reprocessing facility. The model predicts decay heat for the nominal scenario (effective half life due to helium bubbling of 30 sec, and 40 l/d reprocessing for soluble fission products) to be only 4.3% of nominal power directly after shutdown, or approximately 128 MW_{th}, which is in close agreement with results obtained by POLIMI and LPSC predicting 4.3% as well [1]. The temperature increase associated with the decay heat will determine whether it is feasible to use freeze valves to drain the core in case of an emergency, as were used in the MSRE [21]. Figure 4.20 displays decay heat as a function of time after shutdown at $t = 0$, i.e. the flux is zero for $t > 0$.

Although the salt is already in a molten form and a meltdown cannot occur, the salt's boiling point of 2028 K should never be reached[c]. Damage to reactor systems will occur earlier, at around 1200 °C (1473 K) [4] and the safety system is required to drain the fuel before this point is reached. The most recent finding concerning the heat capacity of LiF-ThF_4 (22.5 - 77.5 mol%), although experimental data is scarce, is 1.049 J kg^{-1} K^{-1} [8]. In the Reference Configuration

[c]Calculated by Ondřej Beneš of the Institute for Transuranium Elements (ITU) in Karlsruhe, Germany.

design, a large hotspot exists, increasing the MSFR's average fuel temperature. Curved reactor boundaries will minimize recirculation zones and therefore reduce the average temperature. On the assumption a more optimal geometry will be found[30], two starting temperatures have been chosen: 700 °C (973 K), halfway between the inlet and outlet temperature, and 750 °C (1022 K), the outlet temperature, which approximately equals the average temperature in the core in the current geometry. At t=0, the prompt fission power instantaneously drops to zero, leading to the rise in temperature depicted in figure 4.21. The calculations are conservative as heat loss is not modeled. The 'damage' point is reached in approximately 11 minutes, while the boiling point is then reached after 30 minutes.

To determine the feasibility of a freeze valve, draining the core is analyzed in three scenarios using theory discussed in section 2.5 on page 21. Every time the reactor is modeled as a cylinder with an equal height and volume as the reactor itself, but with different methods of draining, i.e. through a pinhole, a pipe and a pipe with a freeze valve, as displayed in figure 4.22. For all geometries, the velocity at the exit is given by equation 4.1.

$$v_2 = \sqrt{\frac{2gh}{1 + 4f\frac{L}{D} + K_{w,tot}}} \tag{4.1}$$

In the 'pinhole' scenario friction is neglected, i.e. the fuel velocity in the pinhole is dependent only on the fuel level $h(t)$ and the denominator in the square root is 1. In the scenarios with a pipe and with a pipe and a freeze valve, friction is taken into account and is dependent on the velocity itself, a Fanning friction factor (which is chosen conservatively, but constant, $4f = 0.032$) and the geometry. All pipes are 1 meter long and have a 'free jet' (frictionless) exit. This approach to model friction is valid only if Reynolds number $> 10^5$ and for all geometries which could reasonably be used in reality, this is the case.

Draining starts at t=0 when the valves open immediately and driven by gravity the fuel flows in the drainage tanks. Figure 4.23 displays the fuel height as a function of time for different pinhole diameters. On the basis of these calculations, a pinhole diameter of 10 cm empties the reactor in 11.5 minutes. In the actual geometry, a 1 meter thick reflector is at the bottom of the reactor core and no room for a drainage tank exists. Besides, attaching a pipe will decrease the time needed to drain the reactor. Figure 4.24 displays the fuel level as a function of time for different pipe diameters. A pipe with a diameter of 10 cm drains the core in 8.5 minutes, well below the damage point.

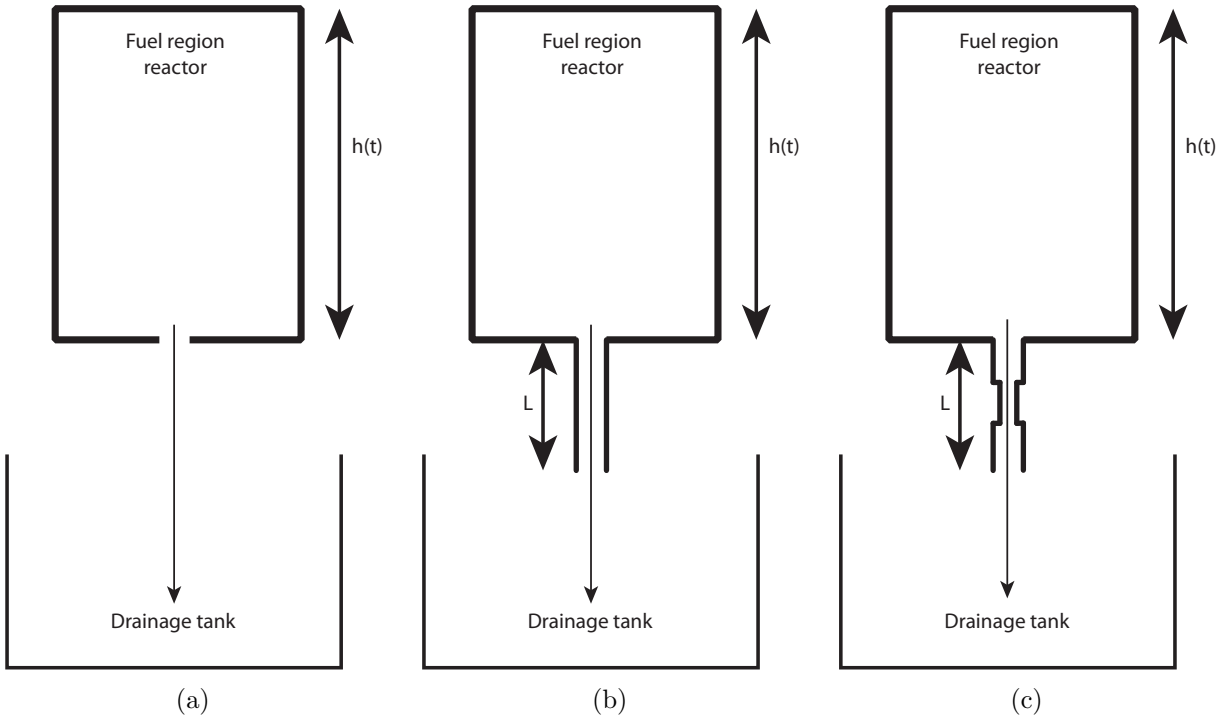

Figure 4.22: **The fuel is drained in different cylindrical configurations: through a pinhole (a), a pipe with a mechanical shutter (b) and a pipe with a freeze valve (c)**

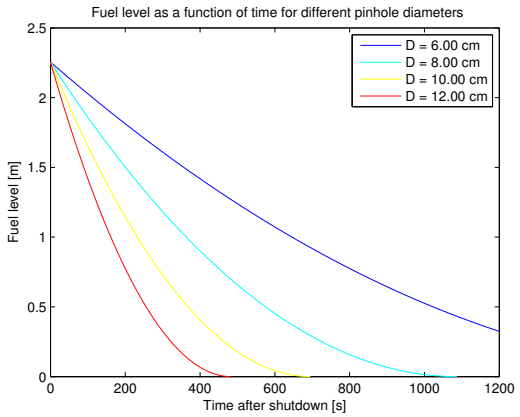

Figure 4.23: **The fuel level as a function of time for different pinhole diameters.**

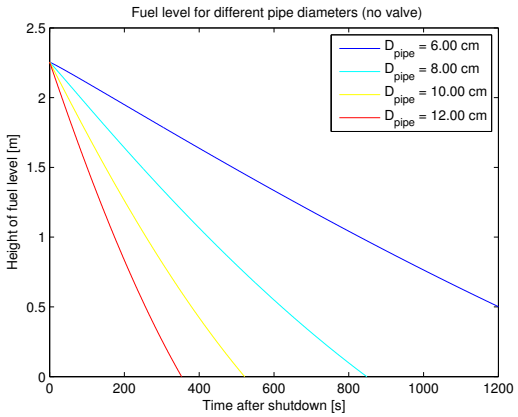

Figure 4.24: **Fuel level as a function of time for different pipe diameters.**

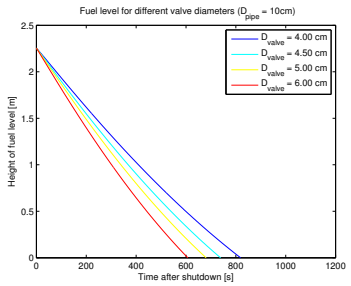

Figure 4.25: **Fuel level as a function of time for different valves.**

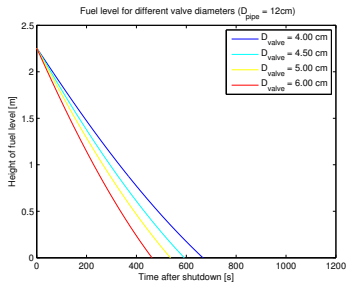

Figure 4.26: **Fuel level as a function of time for different valves.**

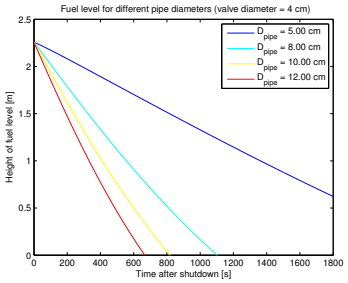

Figure 4.27: **Fuel level as a function of time for different pipes.**

The MSRE used freeze valves of cooled and solidified salt as a plug which could be thawed in case of an emergency. This valve is modeled as a sudden and short contraction in the pipe, as indicated in figure 4.22. Using different pipe and valve diameters, the fuel height as a function of time is modeled and depicted in figures 4.25 through 4.27.

The pipe diameter is still dominant in determining the drainage time, but the freeze valves cause considerable friction and thus delay. Many combinations of valve and pipe diameters would drain the reactor within 10 minutes, as can be seen from the pictures. However, thawing the valve will be the biggest challenge. In the MSRE, the freeze valves could be thawed by either heating them up, or by just stopping the cooling (for instance due to a power outage). In the latter case, thawing would take a bit less than 15 minutes[21], which is too long for use in the MSFR. A mechanical valve, which should require electricity to keep it shut, should be developed and used, unless this thawing time can be greatly reduced.

The pipe length also influences the drainage time greatly and it could in theory be made longer. To address this possibility, figure 4.28 displays the time needed to completely empty the reactor as a function of the length of a pipe with a diameter of 12 cm.

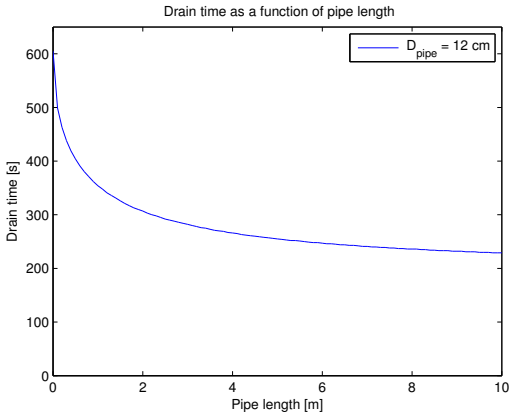

Figure 4.28: **Time to completely drain the reactor for different pipe lengths.**

Chapter 5

Conclusions, discussion and recommendations

5.1 Neutronic benchmark results

The newly developed burnup tool for the MSFR predicts evolution of the fuel composition taking into account online reprocessing and feeding of nuclides in accordance with Monte Carlo simulations performed by Politecnico di Milano (POLIMI) with SERPENT, except for differences in the concentration of ^{232}U and ^{242m}Am. The first discrepancy is due to a not accurate enough description of the fast flux for the important (n,2n) reaction, while the latter is caused by uncertainty in the yields of the transition from ^{241}Am to ^{242m}Am and ^{242}Am. TU Delft's results do not change by increasing resolution in other investigated parameters, including the temperature distribution and size of the burnup step. Because ^{232}U is an important nuclide to evaluate MSFR's proliferation resistance and shielding requirements in the reprocessing facility, a good agreement between different simulations is desirable. In general, the main issue concerning validity of fuel evolution results is the nuclear data used. The capture and fission cross sections (and their ratio) of ^{233}U are quantities needing investigation in order to yield more realistic results, as illustrated by the discrepancy in the ^{234}U concentration found when using the ENDF-B/VII library (TU Delft) or the ENDF-B/VI library (LPSC). A master burnup library with yields and cross sections corresponding more closely to those of the MSFR would increase validity of the results as well.

During the project, some safety aspects were examined and the 'temperature coefficient of reactivity' forms a major part, starting low at -6.95 pcm/K for the MSFR when the core is fresh and as the fuel salt approaches equilibrium the coefficient slightly rises to -5.27 pcm/K, thus remaining strongly negative throughout operation. Flowing fuel causes the effective delayed neutron fraction β_{eff} to be a bit lower than β itself: 290 pcm and 310 pcm at startup respectively. In order to properly investigate β_{eff} for other fuel compositions than the starting composition as well, the neutronic diffusion code DALTON, needs to be adjusted slightly. For safety transients

in which decay heat or changes in fission power are important, DALTON could be updated to include more accurate energy-per-fission and decay heat data, calculated by LOWFAT, the module responsible for burnup calculations.

Another possible addition is modeling of burnup in the fertile blanket, in which formed fission products will have a small influence on the required feeding rates in the core. It would then be possible to evaluate uranium production in the fertile blanket and the true breeding performance.

5.1.1 Recommendations

1. If DALTON would include LOWFAT's energy-per-fission and decay heat data, as well as taking into account fission from multiple actinides to calculate the source in the precursor equations, more realistic (safety) transients could be performed.

2. Differences in the ^{232}U and ^{242m}Am concentration between POLIMI's and TU-Delft's model are probably due to a not accurate enough description of the fast flux and uncertainty in the yield of neutron capture in ^{241}Am, respectively. Noting the importance of ^{232}U concerning proliferation resistance and shielding requirements in the reprocessing facility, further investigation is welcomed.

3. Incorporate burnup in the fertile blanket as well to assess the full breeding capabilities of the MSFR.

4. Study the amount of displacements per atom in the structural material to evaluate its radiation resistance.

5. More accurate nuclear data, especially for the main actinides in the thorium fuel cycle, would greatly increase the validity of the results. More research is needed.

5.2 Reprocessing scenarios

Changing the online fission product reprocessing rate during operation has an immediate and temporary effect on required feeding rates of thorium and fissile material, as well as a delayed and lasting effect. At first, the change in the amount of fission products requires either a one time additional thorium and uranium supply or the opposite, depending on whether the reprocessing rate is lowered or increased, respectively. Changing the rate from 20 liters per day (l/d) to 60 l/d results in a 142 kg ^{233}U inventory excess, which need not supplied extra to the core. The same transient also changes the equilibrium feeding rate from 75 kg/y ^{233}U to 56.3 kg/y, a difference of 25%. The transition investigated here, is a very rapid change in the reprocessing rate. If the change is distributed over a longer time period, then there must exist a function of time, describing the reprocessing rate, which changes the required feeding rate of

fissile material with a step function. For the thorium feed, the effect is small (approximately 2%) and reversed, i.e. if a smaller feed is desired, the feed first increases before decreasing to the new steady state level. All transients take in the order of years to fully set to their new level. Changing the offline reprocessing rate is thus an effective way to influence the required fissile material feeding rate.

Keeping in mind studies[7] showing the possibility of a TRU-started MSFR, changing the feed of fissile material from ^{233}U to a TRU-mixture composed of long-lived waste from current nuclear power plants, will avoid the problem of natural unavailability of ^{233}U and further utilizes MSFR's capability to 'burn' existing waste stockpiles, greatly enhancing sustainability of nuclear power. The reactivity worth of available TRU mixtures is less than pure ^{233}U and therefore the TRU feed will be significantly higher than the ^{233}U feed analyzed in this project. The reactor operator might wish to change the TRU-feed to the reactor depending on future demand of this resource (i.e. nuclear waste) and on the aim or desire to decrease stockpiles. Results obtained in this project attest to MSFR's range of operating possibilities providing this flexibility.

A comprehensive study into the effects of different (TRU-) feeds (both in quantity and composition) would be an interesting follow up to this project. Nuclear waste as a resource of fissile material comes in many isotopic compositions depending on its burnup, number of cycles in the core, reprocessing, storage time and initial composition and influences the higher actinide composition in the MSFR as well as feedback coefficients and β. For some higher actinides, feeding of the isotope will be greater than internal production. Also, solubility limits of for instance plutonium should not be reached.

5.2.1 Recommendations

6. Changing the MSFR model from ^{233}U to TRU-started will result in insight into increased sustainability aspects.

7. Perform a comprehensive investigation into the impact of feeding with different TRU-mixtures into for instance safety features (delayed neutron fraction and feedback coefficients) or isotope accumulation.

5.3 Nuclear waste and radiotoxicity

In an ideal situation where reprocessing of fission products is 100% efficient, i.e. only lanthanides are removed from the core, no long-lived actinide waste need to exist and nuclear waste is thus composed of fission products removed from the core only. The radiotoxicity of reprocessing waste is influenced only a little by the offline lanthanide reprocessing rate and amounts to approximately 390 kg/GWy, the same as for a PWR of the same size. The fission products of the MSFR are however slightly more radiotoxic than those of a PWR, due to the fact that

elements with a high specific radiotoxicity and large absorption cross section are not transmuted in the reactor. Fission products extracted from the MSFR reach radiotoxicity levels of the equivalent amount of natural uranium ore to produce the same quantity of thermal energy in a PWR after approximately 700 years. At first, ^{90}Sr, ^{137}Cs and ^{90}Y form the large part of overall radiotoxicity, but in the long term (i.e. longer than 700 years), ^{99}Tc, ^{129}I and ^{126}Sn determine the waste's radiotoxicity.

However, since the lanthanide and actinide series are chemically similar, offline reprocessing of fission products might prove difficult, if not impossible, to implement without actinide contamination, which will thus form some small quantities of actinide waste. Depending on the size of these inefficiencies, actinide waste may be a significant or prevailing source of long term waste for the MSFR and further investigation of this issue is thus important to fully evaluate MSFR's waste profile.

Once a decision is made to not reuse the fuel salt, the complete inventory at the end of reactor life, consisting of salt, fission products and actinides, should be considered nuclear waste. Per gigawatt of installed thermal power, the MSFR has an inventory of uranium and transuranic elements of 3 tons/GW and including thorium, associated radiotoxicity is $1.06 \cdot 10^{10}$ Sv/GW after ten years of cooling. A traditional PWR produces this amount of radiotoxicity in 13.6 years of operation, although this ratio depends on the time after shutdown due to different decay rates of the components. Radiotoxicity of MSFR's actinides does not diminish as much as PWR's waste does, mainly due to increasing radiotoxicity of decay products of ^{233}U and ^{234}U. All calculations were performed with data according to ICRP 61. It would be prudent to update the data to the latest version.

5.3.1 Recommendations

8. Evaluate the influence of likely inefficiencies in the offline lanthanide reprocessing procedure on MSFR's nuclear waste, possibly in combination with recommendation 7.

9. Update radiotoxicity values to the latest report formulated by the International Commission on Radiological Protection (ICRP).

5.4 Decay heat and draining the core

Decay heat calculations are in good agreement with both POLIMI and LPSC[1], paving the way for performing transients in which decay heat plays a large role, like an 'Unprotected Loss Of Heat Sink' (ULOHS) accident or shutting down the reactor. In this project, feasibility of the freeze valve, used in the MSRE and often cited as a passive safety system for Molten Salt Reactors, was investigated by comparing the predicted temperature rise with what is maximum allowed. Solely due to decay heat, the fuel salt reaches this point of 1473 K, when reactor components start to damage, in only 11 minutes and the salt's boiling temperature of

2028 K in exactly 30 minutes. Freeze valves used in MSRE needed a little less than 15 minutes to melt if no external heat was added and due to this effect alone, the freeze valve's effectiveness in draining MSFR's fuel salt within the required time frame is questionable. A 1 meter long pipe with a diameter of 10 centimeters combined with a mechanical valve requiring electricity to be kept closed, drains the fuel salt in 8.5 minutes, well below the damage point.

However, a wider pipe might be desirable because of other possible scenarios in which the fuel salt will heat up more quickly, like the mentioned ULOHS combined with failing SCRAM mechanisms. In such a scenario, fission power will not be zero and will only be forced down by a temperature increase, which will be significantly more rapid. Probably, a wider (and longer) pipe will be able to drain the fuel salt quickly enough.

5.4.1 Recommendations

10. Perform a more realistic assessment of accident scenarios, most notably a ULOHS-accident to determine the maximum possible temperature increase rate. In this investigation, a more optimal geometry (i.e. no or less hotspots) should be considered as well as heat mixing effects due to natural circulation and residual flow.

A EVOL Reference Configuration

MOLTEN SALT FAST REACTOR

Reference configuration – 15th of March, 2012

The reference MSFR is a 3000 MWth reactor with a fast neutron spectrum and based on the Thorium fuel cycle. It may be started either with ^{233}U, enriched U or TRU elements as initial fissile load.

1 Reactor geometry

1.1 System description

The fuel salt flows upward in the active core until it reaches an extraction area which leads to salt-bubble separators through salt collectors. The salt then flows downward in the fuel salt heat exchangers and the pumps before finally re-entering the bottom of the core through injectors. The injection / extraction of the salt is performed through pipes of ~30 cm of diameter. This very simplified vision of the injection / extraction has to be improved during the EVOL project.

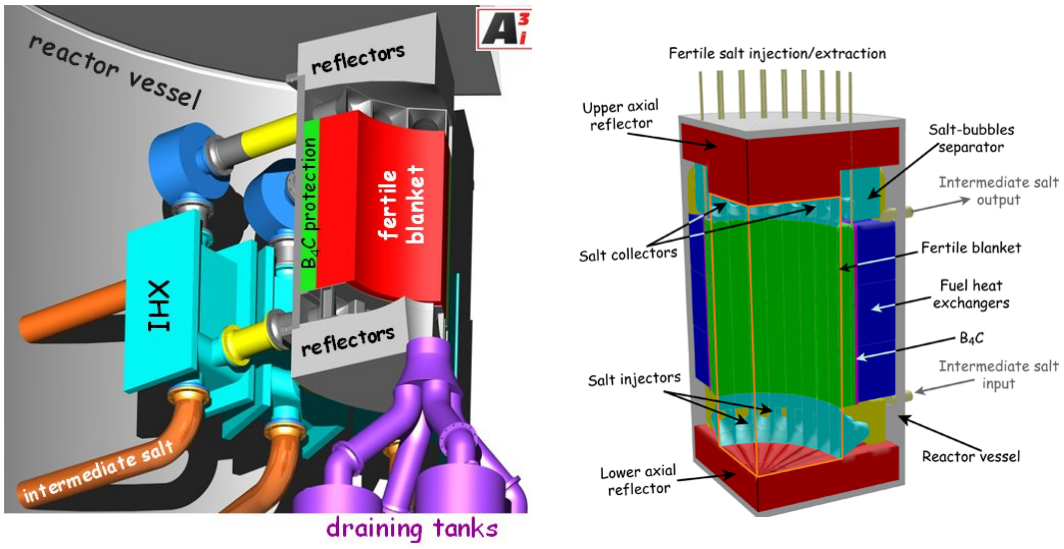

Fig. 1 (Left): *Global view of a quarter of the reactor vessel including the fertile blanket (red), the B_4C protection (green), the structure in Ni-based alloy (grey), the heat exchangers (pale blue) and the draining tanks (purple) -* ***(Right):*** *Schematic view of a quarter of the MSFR, the fuel salt (not represented here) being located within the orange lines*

The external circuit (salt collector, salt-bubble separator, heat exchanger, pump, salt injector and pipes) is broken up in 16 identical modules distributed around the core, outside the fertile blanket and within the reactor vessel. The external circuit is divided in

two parts: the pipes (including the salt-bubble separator, the pump and the injector) and the heat exchanger. The distribution of the salt between these two parts is chosen so as to minimize the pressure drops in the circuit. The fuel salt runs through the total cycle in 3,9 seconds. The salt circulation being considered uniform, the residence time of the salt in each zone of the circuit and the core is proportional to the volume of this zone.

The total fuel salt volume is distributed half ($9m^3$) in the core and half ($9m^3$) in the external circuit.

The external core structures and the heat exchangers are protected by thick reflectors (1m height for the axial reflectors) made of nickel-based alloys which have been designed to absorb more than 99% of the escaping neutron flux.

1.2 Core geometry

As shown in Fig. 2, the core is a single cylinder (the diameter being equal to the height) where the nuclear reactions occur within the flowing fuel salt. The core is composed of three volumes: the active core the upper plenum and the lower plenum. The fuel salt considered in the simulations is a binary salt, LiF - (Heavy Nuclei)F_4, whose (HN)F_4 proportion is set at 22.5 mole % (eutectic point), corresponding to a melting temperature of 565°C. The choice of this fuel salt composition relies on many systematic studies (influence of the chemical reprocessing on the neutronic behaviour, burning capabilities, deterministic safety evaluation and deployment capabilities). This salt composition leads to a fast neutron spectrum in the core.

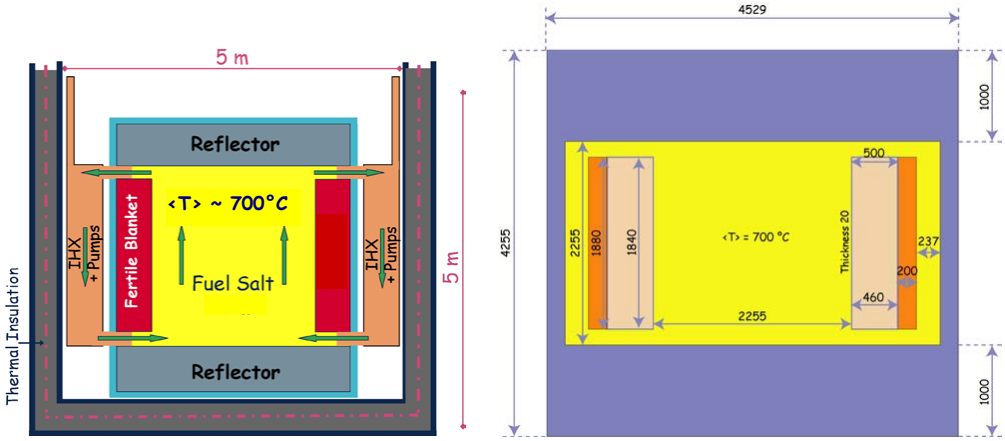

Fig. 2 (Left): *Simplified to scale vertical scheme of the MSFR system including the core, blanket and fuel heat exchangers (IHX) –* ***(Right):*** *Model of the core as used for the neutronic simulations (dimensions given in mm) with the fuel salt (yellow), the fertile salt (pink), the B_4C protection (orange) and the reflectors and 20mm thick walls in Ni-based allow (blue).*

The operating temperatures chosen for our neutronic simulations range between 650°C (input) and 750°C (output), the lower limit due to the salt's melting point, the upper limit estimated from the structural materials chosen for our simulations and detailed in section 5.

1.3 Blanket geometry

As shown in Fig.1 and 2, the radial reflector is a fertile blanket (~50 cm thick) filled with 7.3m^3 of a fertile salt LiF-ThF_4 with molar 22.5% of ^{232}Th. This fertile blanket improves the global breeding ratio of the reactor thanks to a ^{233}U extraction in an around six month period, i.e. 100% of the ^{233}U produced in the blanket is extracted in 192 days (40 liters per day as shown in the lower part of Fig 3). This fertile blanket is surrounded by a 20cm thick neutronic protection of B_4C which absorbs the remaining neutrons and protects the heat exchangers. The thickness of this B_4C protection has been determined so that the neutron flux arriving from the core through it is negligible compared to the flux of delayed neutrons emitted in the heat exchangers.

The radial blanket geometry is an angular section toron of 1.88 m high and 50 cm thick. The 2 cm thick walls are made of Ni-based alloy (see composition in Table 4). A single volume of fertile salt is considered, homogenous and cooled to a mean temperature of 650°C. A temperature variation of the fertile salt of around 30 °C between the bottom and the top of the fertile blanket may be introduced to check its low impact on the reactor evolution.

2 Fuel salt initial composition

The core contains a fluoride fuel salt, composed of 77.5 molar % of LiF enriched in ^{7}Li (99.999 at%) and 22.5 molar % of heavy nuclei (HN) amongst which the fissile element, ^{233}U or Pu. This HN fraction is kept constant during reactor evolution, the produced FPs replacing an equivalent proportion of the lithium.

2.1 ^{233}U-started MSFR

As detailed in table 2, the initial fuel salt is composed in this case of LiF-ThF_4-$^{233}UF_3$, the initial fraction of ^{233}U being adjusted to have an exactly critical reactor.

2.2 TRU-started MSFR

Table 1: *Proportions of transuranic nuclei in UOX fuel after one use in PWR without multi-recycling (burnup of 60 GWd/ton) and after five years of storage*

Isotope	Proportion in the mix
Np 237	6.3 mole%
Pu 238	2.7 mole%
Pu 239	45.9 mole%
Pu 240	21.5 mole%
Pu 241	10.7 mole%
Pu 242	6.7 mole%
Am 241	3.4 mole%

Am 243	1.9 mole%
Cm 244	0.8 mole%
Cm 245	0.1 mole%

The initial fuel salt is composed of LiF-ThF_4-$(TRU)F_3$. More precisely, the reference MSFR is started with a TRU mix of 87.5% of Pu (^{238}Pu 2.7%, ^{239}Pu 45.9% , ^{240}Pu 21.5%, ^{241}Pu 10.7%, and ^{242}Pu 6.7%), 6.3% of Np, 5.3% of Am and 0.9% of Cm, as listed in table 1 and corresponding to the transuranic elements contained in an UOX (60 GWd/ton) fuel after one use in a standard LWR and five years of storage. The amounts of TRU elements initially loaded in the TRU-started MSFR are given in table 2.

Table 2: *Summary of the characteristics of the MSFR*

<table>
<tr><td>Thermal power (MWth)</td><td colspan="5">3000</td></tr>
<tr><td>Electric power (MWe)</td><td colspan="5">1500</td></tr>
<tr><td>Fuel Molten salt initial composition (mol%)</td><td colspan="5">LiF-ThF_4-$^{233}UF_4$ or LiF-ThF_4-$(Pu\text{-}MA)F_3$ with 77.5 % LiF</td></tr>
<tr><td>Fertile Blanket Molten salt initial composition (mol%)</td><td colspan="5">LiF-ThF_4 (77.5%-22.5%)</td></tr>
<tr><td>Melting point (°C)</td><td colspan="5">565</td></tr>
<tr><td>Input/output operating temperature (°C)</td><td colspan="5">650-750[1]</td></tr>
<tr><td rowspan="6">Initial inventory (kg)</td><td colspan="2">^{233}U-started MSFR</td><td colspan="3">TRU-started MSFR</td></tr>
<tr><td>Th</td><td>^{233}U</td><td>Th</td><td colspan="2">Actinide</td></tr>
<tr><td rowspan="4">38 300</td><td rowspan="4">5 060</td><td rowspan="4">30 600</td><td>Pu</td><td>11 200</td></tr>
<tr><td>Np</td><td>800</td></tr>
<tr><td>Am</td><td>680</td></tr>
<tr><td>Cm</td><td>115</td></tr>
<tr><td>Density (g/cm^3)</td><td colspan="5">4.1249</td></tr>
<tr><td>Dilatation coefficient (/°C)</td><td colspan="5">$8{,}82 \cdot 10^{-4}$</td></tr>
<tr><td>Core dimensions (m)</td><td colspan="5">Radius: 1.1275
Height: 2.255</td></tr>
<tr><td>Fuel Salt Volume (m^3)</td><td colspan="5">18
9 out of the core
9 in the core</td></tr>
<tr><td>Blanket Salt Volume (m^3)</td><td colspan="5">7.3</td></tr>
<tr><td>Total fuel salt cycle in the system</td><td colspan="5">4.0 s</td></tr>
</table>

[1] In order to keep the same circulation time, the temperature difference in the core was adjusted regarding the new physico-chemical properties.

Table 3: *Initial critical fissile inventory for the calculation without evolution*

^{233}U-started MSFR		TRU-started MSFR		
Th	^{233}U	Th	Actinide	
38 281 kg 19.985 %mol	4 838 kg 2.515 %mol	30 619 kg 16.068 %mol	Pu	11 079 kg 5.628 %mol
			Np	789 kg 0.405 %mol
			Am	677 kg 0.341 %mol
			Cm	116 kg 0.058 %mol

In fact, the evolution calculation shows that more fissile material is needed to stay critical short time after the starting up.

3 Fuel salt reprocessing

As displayed in Fig. 3, the salt management combines a salt control unit, an online gaseous extraction system and an offline lanthanide extraction component by pyrochemistry.

The gaseous extraction system, where helium bubbles are injected in the core, removes all non-soluble fission products (noble metals and gaseous fission products). This on-line bubbling extraction has a removal period $T_{1/2}$=30 seconds in the simulations. The elements extracted by this system are the following: Z = 1, 2, 7, 8, 10, 18, 36, 41, 42, 43, 44, 45, 46, 47, 51, 52, 54 and 86.

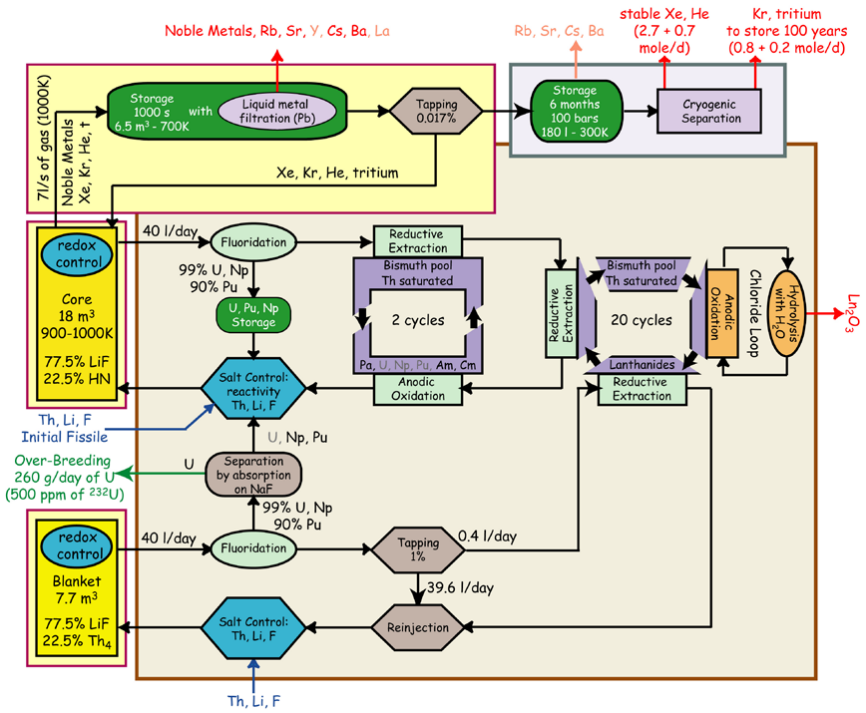

Fig. 3: *Overall scheme of the fuel salt management including the online gaseous extraction (top) and the offline reprocessing unit (bottom) – The yellow boxes surrounded by a red line represent the parts enclosed within the reactor vessel*

A fraction of salt is periodically withdrawn and reprocessed offline in order to extract the lanthanides before it is sent back into the core. The actinides are sent back into the core as soon as possible in order to be burnt. With the online control and adjustment part, the salt composition and properties are checked.

The rate at which this offline salt reprocessing is done depends on the desired breeding performance. In the reference simulations, we have fixed the reprocessing rate at 40 litres per day whatever the fuel salt volume, i.e. the whole core is reprocessed in 450 days. In the simulation of the reactor evolution, this is taken into account through a 100% offline extraction of the following fission products in 450 days: Z = 30, 31, 32, 33, 34, 35, 37, 38, 39, 40, 48, 49, 50, 53, 55, 56, 57, 58, 59, 60, 61, 62, 63, 64, 65, 66, 67, 68, 69, 70

Thanks to this simplified view of the reprocessing, even if not totally realistic, a stationary state may be reached during the reactor evolution. In the following, the extraction efficiencies may be refined in cooperation with WP3.

As displayed in fig 3, the fission products of the fertile blanket are slowly removed, with a rate of 0,4 liter of salt cleaned per day i.e. the whole fertile salt volume ($7.3m^3$) cleaned in 19250 days (52.7 years). The actinides, mostly ^{233}U, are extracted and then re-

injected in the core at a rate of 40 liters of salt cleaned per day. Additionally, the gaseous fission products are extracted in the same way as in the core (see above).

4 Physicochemical properties of the molten salts used in the MSFR

During reactor operation, fission products and new heavy nuclei are produced in the salt up to some mole % only, they do not impact the salt physicochemical properties needed for our studies. In the absence of precise data for the salt chosen in our simulations, we have used the well known characteristics of the LiF (77.5 mole%)-ThF_4 salt, presented in table 3. The last column of Table 1 summarizes the values used in these studies, at a mean temperature of 700°C (halfway between the low and the high operating temperatures).

Table 4: *Physicochemical properties used for the fuel and fertile salt in the Benchmark, measured for the salt 78%mol LiF-22%mol ThF_4 (ISTC Project No. #3749)*

	Formula	Value at 700°C	Validity Range, °C
Density ρ (g/cm^3)	$4{,}094 - 8{,}82 \cdot 10^{-4} (T_{(K)}-1008)$	4,1249	[620-850]
Kinematic Viscosity ν (m²/s)	$5{,}54 \cdot 10^{-8} \exp\{3689/T_{(K)}\}$	$2{,}46 \cdot 10^{-6}$	[625-846]
Dynamic viscosity μ (Pa.s)	$\rho_{(g/cm3)} \cdot 5{,}54 \cdot 10^{-5} \exp\{3689/T_{(K)}\}$	$10{,}1 \cdot 10^{-3}$	[625-846]
Thermal Conductivity λ (W/m/K)	$0{,}928 + 8{,}397 \cdot 10^{-5} \cdot T_{(K)}$	1,0097	[618-747]
Calorific capacity C_p (J/kg/K)	$(-1{,}111 + 0{,}00278 \cdot T_{(K)}) \cdot 10^3$	1594	[594-634][2]

The fertile salt, located in the radial blanket surrounding the core and serving as radial reflector, is composed of 77.5 LiF-22.5 ThF_4 and has similar properties.

The secondary salt is not determined but we have assumed its characteristics to be identical to those of the fuel salt (see table 3). In fact, the constraints on this secondary salt being less stringent than for the primary salt, its capacities in terms of heat transfers will probably be better. Our simulations thus correspond to the worst case.

5 Structural materials

The structural materials of the reactor, even if they are located around the core and not directly in it, have to bear the neutron flux together with high temperatures. We have considered for our simulations a Ni-based alloy containing W and Cr as detailed in tab 4.

[2] In fact, we have to extrapolate the formula of calorific capacity up to 700°C.

Table 5: *Composition (at%) of the Ni-based alloy considered for the simulation of the structural materials of the core*

Ni	W	Cr	Mo	Fe	Ti	C	Mn	Si	Al	B	P	S
79.432	9.976	8.014	0.736	0.632	0.295	0.294	0.257	0.252	0.052	0.033	0.023	0.004

The composition of the material used for the heat exchangers being not yet fixed, we have assumed its thermal conduction to be equal to 24 W/m/K, and typical value for a Ni-based alloy. The density of the Ni-based alloy is equal to 10 (data given by Thierry Auger). This material will not be submitted to a high neutron flux; hence the choice of its composition is not too constrained.

We have considered the composition of natural boron: 19.8% of ^{10}B and 80.2% of ^{11}B. The B_4C density is equal to 2.52016 (data used in SIMMER, given by KIT).

6 Other data

Table 6: *Abundances of seven delayed neutron precursors for two uranium isotopes*

Group	1	2	3	4	5	6	7
Precursor	^{87}Br	^{137}I	^{88}Br	^{93}Rb	^{139}I	^{91}Br	^{96}Rb
Half-Life	55.9 s	24.5 s	16.4 s	5.85 s	2.3 s	0.54 s	0.199 s
Abundances							
^{233}U (fast)	0.0788	0.1666	0.1153	0.1985	0.3522	0.0633	0.0253
^{233}U (thermal)	0.0787	0.1723	0.1355	0.1884	0.3435	0.0605	0.0211
^{235}U (fast)	0.0339	0.1458	0.0847	0.1665	0.4069	0.1278	0.0344
^{235}U (thermal)	0.0321	0.1616	0.0752	0.1815	0.3969	0.1257	0.0270
Mean Value	**0.0742**	**0.1679**	**0.1209**	**0.1915**	**0.3533**	**0.0684**	**0.0240**

Mean values of abundances for the neutron precursors are considered here for fissions that are due to ^{233}U (90%) and ^{235}U (10%) with a spectrum located between a thermal and a fast one (50% of thermal spectrum and 50% of fast spectrum).

B EVOL Neutronic Benchmark Results

Benchmark Calculations to perform for both the 233U-started and the TRU-started MSFR

In order to collect the data of all the partners and compare them to each other, we divided the template in 2 documents: where you have one Word-document and one Excel-file to be completed. The word document, this one, contains small tables (example: quantities at BOL and Steady State (100 years) or mean values), while the Excel-file contains bigger tables with more details (example: evolution of the quantities or flux distribution). Please fill out both documents with the calculation that your tool can perform. If you think that an important quantity was forgotten, please let us know as soon as possible in order to update the template and send it to all participants.

1) Static calculations

Critical Amount:

Since the delayed neutron fraction β_{eff} is not yet compared, we compare the critical amount with $k_{prompt}=1$ with the precision: Δk.

Remark: Feel free to fill out the column with %mol or/and Q[kg]. The comparison will be done for Q[kg]. This remark is valid for all the following tables with %mol and Q[kg] columns.

U233-started MSFR

	%mol	**Q[kg]**	Δk (pcm)
^{232}Th	19.886		
^{233}U	2.614		

This concentration gives k_eff = 1.

1.1) Delayed neutrons fraction

Calculation of the delayed neutrons fraction, please indicate the data basis used, the neutron spectrum used and for which time of the evolution the β fraction was calculated.

	β (pcm)	Fast/thermal/mixed/real (precise how) neutron spectrum	Data basis used
233U-started (initial)	310		ENDF/B-VII
TRU-started (initial)			
Steady State (100 yrs)	322		

Please indicate a short description of the evaluation method used to calculate of the effective delayed neutron fraction, while taking into account the fuel salt circulation out of the core:

	β_{eff} (pcm)	Data basis/ spectrum	Description of the evaluation method
233U-started (initial)	290		Difference between reactivities with and without delayed neutron precursors* (both without flow)
TRU-started (initial)			
Steady State (100 yrs)	307		

* Other computations can also be made. Below are given the reactivities for three different situations for t=0:

- With flow, with delayed neutron precursors, rho = -0.33 pcm (critical)
- Without delayed neutron precursors, rho = -124.60 pcm
- Without flow, with delayed neutron precursors, rho = 165.77 pcm

For t=100 years:

- With flow, with delayed neutron precursors, rho = -1.93 pcm (critical)
- Without delayed neutron precursors, rho = -133.64 pcm
- Without flow, with delayed neutron precursors, rho = 173.62 pcm

1.2) Generation time

	Generation time (μs)	Short description of the evaluation method
233U-started (initial)	1.15	Generation time = (1/v) * 1/nu sigma_f 1/v is spatially and flux averaged
TRU-started (initial)		
Steady State (100 yrs)	1.04	

1.3) Neutron Flux

Mean value of the neutron flux at different location.

	Φ(neutrons/cm²/s)
Mean value of the flux in the core	3.82 E15
Mean value of the flux on the blanket wall	1.14 E15
Mean value of the flux on the upper reflector (on the surface)	1.23 E15
Mean value of the flux on the lower reflector (on the surface)	1.28 E15
Mean value of the flux in the heat exchanger (Fuel salt located behind the B_4C protection)	6.77 E12
Mean value of the flux in the fertile blanket	2.65 E14

Further it is important to compare the neutronic spectrum. Since each participant has its own energy binning, in order to compare them easily we propose to converge into the same binning. Additionally, we ask you to send us your original binning in attached file. So please reevaluate or converge your results regarding the proposed binning A (Binning used by TU Delft):

Energy Groups Binning A (eV)	**Flux (n/cm^{-2}/s)**
2.000E+07 - 1.400E+06	2.84 E14
1.400E+06 - 5.730E+05	3.75 E14
5.730E+05 - 7.300E+04	7.38 E14
7.300E+04 - 2.290E+03	2.00 E15
2.290E+03 - 1.860E+02	3.95 E14
1.860E+02 - 5.200E+01	2.37 E13
5.200E+01 - 3.325E+01	2.04 E12
3.325E+01 - 1.290E+01	1.05 E12
1.290E+01 - 1.000E-05	1.13 E11

For those who work with monte-carlo tool, we propose to send us in attached file, the flux for the following binning B:

from 1e-9 MeV up to 20 MeV with 1031 bins

Find here attached the example file called “Spectrum_U233started.dat”, where you can easily extract the proposed energy binning B.

Additionally you can fill in the following table the flux for the energy binning of your tool.

Your own Energy Binning	**Flux (n/cm^{-2}/s)**
…	…

In order to compare the flux distribution in the core and the blanket, please fill out the following table with the values at indicated points (Z = height, R = radius).

Flux Distribution in the core and fertile blanket [n $cm^{-2}s^{-1}$]									
	Core						Fertile Blanket		
Z	R=0cm	R=22cm	R=44cm	R=66cm	R=88cm	R=112.75 cm	R=114.75 cm	R=137.75 cm	R=160.75 cm
112.75cm	2.23 E15	2.08 E15	1.80 E15	1.42 E15	9.56 E14	4.53 E14	4.14 E14	1.35 E14	3.76 E13
99cm	3.73 E15	3.59 E15	3.09 E15	2.44 E15	1.63 E15	7.17 E14	6.43 E14	1.77 E14	4.27 E13
88cm	4.87 E15	4.55 E15	3.92 E15	3.08 E15	2.05 E15	8.42 E14	6.83 E14	1.62 E14	3.14 E13
77cm	5.92 E15	5.60 E15	4.81 E15	3.77 E15	2.49 E15	1.03 E15	7.69 E14	1.56 E14	2.54 E13
66cm	6.88 E15	6.78 E15	5.80 E15	4.52 E15	2.97 E15	1.20 E15	8.89 E14	1.65 E14	2.37 E13
55cm	7.71 E15	7.48 E15	6.39 E15	4.96 E15	3.25 E15	1.32 E15	9.71 E14	1.76 E14	2.43 E13
44cm	8.43 E15	8.14 E15	6.94 E15	5.38 E15	3.52 E15	1.42 E15	1.05 E15	1.88 E14	2.55 E13
33cm	9.00 E15	8.69 E15	7.40 E15	5.73 E15	3.74 E15	1.51 E15	1.11 E15	1.99 E14	2.68 E13
22cm	9.43 E15	8.78 E15	7.47 E15	5.79 E15	3.79 E15	1.53 E15	1.13 E15	2.00 E14	2.71 E13
11cm	9.68 E15	9.13 E15	7.76 E15	6.00 E15	3.92 E15	1.59 E15	1.17 E15	2.07 E14	2.80 E13
0cm	9.78 E15	9.27 E15	7.87 E15	6.08 E15	3.96 E15	1.61 E15	1.18 E15	2.10 E14	2.83 E13
-11cm	9.73 E15	9.19 E15	7.80 E15	6.02 E15	3.92 E15	1.59 E15	1.17 E15	2.08 E14	2.80 E13
-22cm	9.53 E15	8.89 E15	7.55 E15	5.82 E15	3.80 E15	1.54 E15	1.13 E15	2.01 E14	2.72 E13
-33cm	9.15 E15	8.81 E15	7.49 E15	5.77 E15	3.75 E15	1.52 E15	1.12 E15	2.00 E14	2.69 E13
-44cm	8.60 E15	8.30 E15	7.06 E15	5.44 E15	3.54 E15	1.43 E15	1.06 E15	1.89 E14	2.57 E13
-55cm	7.66 E15	7.66 E15	6.53 E15	5.04 E15	3.27 E15	1.33 E15	9.81 E14	1.77 E14	2.45 E13
-66cm	7.09 E15	6.98 E15	5.95 E15	4.60 E15	2.99 E15	1.22 E15	9.01 E14	1.67 E14	2.40 E13
-77cm	6.12 E15	5.79 E15	4.96 E15	3.86 E15	2.53 E15	1.05 E15	7.84 E14	1.58 E14	2.56 E13
-88cm	5.04 E15	4.71 E15	4.06 E15	3.17 E15	2.10 E15	9.03 E14	7.00 E14	1.65 E14	3.14 E13
-99cm	3.87 E15	3.72 E15	3.21 E15	2.52 E15	1.67 E15	7.35 E14	6.59 E14	1.79 E14	4.18 E13
-112.75cm	2.33 E15	2.18 E15	1.88 E15	1.48 E15	9.89 E14	4.67 E14	4.27 E14	1.38 E14	3.70 E13

1.4) Feedback coefficient

Please fill out the following table with the feedback coefficient and its 2 contributions: the total value and the uncertainty of the total value due to your evaluation. Calculations should be done for ΔT of 100K (calculations performed at 650°C and 750°C). If you did it differently please precise the temperatures used. Concerning the uncertainty on the dϱ/dT calculation, please precise how you evaluate it.

	Density/Void (pcm/K)	Doppler (pcm/K)	Total (pcm/K)	+/- Δ(dϱ /dT) (pcm/K)
233U-started	-2.58	-4.39	-6.97	
TRU-started				
Steady State (100 yrs)			-5.27	

3) Preliminary Thermohyydraulic and coupled comparison: Velocity, Temperature and Precursor distributions

Since no thermohydraulic design was defined until yet, we propose to compare the thermohydraulic results considering the simple initial core geometry (see Benchmark).

Temperature Distribution in the core and fertile blanket [K]

	Core						Fertile Blanket		
Z	R=0cm	R=22cm	R=44cm	R=66cm	R=88cm	R=112.75 cm	R=114.75 cm	R=137.75 cm	R=160.75 cm
112.75cm	1025	1014	1010	1006	1004	1003	1003	1004	1006
99cm	1021	1013	999	991	1002	1037	1039	1035	1030
88cm	1015	1003	987	992	1041	1036	1002	1002	1002
77cm	1012	996	981	1005	1076	1041	1002	1002	1002
66cm	1009	990	977	1023	1100	1045	1002	1002	1002
55cm	1006	985	973	1041	1116	1049	1002	1002	1002
44cm	1003	980	969	1053	1127	1053	1002	1002	1002
33cm	1000	976	966	1059	1135	1056	1002	1002	1002
22cm	998	971	962	1063	1144	1061	1002	1002	1002
11cm	995	967	960	1063	1151	1065	1002	1002	1002
0cm	993	963	955	1060	1159	1069	1002	1002	1002
-11cm	990	959	952	1054	1166	1073	1002	1002	1002
-22cm	988	956	948	1045	1172	1077	1002	1002	1002
-33cm	986	952	943	1029	1180	1082	1002	1002	1002
-44cm	985	949	940	1013	1185	1085	1002	1002	1002
-55cm	985	946	936	989	1189	1089	1002	1002	1002
-66cm	986	944	933	958	1189	1092	1002	1002	1002
-77cm	988	944	931	933	1152	1096	1002	1002	1002
-88cm	995	947	930	925	954	1100	1002	1002	1002
-99cm	1007	964	930	925	922	919	919	918	917
-112.75cm	1031	1012	976	964	963	955	962	963	963

Axial Component of Velocity in the core [m/s]

Z	R=0cm	R=22cm	R=44cm	R=66cm	R=88cm	R=112.75cm
112.75cm	0	0	0	0	0	0
99cm	6.35 E-1	8.19 E-1	1.01	9.88 E-1	7.65 E-1	1.01
88cm	1.21	1.47	1.71	1.59	9.28 E-1	2.02 E-1
77cm	1.70	2.04	2.26	1.92	7.82 E-1	-5.47 E-1
66cm	2.15	2.53	2.69	2.05	5.71 E-1	-7.81 E-1

55cm	2.56	2.94	3.02	2.04	3.82 E-1	-8.17 E-1
44cm	2.87	3.22	3.22	1.98	2.54 E-1	-7.78 E-1
33cm	3.06	3.38	3.33	1.93	1.77 E-1	-7.29 E-1
22cm	3.24	3.53	3.43	1.88	9.45 E-2	-6.66 E-1
11cm	3.32	3.60	3.47	1.87	4.66 E-2	-6.20 E-1
0cm	3.35	3.62	3.50	1.89	7.94 E-3	-5.80 E-1
-11cm	3.33	3.60	3.50	1.93	-2.25 E-2	-5.43 E-1
-22cm	3.26	3.54	3.49	1.99	-4.57 E-2	-5.07 E-1
-33cm	3.08	3.37	3.42	2.13	-6.65 E-2	-4.60 E-1
-44cm	2.84	3.17	3.33	2.25	-7.38 E-2	-4.17 E-1
-55cm	2.45	2.83	3.13	2.42	-7.13 E-2	-3.60 E-1
-66cm	1.88	2.31	2.78	2.54	-3.03 E-2	-2.90 E-1
-77cm	1.19	1.69	2.32	2.38	3.96 E-1	-2.12 E-1
-88cm	4.64 E-1	1.01	1.76	1.90	1.46	-1.28 E-1
-99cm	-4.72 E-2	2.57 E-1	9.78 E-1	1.16	9.37 E-1	2.42 E-1
-112.75cm	0	0	0	0	0	0

Radial Component of Velocity in the core [m/s]						
Z	**R=0cm**	**R=22cm**	**R=44cm**	**R=66cm**	**R=88cm**	**R=112.75cm**
112.75cm	0.00	4.17 E-1	1.06	1.71	2.10	2.57
99cm	0.00	6.00 E-1	1.35	2.16	2.63	3.12
88cm	0.00	5.76 E-1	1.22	1.79	1.76	0
77cm	0.00	5.13 E-1	1.03	1.38	1.04	0
66cm	0.00	4.24 E-1	8.11 E-1	9.41 E-1	5.41 E-1	0
55cm	0.00	3.24 E-1	5.92 E-1	6.17 E-1	2.42 E-1	0
44cm	0.00	2.37 E-1	4.18 E-1	3.93 E-1	1.02 E-1	0
33cm	0.00	1.74 E-1	3.00 E-1	2.70 E-1	4.54 E-2	0
22cm	0.00	1.01 E-1	1.76 E-1	1.67 E-1	1.39 E-2	0
11cm	0.00	5.15 E-2	9.80 E-2	1.12 E-1	3.64 E-3	0
0cm	0.00	4.15 E-3	2.65 E-2	6.59 E-2	-4.26 E-3	0
-11cm	0.00	-4.63 E-1	-4.81 E-2	-1.64 E-2	-1.43 E-2	0
-22cm	0.00	-1.05 E-1	-1.37 E-1	-4.68 E-2	-2.76 E-2	0
-33cm	0.00	-2.01 E-1	-2.86 E-1	-1.65 E-1	-5.00 E-2	0
-44cm	0.00	-2.91 E-1	-4.38 E-1	-3.07 E-1	-7.16 E-2	0
-55cm	0.00	-4.22 E -1	-6.71 E-1	-5.80 E-1	-1.03 E-1	0
-66cm	0.00	-5.81 E-1	-9.74 E-1	-1.06	-1.53 E-1	0
-77cm	0.00	-7.08 E-1	-1.26	-1.65	-4.76 E-1	0
-88cm	0.00	-7.21 E-1	-1.47	-2.10	-2.40	0
-99cm	0.00	-4.27 E-1	-1.43	-2.32	-3.08	-3.30
-112.75cm	0.00	1.22 E-1	5.44 E-2	-3.61 E-1	-1.07	-1.57

Precursors Density Distribution group 1 [E11 at/cm^3] (see explanation)						
Z	**R=0cm**	**R=22cm**	**R=44cm**	**R=66cm**	**R=88cm**	**R=112.75cm**
112.75cm	2.31	1.37	1.37	1.36	1.36	1.60
99cm	2.74	2.72	2.71	2.71	2.71	2.72
88cm	2.73	2.72	2.71	2.71	2.72	1.37
77cm	2.73	2.71	2.71	2.71	2.74	1.37
66cm	2.73	2.71	2.70	2.71	2.77	1.37
55cm	2.72	2.70	2.70	2.72	2.78	1.36
44cm	2.72	2.70	2.70	2.72	2.79	1.36
33cm	2.71	2.70	2.69	2.72	2.80	1.36
22cm	2.71	2.70	2.70	2.72	2.80	1.36
11cm	2.71	2.69	2.69	2.72	2.81	1.36
0cm	2.70	2.69	2.68	2.72	2.81	1.36
-11cm	2.70	2.68	2.68	2.71	2.81	1.36
-22cm	2.69	2.69	2.68	2.70	2.81	1.36
-33cm	2.69	2.68	2.68	2.70	2.81	1.36
-44cm	2.68	2.67	2.67	2.69	2.81	1.36
-55cm	2.68	2.67	2.67	2.69	2.81	1.36
-66cm	2.68	2.67	2.66	2.68	2.80	1.36
-77cm	2.67	2.66	2.66	2.66	2.74	1.36
-88cm	2.67	2.66	2.66	2.65	2.66	1.36
-99cm	2.68	2.65	2.65	2.65	2.65	2.65
-112.75cm	2.32	1.36	1.28	1.22	1.26	1.54

Precursors Density Distribution group 6 [at/cm^3] (see explanation)						
Z	**R=0cm**	**R=22cm**	**R=44cm**	**R=66cm**	**R=88cm**	**R=112.75cm**
112.75cm	4.50 E8	2.72 E8	2.73 E8	2.63 E8	2.46 E8	2.63 E8
99cm	9.86 E8	9.64 E8	9.00 E8	8.14 E8	7.08 E8	5.44 E8
88cm	1.13 E9	1.06 E9	9.52 E8	8.38 E8	6.97 E8	1.68 E8
77cm	1.19 E9	1.10 E9	9.63 E8	8.40 E8	6.67 E8	1.39 E8
66cm	1.22 E9	1.11 E9	9.54 E8	8.35 E8	6.27 E8	1.28 E8
55cm	1.24 E9	1.10 E9	9.38 E8	8.30 E8	6.05 E8	1.26 E8
44cm	1.23 E9	1.08 E9	9.12 E8	8.21 E8	5.98 E8	1.27 E8
33cm	1.22 E9	1.05 E9	8.75 E8	8.05 E8	6.04 E8	1.31 E8
22cm	1.19 E9	1.04 E9	8.67 E8	8.00 E8	6.06 E8	1.32 E8
11cm	1.16 E9	9.90 E8	8.15 E8	7.68 E8	6.13 E8	1.37 E8
0cm	1.11 E9	9.27 E8	7.53 E8	7.21 E8	6.14 E8	1.40 E8
-11cm	1.06 E9	8.55 E8	6.81 E8	6.58 E8	6.03 E8	1.42 E8
-22cm	1.00 E9	7.76 E8	6.04 E8	5.81 E8	5.80 E8	1.41 E8

-33cm	9.43 E8	7.62 E8	5.90 E8	5.64 E8	5.73 E8	1.40 E8
-44cm	8.77 E8	6.83 E8	5.11 E8	4.78 E8	5.38 E8	1.35 E8
-55cm	8.10 E8	6.09 E8	4.38 E8	3.93 E8	4.96 E8	1.28 E8
-66cm	7.43 E8	5.44 E8	3.74 E8	3.15 E8	4.46 E8	1.20 E8
-77cm	6.78 E8	4.57 E8	2.88 E8	2.09 E8	2.93 E8	1.05 E8
-88cm	6.22 E8	4.06 E8	2.32 E8	1.42 E8	1.04 E8	8.85 E7
-99cm	5.88 E8	3.99 E8	2.05 E8	1.16 E8	6.05 E7	2.28 E7
-112.75cm	3.85 E8	2.12 E8	1.56 E8	6.58 E7	2.90 E7	1.14 E7

Fissile salt Composition: 233U-started MSFR

	BOL		6 months		1 year		2 years		5 years	
	mol%	Q [kg]	mol%	Q [kg]	mol%	Q [kg]	mol%	Q [kg]	mol%	Q [kg]
Li		4,49E+03		4,49E+03		4,49E+03		4,49E+03		4,49E+03
F		2,63E+04		2,63E+04		2,63E+04		2,63E+04		2,63E+04
Nb		0,00E+00		9,09E-05		9,34E-05		9,35E-05		9,36E-05
Xe		0,00E+00		2,73E-04		2,73E-04		2,73E-04		2,72E-04
tot FP		0,00E+00		2,37E+02		4,07E+02		5,33E+02		6,24E+02
232Th		3,81E+04		3,79E+04		3,78E+04		3,77E+04		3,72E+04
231Pa		0,00E+00		1,86E+00		3,58E+00		6,60E+00		1,31E+01
233Pa		0,00E+00		1,34E+02		1,34E+02		1,32E+02		1,29E+02
tot Pa		0,00E+00		1,36E+02		1,38E+02		1,39E+02		1,43E+02
232U		0,00E+00		1,27E-01		3,79E-01		1,15E+00		4,44E+00
233U		5,01E+03		5,16E+03		5,19E+03		5,23E+03		5,22E+03
234U		0,00E+00		9,50E+01		1,88E+02		3,63E+02		8,13E+02
235U		0,00E+00		1,44E+00		5,44E+00		1,94E+01		8,78E+01
236U		0,00E+00		1,57E-02		1,19E-01		8,55E-01		9,74E+00
tot U		5,01E+03		5,28E+03		5,44E+03		5,67E+03		6,18E+03
tot Np		0,00E+00		1,41E-04		3,44E-03		3,25E-02		6,56E-01
238Pu		0,00E+00		1,45E-06		4,95E-05		1,48E-03		9,62E-02
239Pu		0,00E+00		1,10E-08		7,15E-07		4,17E-05		6,29E-03
240Pu		0,00E+00		5,98E-11		7,54E-09		8,81E-07		3,28E-04
241Pu		0,00E+00		2,92E-13		6,22E-11		1,42E-08		1,21E-05
242Pu		0,00E+00		5,20E-14		4,06E-13		1,66E-10		3,53E-07
tot Pu		0,00E+00		2,76E-06		1,58E-04		2,74E-03		1,29E-01
241Am		0,00E+00		4,05E-14		3,70E-13		1,55E-10		3,20E-07
242Am		0,00E+00		2,41E-17		1,80E-16		7,35E-14		1,50E-10
242mAm		0,00E+00		3,73E-14		3,26E-14		5,53E-13		2,55E-09
243Am		0,00E+00		4,21E-14		4,24E-14		1,82E-12		9,18E-09
Tot Am		0,00E+00		1,20E-13		2,71E-12		4,49E-10		5,03E-07
242Cm		0,00E+00		3,82E-14		2,39E-14		3,69E-12		1,41E-08
243Cm		0,00E+00		3,81E-14		3,27E-14		5,85E-14		3,12E-10
244Cm		0,00E+00		4,57E-14		4,70E-14		1,05E-13		7,18E-10
245Cm		0,00E+00		3,96E-14		3,58E-14		3,07E-14		2,32E-11
tot Cm		0,00E+00		1,58E-13		1,71E-13		1,20E-11		2,36E-08
total Heavy Nuclei *		4,31E+04		4,33E+04		4,34E+04		4,35E+04		4,35E+04

* Heavy Nuclei = (88<Z<99)

Fissile salt Composition: 233U-started MSFR

	10 years		20 years		50 years		100 years		200 years	
	mol%	Q [kg]	mol%	Q [kg]	mol%	Q [kg]	mol%	Q [kg]	mol%	Q [kg]
Li		4,49E+03		4,49E+03		4,49E+03		4,49E+03		4,49E+03
F		2,62E+04		2,62E+04		2,61E+04		2,59E+04		2,55E+04
Nb		9,39E-05		9,42E-05		9,43E-05		9,42E-05		9,42E-05
Xe		2,72E-04		2,71E-04		2,70E-04		2,70E-04		2,70E-04
tot FP		6,33E+02		6,33E+02		6,32E+02		6,33E+02		6,37E+02
232Th		3,66E+04		3,58E+04		3,46E+04		3,42E+04		3,41E+04
231Pa		1,88E+01		2,24E+01		2,33E+01		2,35E+01		2,37E+01
233Pa		1,26E+02		1,21E+02		1,16E+02		1,14E+02		1,14E+02
tot Pa		1,45E+02		1,43E+02		1,39E+02		1,37E+02		1,37E+02
232U		9,69E+00		1,49E+01		1,67E+01		1,68E+01		1,70E+01
233U		5,16E+03		5,05E+03		4,91E+03		4,86E+03		4,84E+03
234U		1,37E+03		2,01E+03		2,53E+03		2,59E+03		2,58E+03
235U		2,21E+02		4,15E+02		5,86E+02		6,05E+02		6,02E+02
236U		4,97E+01		1,84E+02		5,26E+02		6,72E+02		6,84E+02
tot U		6,88E+03		7,79E+03		8,59E+03		8,74E+03		8,73E+03
tot Np		6,08E+00		3,59E+01		1,22E+02		1,63E+02		1,66E+02
238Pu		1,65E+00		1,69E+01		1,11E+02		1,75E+02		1,82E+02
239Pu		1,99E-01		3,50E+00		3,74E+01		6,70E+01		7,07E+01
240Pu		2,10E-02		7,51E-01		1,92E+01		5,20E+01		5,98E+01
241Pu		1,38E-03		8,00E-02		3,13E+00		9,63E+00		1,13E+01
242Pu		8,44E-05		1,05E-02		1,17E+00		6,80E+00		9,76E+00
tot Pu		2,42E+00		2,82E+01		1,81E+02		3,12E+02		3,33E+02
241Am		7,11E-05		7,71E-03		5,81E-01		2,28E+00		2,80E+00
242Am		3,29E-08		3,50E-06		2,58E-04		1,01E-03		1,23E-03
242mAm		1,05E-06		1,95E-04		2,48E-02		1,17E-01		1,48E-01
243Am		4,27E-06		1,00E-03		2,26E-01		1,81E+00		2,84E+00
Tot Am		1,26E-04		1,59E-02		9,53E-01		4,31E+00		5,79E+00
242Cm		4,34E-06		5,71E-04		4,83E-02		1,95E-01		2,40E-01
243Cm		1,79E-07		4,02E-05		5,60E-03		2,67E-02		3,39E-02
244Cm		6,63E-07		3,01E-04		1,49E-01		1,82E+00		3,27E+00
245Cm		4,01E-08		3,21E-05		2,86E-02		4,54E-01		8,77E-01
tot Cm		8,95E-06		1,82E-03		2,90E-01		2,90E+00		5,31E+00
total Heavy Nuclei *		4,36E+04		4,36E+04		4,36E+04		4,35E+04		4,35E+04

* Heavy Nuclei = (88<Z<99)

Neutronic Characteristics of the 233U-started MSFR										
	BOL	6 months	1 year	2 years	5 years	10 years	20 years	50 years	100 years	200 years
Breeding Ratio (as defined in benchmark word template)**	-	0.95	0.95	0.95	0.94	0.94	0.95	0.94	0.944	0.945
233U production in the core [kg/an]	-	-142.0	-109.8	-89.0	-69.8	-63.4	-58.5	-61.7	-61.7	-60.6
233U production extracted out of blanket [kg/an]										
Breeding Gain [kg/an]										
Thorium supply core [kg/year]	-	1205.1	1234.7	1228.4	1099.6	1115.7	1097.5	1097.8	1098.3	1099.5
Thorium supply core and blanket [kg/year]										
Balance of HN [kg] (« total HN inventory at time t »- « Init. inventory »- « supply up to t » + « extracted »)										
dk/dT (Doppler) [pcm/K]										
dk/dT (density) [pcm/K]										
dk/dT (total) [pcm/K]	-6,97	-6,68	-6,57	-6,43	-6,22	-6,04	-5,73	-5,39	-5,27	-5,23
Fraction of delayed neutrons [pcm] *	310								322	

* without taking in account recirculation

** Only takes into account the core (burnup in fertile blanket is not modeled).

Bibliography

[1] M. Aufiero, A. Cammi, and C. Fiorina et al. An Extended Version of the SERPENT-2 code to Investigate fuel Burn-up and Core Material Evolution of the Molten Salt Fast Reactor. Preprint, 2013.

[2] S.E. Beall and P.N. Haubenreich et. al. MSRE Design and Operations Report. Technical report, Oak Ridge National Laboratory, 1964.

[3] A.J.J. Bos, F.S. Draaisma, and W.J.C. Okx. *Inleiding tot de Stralingshygiëne*. Sdu Uitgevers, 2007.

[4] M. Brovchenko. Preliminary Safety Studies of the MSFR. Presented during EVOL meeting.

[5] P.N. Brown and G.D. Byrne; A.C. Hindmarsh. Vode: a Variable-Coefficient ODE solver. *SIAM Journal on Scientific and Statistical Computing*, 10(5):1038–1051, September 1989.

[6] Nuclear Fuel Cycle and Materials Section. Thorium fuel cycle - Potential Benefits and Challenges. Technical report, International Atomic Energy Agency, Wagramer Strasse 5, A-1400 Vienna, Austria, May 2005.

[7] E. Merle-Lucotte et al. D. Heuer. Possible Configurations for the Thorium Molten Salt Reactor and Advantages of the Fast Nonmoderated Version. *Nuclear Science and Engineering*, 161:78–89, 2008.

[8] L.C. Dewan and C. Simon et al. Molecular Dynamics Simulation of the Thermodynamic and Transport Properties of the Molten Salt Fast Reactor Fuel LiF-ThF_4. *Journal of Nuclear Materials*, December 2012.

[9] J. J. Duderstadt and L. J. Hamilton. *Nuclear Reactor Analysis*. John Wiley & Sons, 1976.

[10] S.M. Bowman; M.E. Dunn. *Scale Cross-Section libraries*. Oak Ridge National Laboratory, Tennessee, United States, six edition, January 2009.

[11] A. Evans-Pritchard. China blazes trail for 'clean' nuclear power from thorium. The Telegraph, January 2013.

[12] EVOL. http://www.li2c.upmc.fr/. Webpage.

[13] EVOL. MOLTEN SALT FAST REACTOR - Reference Configuration, March 2012.

[14] The Weinberg Foundation. Do Molten Salt Reactor Have a Lithium Problem. Webpage, June 2013.

[15] I.C. Gauld and O.W. Hermann. *Couple: Scale System Module to Process Problem-Dependent Cross Sections and Neutron Spectral Data for Origen-S Analysis*. Oak Ridge National Laboratory, Tennessee, United States, six edition, January 2009.

[16] I.C. Gauld, B.D. Murphy, and M.L. Williams. *ORIGEN-S data libraries*. Oak Ridge National Laboratory, Tennessee, United States, six edition, January 2009.

[17] GEN4. http://www.gen-4.org/. Webpage, September 2010.

[18] S. Goluoglu and D.F. Hollenbach et. al. *The Information Material Processor for Scale*. Oak Ridge National Laboratory, Tennessee, United States, 6 edition, January 2009.

[19] N.M. Green and L.M. Petrie. *XSDRNPM: a One-Dimensional Discrete-Ordinates Code for Transport Analysis*. Oak Ridge National Laboratory, Tennessee, United States, six edition, January 2009.

[20] N.M. Green, L.M. Petrie, and S.K. Fraley. *ICE: Module to Mix Multigroup Cross Sections*. Oak Ridge National Laboratory, Tennessee, United States, six edition, January 2009.

[21] D.E. Holcomb and S.M. Cetiner. An Overview of Liquid-Fluoride-Salt Heat Transport Systems. Technical report, Oak Ridge National Laboratory, Tennessee, United States, September 2010.

[22] ICRP. Annual Limits on Intake of Radionuclides by Workers Based on the 1990 Recommendations. Technical report, ICRP, 1990.

[23] L.P.B.M. Janssen and M.M.C.G. Warmoeskerken. *Transport Phenomena Data Companion*. VSSD, Delft, Netherlands, 2012.

[24] D. Kotlyar, Y. Shaposhnik, E. Fridman, and E. Shwageraus. Coupled Neutronic Thermo-Hydraulic Analysis of Full PWR Core with Monte-Carlo Based BGCore System. *Nuclear Engineering and Design*, pages 3777–3786, 2011.

[25] R.W. Moir and E. Teller. Thorium-Fueled Underground Power Plant Based on Molten Salt Technology. *Nuclear Technology*, 151:334 – 340, September 2005.

[26] NIST. Atomic Weights and Isotope Compositions. Webpage, 2013.

[27] European Union Publication Office. http://cordis.europa.eu/. Webpage.

[28] R.C. Robertson. MSRE Design and Operations Report, January 1965.

[29] M.W. Rosenthal, P.R. Kasten, and R.B. Briggs. Molten-Salt Reactors - History, Status and Potential. *Nuclear Applications and Technology*, 8(107), 1970.

[30] H. Rouch and P. Rubiolo. MSFR Thermal Hydraulics Benchmark Specifications. EVOL internal report.

[31] Y. Saad. *Numerical Methods for Large Eigenvalue Problems.* Society for Industrial and Applied Mathematics, 2011.

[32] R.D. Skeel. Construction of Variable-Stepsize Multistep Formulas. *Mathematics of Computation*, 47(176):503–510, October 1986.

[33] W.F. Smith. *Principles of Materials Science and Engineering.* McGraw-Hill, third edition, 1995.

[34] S. Tabuchi and T. Aoyama. Lumped Group Constants of FP Nuclides for Fast Reactor Shielding Calculation Based on JENDL-3.2. Technical report, Japan Nuclear Cycle Development Institute, Ibaraki, Japan, 2001.

[35] H. van den Akker and R. Mudde. *Fysische Transportverschijnselen.* VSSD, 2008.

[36] Erik van der Linden. Coupled neutronics and computational fluid dynamics for the molten salt fast reactor. Master's thesis, Delft University of Technology, 2012.

[37] H.K. Versteeg and W. Malalasekera. *An Introduction to Computational Fluid Dynamics - The Finite Volume Method.* Pearson Eduction Limited, Harlow, England, second edition, 2007.

[38] D.C. Wilcox, editor. *Turbulence modeling for CFD.* DCW Industries, La Canada, California, United States, second edition, November 1994.